Title

Economically driven constrained optimization and control: Algorithms, formal guarantees, and applications in optimal microgrid sizing and dispatch

ISBN
9798293838097

Author
Ghosh, Avik

Publication Date
2025-09-13

UNIVERSITY OF CALIFORNIA SAN DIEGO

Economically driven constrained optimization and control: Algorithms, formal guarantees, and applications in optimal microgrid sizing and dispatch

A dissertation submitted in partial satisfaction of the
requirements for the degree Doctor of Philosophy

in

Engineering Sciences (Mechanical Engineering)

by

Avik Ghosh

Committee in charge:

Professor Jan Kleissl, Chair
Professor Sonia Martínez, Co-Chair
Professor Patricia Hidalgo-Gonzalez
Professor Yuanyuan Shi

2025

The Dissertation of Avik Ghosh is approved, and it is acceptable in quality and form for publication on microfilm and electronically.

University of California San Diego

2025

DEDICATION

To my family, and to all the tireless souls who, in myriad ways, uphold *Dharma* and serve *Bharatmata* — upon whose quiet strength, labor and sacrifice, we march into the future with ever nobler dreams and even higher ideals.

EPIGRAPH

চিত্ত যেথা ভয়শূন্য, উচ্চ যেথা শির,
জ্ঞান যেথা মুক্ত, যেথা গৃহের প্রাচীর
আপন প্রাঙ্গণতলে দিবসশর্বরী
বসুধারে রাখে নাই খণ্ড ক্ষুদ্র করি,
যেথা বাক্য হৃদয়ের উৎসমুখ হতে
উচ্ছ্বসিয়া উঠে, যেথা নির্বারিত স্রোতে
দেশে দেশে দিশে দিশে কর্মধারা ধায়
অজস্র সহস্রবিধ চরিতার্থতায়,
যেথা তুচ্ছ আচারের মরুবালুরাশি
বিচারের স্রোতঃপথ ফেলে নাই গ্রাসি,
পৌরুষেরে করে নি শতধা, নিত্য যেথা
তুমি সর্ব কর্ম চিন্তা আনন্দের নেতা,
নিজ হস্তে নির্দয় আঘাত করি, পিতঃ;
ভারতেরে সেই স্বর্গে করো জাগরিত।

রবীন্দ্রনাথ ঠাকুর

Where the mind is without fear and the head is held high;
Where knowledge is free;
Where the world has not been broken up into fragments by narrow domestic walls;
Where words come out from the depth of truth;
Where tireless striving stretches its arms towards perfection;
Where the clear stream of reason has not lost its way into the dreary desert sand of dead habit;
Where the mind is led forward by thee into ever-widening thought and action—
Into that heaven of freedom, my Father, let my country, *Bharat*, awake.

Rabindranath Tagore

The above is a poem from *'Gitanjali'*, originally written in Bengali (and then translated to English) by Rabindranath Tagore, a Bengali polymath who worked as a poet, writer, playwright, composer, philosopher, social reformer, and painter of the Bengal Renaissance — who reshaped literature and music as well as Indian art with contextual modernism in the late 19th and early 20th centuries. He was awarded the Nobel Prize in Literature in 1913, the first Asian to receive so, *"because of his profoundly sensitive, fresh and beautiful verse, by which, with consummate skill, he has made his poetic thought, expressed in his own English words, a part of the literature of the West."*

TABLE OF CONTENTS

NOMENCLATURE

α	Maximum probability of violation of state constraints
γ	Constant of proportionality in online h update rule
$\hat{w}$	Width of the critical region
κ, κ'	Critical region
$\mathbb{P}$	Probability measure
$\mathscr{F}_t$	Filtration
$\tilde{h}$	Adaptive state constraint tightening parameter
m'	Month index of year
Δt	Sampling time
A	System state transition matrix
B	System control input matrix
BC	EV battery capacity (kWh)
BE	EV battery energy (kWh)
BESS	Battery energy storage system
CD	EV charging demand (kWh)
c	Control input coupling vector
d	Date index of month/Control input coupling vector dimension
E	System state uncertainty matrix
EC	Energy charges ($)
ED	Energy demand (kWh)
EMPC	Economic MPC
EV	Electric vehicle/Electric vehicle charging rate (kW)
F	Control input uncertainty matrix
G	State chance constraint matrix

g	State chance constraint vector
h	Adaptive state constraint relaxing parameter
k	Time index
JCC	Joint chance constraints
L	Original building/microgrid load (kW)
LTI	Linear time invariant
M	Control input coupling matrix
MG	Microgrid
MPC	Model predictive control(ler)
m	Number of days in a month/Control input dimension
N	MPC prediction horizon length
NC	Non-coincident
NCDC	Non-coincident demand charge ($)
NCDP	Non-coincident demand peak (kW)
NL	Optimized net load of buildings (kW)
n	Total number of EVs/State dimension
OC	Other charges ($)
OP	On-peak
OPDC	On-peak demand charge ($)
OPDP	On-peak demand peak (kW)
PV	Photovoltaic/Photovoltaic power generation (kW)
p	Uncertainty dimension/Probability of violation of state constraints
q	Control input constraint vector dimension
R	Rate of energy charges ($/kWh)/Rate of demand charges ($/kW)
RT	Regularization term

r	State chance constraint vector dimension
S	Control input constraint matrix
SMPC	Stochastic MPC
SOC	State of charge of EV/BESS
s	Control input constraint vector
t	Time index/Time in hours
u	Control input
V	State constraint violation tracker
VRES	Variable renewable energy sources
w	Uncertainty
w_f	Weighing factor for regularization term
w_{site}	Weights for different sites
x	State
Y	Time-average of state constraint violations
Z	Absolute difference between α and Y

LIST OF SUPPLEMENTAL TABLES

LIST OF FIGURES

LIST OF TABLES

ACKNOWLEDGEMENTS

First and foremost, I would like to thank my advisor, Prof. Jan Kleissl for his constant support and encouragement through the duration of my Ph.D. Jan has been gentle, kind, and left no stone unturned to help me in this journey, whether it be in scientific scholarship, or in financial or emotional support. I joined the group with little to no technical knowledge of controls and optimization; I only had a passion to work for a cleaner energy powered future. Words will fail to express what an amazing advisor and mentor Jan has been: he gave me the freedom to explore science without worrying too much about the end results, silently nurtured my spirit for scientific inquiry, instilled within me a reverence for openness in scientific thought, discourse and collaboration, refined my early and unpolished drafts into articulate and compelling papers, especially in the initial stages of my Ph.D., and has been a role model in being evenhanded and fair to me throughout — values I will seek to carry forward in my scientific journey. I would not have made it but for his kind support and patience with me during the tumultuous COVID phase. This space is not enough to express the profound impact he has had upon me, and I sincerely hope we keep collaborating in the future. Jan has exemplified the ideal Ph.D. advisor — one I had only heard of in lectures and interviews of esteemed scientists since my childhood.

I would also like to extend my deepest gratitude to my co-advisor, Prof. Sonia Martínez. Although I started working with Prof. Martínez only after my candidacy, I have learnt and picked up a great deal about controls and research in general since then through my interactions with her — both individually and also through the MURO group meetings. I admire and look upto how she is able to so quickly parse through a scientific problem, give deep technical insights, and give directions to attack the problem from multiple angles. I thank Sonia for welcoming me into her group and pushing me adequately, whether it be in asking the deep and challenging scientific questions, helping me prepare intuitive but

technically demanding presentations, or in writing papers. My only regret would be to not start working with her earlier, but I hope that I would make up for it by a lifetime of collaboration going forward.

I would like to thank my committee members: Prof. Patricia Hidalgo-Gonzalez and Prof. Yuanyuan Shi for their technical insights on my dissertation and suggestions about pursuing postdoctoral research. They both have been instrumental in organizing the PES Seminars in UCSD which has been an excellent venue to present my research and hear about others'.

I would also like to thank my instructors, especially Prof. Mauricio de Oliveira and Prof. Miroslav Krstić for their insightful courses which have shaped my dissertation implcitly and has given me ideas to explore later in my scientific career. Prof. de Oliveira's *MAE 280B: Linear Control Design* and Prof. Krstić's *MAE 281A: Nonlinear Systems* have been the highlight courses of my graduate studies. Special thanks to Prof. Jorge Cortés for his insightful critiques during the MURO group presentations. Thanks also to Prof. Mamadou Diagne for the mentorship and advice during my postdoctoral job search.

Over the years, I have had the fortune of collaborating with amazing researchers, the foremost among them being Dr. Adil Khurram, who joined as the postdoc and is now a Research Scientist in the GrID Lab. Adil introduced me to model predictive controllers which is the major focus of my dissertation, and patiently and painstakingly worked with me initially when I was a novice in developing formal proofs. I cherish our scientific discussions which stretched hours and sometimes multiple days — and in the end I believe of all things in my graduate experience, I learnt the most through them. Adil's calm but deeply critical questions and comments pushed me to develop better proofs, coming up with better technical arguments, writing more clearly but concisely, and presenting in a more audience friendly format. I appreciated his help through the multiple initial drafts and scribbled notes — my advisors saw mostly the polished draft, but Adil had to work with the crappy versions and I cannot thank him enough for it. I knew if I could justify

my work with Adil, I could with others. I am extremely proud of the work we did together, and it is only because of him that I mustered the courage to delve into theory, despite not having the formal math background for it — all of which made my dissertation richer and gave me a vision for what I want to do in the future – I could not have done it without him and I hope we keep collaborating in the future.

I want to take this opportunity to thank my labmates, both former and present from the GrID Lab: Elynn, Monica, Changfu, Manasa, Cristian, Sushil, Yi-An, Ryan, Graham, Melvin, Melek, Mohammed, Kohei, Chi, Yizhan, Ben, Lola, Lennard, Latetia, Yuying, and Isabel. Thank you for the lab lunches and making the office a fun place to work in. Thanks to Monica for getting me started on the research journey with her initial work on the Nuvve Project, which ultimately became my first paper. Thanks to Cristian and Manasa for their timely advice when I was starting out — in many instances they were the first to tread the unknown when our lab shifted research directions, from which the rest of us learnt. I also want to thank Cristian and Yi-An for the collaboration and help on the San Diego Port project.

Graham and Melvin were the best cohort mates I could have asked for. Taking classes together was challenging but fun. Both of them helped me get accustomed to the SoCal and unspoken rules of an American life, which I was not aware of when I came here. Thanks to Graham for the multiple collaborations we have had during the Ph.D. I respect his discipline, ability to balance work with life, and having the capacity to make us all realize that some of life needs to be for fun to keep us from burning out, especially during a Ph.D. Melvin was my friend, philosopher and guide, especially in my first year when I was naive and knew nothing about living abroad. I thank him for the wonderful and deep conversations we have had — it gave me a perspective which I had never had thus far in my life. I also thank him for being a straight shooter from whom I have learnt a great deal, and with his help I have even been able to get rid of some of my erstwhile bad habits. Melvin's wisdom helped me overcome a particularly challenging phase of my life

post COVID, without which my Ph.D. would have been in jeopardy. I would also like to extend my deepest gratitude and thanks to Ryan, with whom I have spent the longest amount of time in the lab. There were many a times when we both had all our meals — breakfast, lunch, coffee breaks, and dinner in the lab — and through myraid conversations with him spanning a great range — from dating to technical issues in research to a life in academia — his kindness, insights and wisdom left a deep imprint on me. It was nice to have him around when we both were burning the midnight oil in the lab: I knew he was going through it with me and it helped inspire, sustain and push me, especially when the going got tough.

Thanks to Melek for taking the initiative for a lot of new things in our lab (the new white board, lab website, PES seminars, lab potluck, among others). We have all benefited from his enthusiasm. Thanks to Yizhan for the collaboration and help on the UpSCALEDEV project. Of late, Chi has been the official prankster of the GrID lab, and I thoroughly enjoy being around him — his comically timed quips along with a relaxed attitude helped maintain a jovial and light mood in the lab. Chi, we are absolutely writing a paper together — ideally on controls and optimization, but I'm also open to groundbreaking research on comedic timing and the art of the perfect prank!

I also want to thank all members of the MURO Lab, both former and present: Scott Brown, Nirabhra, Ahmed, Zhenyi, Jun, Masih, Michael, Mohammed Alyaseen, Mohammad Khajenejad, Paul, Pol, Scott Addams, Neilabh, Benjamin, Dhruv, Azra, Steven, Xuting, Yinzhuang, Ana, Arnau, William, Meghan, Aleix and Guillem for their pertinent group presentations from which I learnt a lot. I want to extend a special thank you to both Scott Brown and Nirabhra for helping me prepare and give better technical presentations. Nirabhra's help when I presented my first paper in the group meeting was extremely important and it helped me be more confident in my explanations. Thanks to Scott for driving me to the Southern California Control Workshops and being always willing to extend help.

I would like to thank my undergraduate professors from IIEST, Shibpur, especially Prof. Aritra Ganguly and Prof. Bijan Kumar Mandal for their early research guidance and support during my graduate school applications. Prof. Jishnu Bhattacharya from IIT, Kanpur whom I interned with also played an instrumental rule in shaping my scientific career in my bachelor's days. Thanks to Prof. Anindya Chatterjee and the Late Prof. Sameer Khandekar from IIT, Kanpur, Prof. Partha Pratim Chakrabarti from IIT, Kharagpur and Prof. Sudhir Kumar Jain from IIT Gandhinagar for their insightful advice on social media (LinkedIn/Youtube/Quora) to young Indian scientists which I have grown up listening to and which inspires me to this day.

Thanks to my high school and undergraduate friends — Pinaki, Prithviraj, Soham, Soudip, Pulasta, Abhinaba, Arani, Sayan, Ghorai, Rajdip, Debjyoti, Debashish, Dhritiman and Souvik *Da* for keeping me sane by reminiscing our wonderful Kidderpore/Shibpur days, and always being just one phone call away despite months of no-contact sometimes. To all my friends in San Diego and the US — Sombuddha, Anshu, Atishna, Ushashi, Subhechchha, Nikhil, Prabhav, Shravan, and Arijit *Da*: thank you for your friendship, impromptu parties, celebrations on festivals, and occasional dozes of encouragement. Thanks to Soumya for giving me a place to stay when I first arrived in the US and did not have housing. I am especially grateful to Abhinaba, my former undergraduate roommate, whose presence in San Diego was of great comfort during the challenging period of my postdoc job search. His homecooked meals and thoughtful advice provided much-needed warmth and support. Special thanks to both Souvik *Da* and Arijit *Da* for your wisdom on life and for helping me selflessly many a times.

I would like to thank my family — *Baba, Ma*, and *Dada* for their unconditional love and for supporting me through this journey. Staying away from family is hard, and this journey is as much theirs as it is mine. I thank *Baba* and *Ma* for all the sacrifices they made from my childhood so that I could have the platform to do my Ph.D. It is rare to connect with someone for both crass humor and sophisticated political discussions: *Dada*

is a comfortable contender for that spot, which has kept me grounded and connected to my roots many a times during the Ph.D. journey. I thank *Manapishi* for her tireless and selfless help in bringing me up. Though she dances among the stars now, I find solace in her silent blessings, ever watching, ever near, from the heavens above.

Last, but not the least, I want to thank my partner Shirsha for being the bundle of joy she is and for always inspiring me. Her love and belief in me has helped me immensely in this journey. She has helped me grow and pushed me to be better than what I thought I was capable of. It would be foolish of me (anyway she thinks she is smarter than me, which she is right about) to try to encapsulate her contributions in words, so I would rather not try. Also, because of Shirsha I have another family now — and knowing their thoughts are with me made many difficult things easier to deal with.

Chapter 1, in part, is a reprint of the material as it appears in 'Effects of number of electric vehicles charging/discharging on total electricity costs in commercial buildings with time-of-use energy and demand charges' authored by Avik Ghosh, Monica Zamora Zapata, Sushil Silwal, Adil Khurram, and Jan Kleissl, in the Journal of Renewable and Sustainable Energy, 2022; and 'Adaptive Chance Constrained MPC under Load and PV Forecast Uncertainties' authored by Avik Ghosh, Cristian Cortes-Aguirre, Yi-An Chen, Adil Khurram, and Jan Kleissl, in the 2023 IEEE PES Grid Edge Technologies Conference & Exposition; and 'Adaptive Relaxation-Based Nonconservative Chance Constrained Stochastic MPC' authored by Avik Ghosh, Cristian Cortes-Aguirre, Yi-An Chen, Adil Khurram, and Jan Kleissl, in the IEEE Transactions on Control Systems Technology, 2025; as well as 'Economic Model Predictive Control with a Non-Fixed Reference Trajectory for Optimal Microgrid Dispatch' authored by Avik Ghosh, Adil Khurram, Jan Kleissl, and Sonia Martínez, which is currently being prepared for submission for publication in Automatica. The dissertation author was the primary investigator and author of these papers.

Chapter 3, in full, is a reprint of the material as it appears in 'Effects of number of electric vehicles charging/discharging on total electricity costs in commercial buildings with time-of-use energy and demand charges' authored by Avik Ghosh, Monica Zamora Zapata, Sushil Silwal, Adil Khurram, and Jan Kleissl, in the Journal of Renewable and Sustainable Energy, 2022. The dissertation author was the primary investigator and author of this paper.

Chapter 4, in full, is a reprint of the material as it appears in 'Adaptive Relaxation-Based Nonconservative Chance Constrained Stochastic MPC' authored by Avik Ghosh, Cristian Cortes-Aguirre, Yi-An Chen, Adil Khurram, and Jan Kleissl, in the IEEE Transactions on Control Systems Technology, 2025. The dissertation author was the primary investigator and author of this paper.

Chapter 5, in full, is currently being prepared for submission for publication of the material as 'Economic Model Predictive Control with a Non-Fixed Reference Trajectory for Optimal Microgrid Dispatch' authored by Avik Ghosh, Adil Khurram, Jan Kleissl, and Sonia Martínez, in Automatica. The dissertation author was the primary investigator and author of this paper.

Chapter 6, in part, is a reprint of the material as it appears in 'Effects of number of electric vehicles charging/discharging on total electricity costs in commercial buildings with time-of-use energy and demand charges' authored by Avik Ghosh, Monica Zamora Zapata, Sushil Silwal, Adil Khurram, and Jan Kleissl, in the Journal of Renewable and Sustainable Energy, 2022; and 'Adaptive Relaxation-Based Nonconservative Chance Constrained Stochastic MPC' authored by Avik Ghosh, Cristian Cortes-Aguirre, Yi-An Chen, Adil Khurram, and Jan Kleissl, in the IEEE Transactions on Control Systems Technology, 2025; as well as 'Economic Model Predictive Control with a Non-Fixed Reference Trajectory for Optimal Microgrid Dispatch' authored by Avik Ghosh, Adil Khurram, Jan Kleissl, and Sonia Martínez, which is currently being prepared for submission for publication in Automatica. The dissertation author was the primary investigator and author of these papers.

VITA

2019	Bachelor of Technology in Mechanical Engineering, Indian Institute of Engineering Science and Technology, Shibpur
2021	Master of Science in Engineering Sciences (Mechanical Engineering), University of California San Diego
2025	Doctor of Philosophy in Engineering Sciences (Mechanical Engineering), University of California San Diego

PUBLICATIONS

Journal papers:

1. **Ghosh, A.**, Khurram, A., Kleissl, J., Martínez, S., 2025. Economic Model Predictive Control with a Non-Fixed Reference Trajectory for Optimal Microgrid Dispatch. *In preparation for submission to Automatica.*

2. **Ghosh, A.**, Cortes-Aguirre, C., Chen, Y., Khurram, A., Kleissl, J., 2025. Adaptive Relaxation-Based Nonconservative Chance Constrained Stochastic MPC. *IEEE Transactions on Control Systems Technology.*

3. Cortes-Aguirre, C.*, Chen, Y.* **Ghosh, A.**, Kleissl, J., Khurram, A., 2024. Economic MPC with an Online Reference Trajectory for Battery Scheduling Considering Demand Charge Management. *Under review in IEEE Transactions on Smart Grids.*

4. McClone, G., **Ghosh, A.**, Khurram, A., Washom, B., Kleissl, J., 2023. Hybrid Machine Learning Forecasting for Online MPC of Work Place Electric Vehicle Charging. *IEEE Transactions on Smart Grids.*

5. **Ghosh, A.**, Zapata, M.Z., Silwal, S., Khurram, A., Kleissl, J., 2022. Effects of number of electric vehicles charging/discharging on total electricity costs in commercial buildings with time-of-use energy and demand charges. *Journal of Renewable and Sustainable Energy.*

6. **Ghosh, A.**, Bhattacharya, J., 2021. A solar regenerated liquid desiccant evaporative cooling system for office building application in hot and humid climate. *Thermal Science and Engineering Progress.*

7. **Ghosh, A.**, Ganguly, A., 2017. Performance analysis of a partially closed solar regenerated desiccant assisted cooling system for greenhouse lettuce cultivation. *Solar Energy.*

Conference papers:

8. **Ghosh, A.**, Lu, X., Adetola, V., 2024. Advanced Predictive Rule-based Control for HVAC Cost Reduction Under Dynamic Electricity Pricing in Residential Buildings. In *8th International High Performance Buildings Conference at Purdue.*

9. **Ghosh, A.***, Cortes-Aguirre, C.*, Chen, Y.*, Khurram, A., Kleissl, J., 2023. Adaptive Chance Constrained MPC under Load and PV Forecast Uncertainties. In *2023 IEEE PES Grid Edge Technologies Conference & Exposition (Grid Edge), San Diego, CA, USA.*

10. **Ghosh, A.**, Ganguly, A., Bhattacharya, J., 2019. Exergy analysis of a solar regenerated liquid desiccant assisted air conditioning system for hot and humid climates. In *Journal of Physics: Conference Series, 2nd International Conference on New Frontiers in Engineering, Science & Technology (NFEST) 2019, Kurukshetra, Haryana, India.*

11. **Ghosh, A.**, Ganguly, A., 2018. Thermal model development of a partially closed solar desiccant assisted greenhouse cooling system. In *A. Mukhopadhyay, P. Sahoo & S. Sen (Ed.), Proceedings of the 1st International Conference on Mechanical Engineering. Jadavpur University Press, Kolkata, pp. 614-617.*

ABSTRACT OF THE DISSERTATION

Economically driven constrained optimization and control: Algorithms, formal guarantees, and applications in optimal microgrid sizing and dispatch

by

Avik Ghosh

Doctor of Philosophy in Engineering Sciences (Mechanical Engineering)

University of California San Diego, 2025

Professor Jan Kleissl, Chair
Professor Sonia Martínez, Co-Chair

The modern electricity grid is fast changing with a shift from traditional centralized generation sources like fossil-fuel and nuclear power plants to distributed variable renewable energy sources (VRES) like wind and photovoltaic (PV) generators. However, VRES are intermittent in nature which can potentially lead to power imbalance in the electric grid, thereby risking grid stability. A cost-effective approach to mitigate these intermittencies is by integrating dispatchable energy resources like electric vehicles (EVs) and battery energy storage systems (BESS) in commercial microgrids to minimize the power fluctuations and provide additional grid services. However, for commercial microgrid operators to avail the

maximum benefits from the dispatchable energy resources, it is important to appropriately size them during installation, and once installed it is vital to optimally dispatch them in real-time to realize the maximum electricity cost savings — two critical directions of research we contribute to, in this dissertation.

In the first part of the dissertation, we focus on developing EV charging infrastructure sizing solutions — to assist building owners in making a quick and informed choice for different ‘smart’/‘dumb’ and unidirectional/bidirectional EV charging strategies (V0G/V1G/V2G). We first analyzed the impact of an idealized EV commuter fleet workplace charging on commercial building electricity costs following the installation of a variable number of EV charging stations by leveraging an economic optimization model. Next, we developed accurate analytical expressions to estimate the optimal EV charging behavior and benefits even without economic optimization using the exogenous model inputs.

In the second part of the dissertation, we first focus on developing application-agnostic, computationally inexpensive, real-time model predictive control (MPC) algorithms with provable guarantees. Here, we developed an adaptive relaxation-based stochastic MPC framework for generic discrete linear time invariant systems with provable nonconservative chance constraint satisfaction in closed-loop. Next, we proposed an economic MPC formulation for generic deterministic discrete non-linear time varying systems, with provable no-worse closed-loop asymptotic economic cost guarantees as compared to any arbitrary solution of the system under the same constraints, known only until the current time-step. Second, we demonstrated that both our proposed methods, when implemented for a real-life microgrid with BESS, VRE generation and load demand, shows superior electricity cost savings as compared to the traditional and state-of-the-art methods.

Chapter 1

Introduction

Recently, there has been a huge thrust to integrate variable renewable energy sources (VRES), such as wind and PV generators, in electricity grids to produce cleaner power. However, power generation from VRES are intermittent in nature and depend upon the weather conditions as well as the location where these sources are placed. The intermittency of VRES can potentially lead to power imbalance in the electric grid and, therefore, affects grid stability [1].

Dispatchable energy resources like electric vehicles (EVs) and battery energy storage systems (BESS) can be used to minimize power fluctuations caused by integrating VRES into the grid [1]. Furthermore, BESS and EVs can be used for energy arbitrage, peak load shaving, and to provide ancillary services. The declining costs of BESS [2] and EVs (and their associated charging infrastructure) [3] is a major driving force behind their wide scale adoption in commercial microgrids (MG) [4], which can defer extensive grid upgrades. However, for commercial MG operators to avail the maximum benefits from the dispatchable energy resources, it is important to appropriately size them during installation, and once installed it is vital to optimally dispatch them in real-time to realize the maximum electricity cost savings.

The appropriate sizing and dispatch of EVs/BESS inherently lead to constrained optimization problems, wherein the constraints reflect the physical and design limitations of the system (such as maximum power capacity, state of charge update/bounds of the BESS/EVs, etc.). Although the objective of the constrained optimization problem can differ, a natural choice is economic optimization, where the goal is to minimize the actual electricity cost of the MG (i.e., the monthly electricity bill), thereby maximizing electricity cost savings. Control algorithms developed based on such constrained economic optimization problems can be leveraged to optimally dispatch BESS/EVs, with model predictive controllers (MPC) being a popular choice. A MPC with an economic objective function is referred to as economic MPC (EMPC). Henceforth, we will use the abbreviation MPC for both model predictive control and model predictive controllers, wherever appropriate.

Despite the growing integration of dispatchable energy resources like EVs and BESS in MGs, there remain several open challenges that hinder their full economic potential. Broadly, these challenges can be categorized into three interrelated areas. First, while there has been extensive research on the benefits of EV charging and discharging strategies (such as V0G, V1G, and V2G/V2B), the impact of these strategies on commercial building electricity costs, especially in the presence of demand charges,[1] remains underexplored. Most existing studies evaluate cost savings over short durations and often overlook demand charges, which can constitute a significant fraction (30 – 70 %) of monthly electricity bills for commercial and industrial consumers. As a result, there is a critical need for long-term, realistic analyses of smart EV charging strategies that explicitly incorporate demand charges into the economic optimization framework. Moreover, there is also a need for developing an analytical framework to estimate the optimal EV charging behavior, benefits and metrics, even without economic optimization using the exogenous model

[1]Electricity costs incurred by a commercial building/MG to the utility involve time-of-use energy charges and demand charges. Energy charges ($/kWh) are incurred based on the volumetric import of electricity from the grid, while demand charges ($/kW) are incurred based on the maximum load import from the grid over the month. Two distinct time-of-use demand charges are used: one based on maximum grid imports for the whole month called non-coincident demand peak (NCDP), added on top of maximum grid import between 16:00 – 21:00 h of all days of the month, called on-peak demand peak (OPDP). The demand charges associated with NCDP and OPDP are called non-coincident demand charges (NCDC), and on-peak demand charges (OPDC) respectively.

inputs — which can assist building owners in making a quick and informed choice about EV charging infrastructure sizing solutions worldwide.

Second, although stochastic MPC (SMPC) has emerged as a powerful framework for real-time dispatch of BESS under forecast uncertainty, many existing SMPC formulations are either overly conservative or computationally intensive, or require a-priori knowledge of uncertainty distribution/statistics/samples — limiting their practical application. There is thus a pressing need for computationally tractable, nonconservative SMPC algorithms with provable guarantees that do not rely on strong assumptions about the uncertainty.

Third, EMPC is gaining popularity as a tool to minimize electricity costs in real time by optimally dispatching BESS and other controllable resources. However, most existing EMPC literature focuses on asymptotic stability and performance with respect to known steady-state or periodic reference trajectories, which may not exist or be known in economic MG dispatch applications. Moreover, the inclusion of demand charges in the electricity cost objective introduces time-scale mismatches and violates standard assumptions (such as the principle of optimality), thereby complicating the theoretical guarantees. Therefore, EMPC formulations that provide performance guarantees with respect to arbitrary, non-fixed reference trajectories (which may be generated online by MG operators with some rule-of-thumb or other optimization methods which can outperform the standard EMPC with respect to closed-loop economic performance), particularly under time-varying system dynamics, are of substantial practical value.

To address these gaps, this dissertation is organized into two major parts, each targeting one or more of the aforementioned challenges. The first part examines the impact of different EV charging strategies, and infrastructure sizing solutions on electricity costs in commercial MGs, with special attention to demand charges and development of an analytical framework to accurately estimate optimal EV charging benefits and metrics. The second part develops and analyzes novel MPC algorithms for economic dispatch of BESS, under both uncertainty (via adaptive SMPC) and deterministic forecasts (via

EMPC). In each case, we aim to bridge theoretical advances with practical implementation challenges, enabling improved operational decision-making for MG operators.

1.1 Organization of the dissertation

This chapter (Chapter 1) introduces the problems we attempt to solve in this dissertation, discusses the relevant literature, and outlines the contributions of the dissertation. Chapter 2 introduces the notations that are common to all the works in the dissertation and mathematical preliminaries. Chapter 3 constitutes the first part of the dissertation focusing on EV charging effects on building electricity costs and appropriate sizing of EV charging infrastructure. Chapters 4 and 5 constitute the second part of the dissertation, focusing on the development of computationally inexpensive, real-time MPC algorithms with provable guarantees. Chapter 4 focuses on the development of an adaptive relaxation-based provably nonconservative chance constrained SMPC framework for generic discrete LTI systems. Chapter 5 focuses on the development of an EMPC formulation for generic deterministic discrete non-linear time varying systems with economic performance guarantees. Finally, Chapter 6 summarizes the conclusions from the dissertation and suggests directions for future work.

1.2 Literature review

1.2.1 Effects of EV charging/discharging on commercial building electricity costs

The use of electric vehicles (EVs) has significantly increased in the past decade and is projected to increase even more in the coming decade. The push toward the increasing market penetration of EVs has also been complemented by the strong growth of EV charging infrastructure along interstate highways, at workplaces, and at public parking lots [5]. There are three popular types of EV charging: V0G ("dumb" charging at constant full power from when the vehicles are plugged in until they are unplugged or full, whichever occurs first), V1G (unidirectional, grid-to-vehicle variable smart charging), and V2G (bidirectional, grid-to-vehicle, and vehicle-to-grid variable smart charging). V2B (bidirectional, grid-to-vehicle, and vehicle-to-building variable smart charging) is a variant of V2G, where the EVs, instead of feeding back energy directly to the grid, reduce the building's net load peak (grid import). Smart charging optimally charges and discharges (in the case of V2G/V2B) the EVs to provide economic benefit to EV owners, MG/EV charging station operators, and/or grid operators [6].

V2G chargers are gaining importance and making a stronger business case because of value streams associated with operational flexibility as compared to V1G chargers. While the EV charging literature is vast, the following literature in this paragraph only discusses studies that incorporate V2G charging. Alusio et al. [6] described an optimal day ahead operating strategy for MGs with V2G EVs to minimize operating costs based on forecasted load demand and renewable generation. The authors used time-of-use energy rates for the analysis and demonstrated the optimization algorithm on a test MG. In [7], the authors carried out a techno-economic analysis of V2G in the Indonesian power grid considering 3 different tariffs: i) a fixed tariff which provided flat charging and discharging energy rates to EV owners, ii) a "natural" tariff which provided energy rates based on the electric generating resources, for example, geothermal, hydro, coal etc., iii) a demand response tariff which provided energy rates and incentives depending upon the amount of electricity supply and demand, i.e. the demand response tariff will increase when demand is high. The authors reported the environmental and economic advantages of incorporating V2G charging for both EV owners and utility companies. The authors in [8] presented an adjustable robust optimization scheduling model for a MG with renewable energy generation, V2G EVs, and time-of-use energy rates. Results showed improvements in the operational stability and economic performance of the MG, such as increasing the wind energy utilization, reducing peak-loads, and increasing minimum loads. Kiaee et al. [9] developed a V2G simulator to undertake power flow analyses to compare the total charging cost of EVs with and without V2G technology within a power system consisting of 5,000 EVs using time-of-use energy rates. The control algorithm took advantage of arbitrage, while considering the EV capacity, the SOC, vehicle movement within the system and the requirements of drivers and power system operators. V2G charging achieved a 13.6% reduction in charging cost. A review paper [10] sheds light on various optimization algorithms used for EV scheduling for grid integration.

Schuller et al. [11] compared the weekly charging cost of EVs owned by different socio-economic groups by implementing V0G, V1G, and V2G charging strategies for residential charging with a time-of-use energy rate. Employees and retirees are the two socio-economic groups with the greatest contrast in driving behavior, driving 228 km and 119 km on average per week, respectively. For employees, weekly average costs are 32% and 45% less for V1G and V2G charging respectively as compared to V0G. For retirees, V1G and V2G charging saved about 51% and 62% respectively as compared to V0G. Datta et al. [12] proposed a charging/discharging strategy according to the price of electricity during off and on peak hours (i.e., time-of-use energy rates), and illustrated that the monthly cost savings associated with V2B is 11.6% as compared to V1G. Zhou et al. [13] optimized the provision of ancillary services to bring economic benefits to V2G EV owners in China under time-of-use energy rates. The works in [14, 15] further shed light on the capability of V2G EVs to shift charging from peak to off peak periods depending on time of use energy rates and demand response programs.

None of the studies discussed in the above literature review considered the effect of demand charges while optimizing V2G/V2B EV charge scheduling, even though demand charges are a significant portion (30 – 70%) of the electricity bill for commercial and industrial customers [16]. Very few studies directly deal with demand charges for EV charging [17]. Zhang et al. [17] proposed a V1G charging scheme for demand charge reductions, with the EV charging stations installed at four locations: large and small retail, recreation area, and workplace. The authors used real world Level 2 EV charging data for the analyses, where for the large retail (which is least flexible due to shorter charging events and higher EV mobility), 80% of the charging events were shorter than 3 hours. The proposed V1G smart charging scheme reduced monthly demand charges for large retail by 20 – 35% as compared to no-control charging for 30% EV demand penetration level, which is the percentage of EV energy demand with respect to the original (pre-EV) energy demand of the building. The authors in [18, 19] considered demand charges for electric bus V1G fast charging stations but charging schedules of public buses differ from passenger EVs with bus driving schedules being longer and rigid and energy requirements larger [18], and thus public bus charging is a unique problem [19]. Additionally, to the best of the authors' knowledge, only one previous work [11] presented a direct economic performance comparison of both V2G and V1G charging. Also, no previous work incorporated demand charges for commuter V2G/V2B EVs which the present work considers. Although V2G/V2B scheduling strategies for economic cost optimization for time-of-use energy rates have been investigated previously, there are very few works on the long-term economic impact of smart charging. Most of the literature present case studies over a single day, week, or month to prove the efficacy of the schemes conceptually, as summarized in Table 1.1. However, at least year-long studies are needed to capture seasonal variations in building loads, EV demand, and tariffs.

1.2.2 Nonconservative chance constrained SMPC

MPC based scheduling algorithms that include grid constraints can be used to optimally schedule BESS dispatch in MGs. In MPC, an objective function (for example, electricity cost) is minimized to compute a sequence of optimal control inputs (i.e., BESS dispatch) based on forecasts of load and VRES, internal plant model (i.e., MG operational constraints), and initial system state (BESS state of charge) over a finite prediction horizon. The prediction horizon is divided into a specific number of time-steps. For example, an

Table 1.1. Simulation duration of other studies in the literature

Work	Duration
Alusio et al. [6]	1 day
Shi et al. [8]	1 day
Zhou et al. [13]	1 day
Onishi et al. [14]	1 day
Zhang et al. [17]	1 day
Kiaee et al. [9]	5 weekdays
Schuller et al. [11]	7 days/1 week
Datta et al. [12]	30 days/1 month
Huda et al. [7]	1 year
Our work (Described later in Chapter 3)	1 year
Li et al. [15]	10 years

MPC can minimize an objective function to predict a sequence of optimal control inputs based on day-ahead (24 h) forecasts, with the 24 h prediction horizon being divided into 96 15-minute time-steps. During execution, only the first computed control input of the prediction horizon is implemented, after which the system state evolves as it moves to the next time-step. Thereafter, forecasts are updated, and the MPC optimization is solved again from the new initial system state and time-step. Receding horizon MPC are popular in VRE based systems, which are run for the same specified horizon (such as 24 h) at every time-step [1].

However, uncertainty in forecasts can significantly reduce performance and should be taken into account when formulating MPCs. Classical open-loop min-max formulation based robust MPC can be used to factor in uncertainty but it leads to over-conservative solutions which may not be economical from an operational perspective [20]. Other variations of robust MPC such as closed-loop min-max formulation (commonly known as "Feedback MPC") suffer from prohibitive complexity [20]. Tube-based MPC requires specification of a bounded uncertainty set a-priori [21] (a problem in common with robust MPC), which may be difficult to specify nonconservatively for a complex practical system such as a VRES integrated MG, which involves a variety of forecasts. An over-conservative uncertainty set negatively impacts economical system performance.

SMPC methods based on chance constraints strike a trade off between economic operation and full constraint satisfaction [21]. Chance constraints allow for the MPC to operate in a more economical way by respecting a maximum probability of constraint violation. The superior economic performance, lower complexity, and weaker assumption requirements of chance constrained SMPC is desirable for BESS operation in VRES intensive MGs, especially under uncertainty in VRES and load forecasts, and is thus the primary focus of our work.

Chance constrained SMPC algorithms have found applications in problems involving building climate control [21, 22, 23, 24], optimal power flow [25], and optimal MG dispatch [26, 27, 28, 29, 30, 31, 32, 33, 34, 35]. Chance-constrained SMPC problems are solved by converting them into an approximate deterministic form. If the uncertainties are Gaussian, or follow other known distributions [36, 37], standard procedures exist to convert the stochastic problem into a deterministic one. However, in practical scenarios such as VRES and load forecasts, the uncertainty distributions, and additionally, uncertainty statistics (moments like mean, variance, skewness, etc.) may be unknown and can vary with time (i.e., seasonally/yearly). Other methods of reformulating the SMPC problem into a deterministic one, such as using Chebyshev inequalities [38] require a-priori knowledge about the uncertainty statistics (mean and covariance), while using Chernoff bounds suffer from high conservatism [21]. Sampling based approaches [39, 40] suffer from high computational demand and may require a prohibitive number of samples [21].

Chance constraints are generally enforced pointwise-in-time within an MPC prediction horizon, without including past behavior of the system, which can also lead to over-conservativeness (i.e., less than desired constraint violations) in closed-loop [22, 24]. However, reducing over-conservativeness is of paramount importance for MG operators to reduce electricity costs. Thus, in our work we re-interpret the pointwise-in-time chance constraints as time-average of violations (or time-average of some loss function of violations) in closed-loop similar to [21, 22, 24, 41, 42], and first focus our literature review specifically on such online chance constrained SMPC methods with theoretical advancements. The re-interpretation keeps the spirit of occasional constraint violations of the original chance constraint [22] while keeping memory of past behavior of the system to aid in reducing over-conservativeness in closed-loop.

Review of works focused on theoretical advancements

The work in [24] adaptively relaxed and tightened the MPC state constraints online aided by the amount of violations quantified by a loss function empirically weighted averaged over time. The authors defined a family of stochastic robust control invariant (SRCI) sets for implementing their control online and proved that the empirical weighted average loss is bounded either in expected value or robustly with probability 1, and derived bounds on the convergence time. However, drawbacks of the work include high computational cost to parameterize the SRCI sets, and a-priori knowledge about the distribution/statistics of the uncertainty.

The authors in [41] adaptively relaxed the MPC state constraints online based on the time-average of (i) the number of constraint violations in the first method, and (ii) a loss metric based on a convex loss function of constraint violations in the other method. Instead of providing asymptotic bounds on constraint violations as done in previous works like [21, 22], the authors provided stronger robust bounds in closed-loop over finite time periods. A practical limitation of [41] for our application (economic MG dispatch) is the assumption of an objective function that is composed of stage costs with quadratic penalties on predicted control inputs and state deviations from an a-priori defined robust positively invariant target set. Construction of a nonconservative robust positively invariant target state set is difficult. Additionally, electricity costs due to grid imports in a MG with BESS cannot be expressed by stage costs with quadratic penalties on control inputs and state deviations, because economic stage costs are not necessarily positive definite with respect to the target set of states and/or control inputs [43].[2] Moreover, the uncertainty is incorporated by bounding the predicted states in state tubes which require a-priori specification of the uncertainty set, and the computation time is similar to a corresponding robust MPC problem which is more expensive than the nominal MPC.

The authors in [21, 22, 42] adaptively tightened the state constraints online during MPC computations: (i) using an update rule based on the time-average of past state constraint violations in [21, 22], and (ii) by iteratively employing a data-driven Gaussian process binary regression based approach depending on the observed state constraint violations in the training data in [42]. In [22], using stochastic approximation, the authors also proved the convergence of the time-average of constraint violations in probability to the allowable 'least conservative' level. A few limitations of [22] are the a-priori assumption of the uncertainty distribution, and the strong assumption of terminal stability region of the state in closed-loop, which is unrealistic for economic MG dispatch using BESS. While [42] relaxes the requirement of a-priori knowledge of the uncertainty distribution, iteratively learning the final optimal tightening parameter is data-intensive. The entire solution framework exhibits significantly more computation cost for satisfying the chance constraints in the long run as compared to the nominal MPC. For our application, [42] may be unable to perform economically or may cause significant violation of the chance constraints if the underlying uncertainty distribution changes with time (as the final optimal tightening parameter is learned from past data), which is undesirable for economic MG operation.

Some of the limitations of [22, 24, 41, 42] are avoided by [21] which can be applied to systems with unknown uncertainty distribution/statistics. Also, [21] does not need the assumptions of terminal stability of the state and the type of the objective function (except convexity assumptions), and the implementation of the SMPC is computationally

[2]Economic MG dispatch involves usage of the electricity cost function directly as the objective function of the MPC.

inexpensive and has similar computation cost as that of a nominal MPC. The above mentioned properties make the work in [21] ideal for economic MG dispatch, and forms the primary reference on which we develop our work.

In [21], the authors developed an adaptive state constraint tightening rule that allows the time-average of violations of the system to converge to the maximum allowable violation probability in closed-loop under an ideal control policy assumption (which may be unmet for practical implementation). However, as clarified by the authors, the convergence was argued intuitively without rigorous proof. Also, despite its advantages, [21] is still not robust to significant violation of chance constraints under time varying uncertainty distribution.

Review of works focused on economic MG dispatch

While significant theoretical advancements have been made to develop SMPC with varying degrees of simplifying assumptions, computational cost, and ability to avoid over-conservativeness in closed-loop chance constraint satisfaction, there exists a gap in the literature of exploiting these nonconservative methods for economic MG dispatch under uncertainty. Some recent applied works involving economic MG dispatch in VRES intensive grids with chance constraints are explored in [26, 27, 28, 29, 30, 31, 32, 33, 34].

The authors in [26] minimized the operational cost of a VRE integrated MG with flexible EV charging that included chance constraints on EV dispatch power and state of charge (SOC). Flexible EV charging was used for alleviating real-time load and VRE forecast uncertainties. The work in [27] presented an optimal VRE integrated MG scheduling strategy that minimized operational cost subject to chance constraints on islanding capability from the main grid. Islanding capability means that a MG maintains enough spinning reserve (both up and down) to meet local demand and accommodate local VRE after instantaneously disconnecting from the main grid. The authors in [29] presented a SMPC for demand response (DR) for a home energy management system consisting of a PV array, HVAC, BESS, and uncontrollable loads. The controller minimized the PV curtailment and grid import costs with chance constraints ensuring that both DR and thermal comfort conditions are satisfied with a high probability under uncertainties in PV and outdoor temperature forecasts. The authors in [30] proposed a SMPC to minimize grid import costs for a residential DC MG consisting of a PV array, fuel cells, BESS, and load. The MG power exchange with the main grid was reformulated into chance constraints. The authors in [32] presented a day-ahead scheduling framework for multiple MGs under wind, solar, and load forecast uncertainties. The algorithm minimizes the MG operational and emissions costs with chance constraints being considered for the MG power balance. The authors in [33] proposed an optimal VRE integrated MG scheduling model that minimizes MG operational and emissions cost with chance constraints on reserve power constraints.

The authors in [28] proposed a two stage MG scheduling model that minimized operational cost under load and VRE uncertainties. In the day-ahead stage, the uncertainties are modeled using historical data based on a Wasserstein ambiguity set (a ball which contains all possible uncertainty distributions centred at the reference distribution) and a dispatch schedule is generated by solving a distributionally robust chance constrained (DRCC) optimization. In the real-time stage, the deviation of the dispatch schedule from the day-ahead schedule is minimized in an MPC subject to MG constraints. The authors in [31] proposed an evolutionary algorithm that solves a distributionally robust joint chance constrained problem for networked DC MGs. The algorithm optimizes MG operational cost under uncertain VRE forecasts, which is modeled by ambiguity sets from historical data. The authors in [34] presented a non-parametric chance constrained model for day ahead MG scheduling without any a-priori assumption about uncertainty distribution. The algorithm minimizes MG operational costs with chance constraints on the MG electric and thermal power balance, and virtual solar+BESS generator smoothness. The authors used adaptive kernel density estimation to estimate the nonparametric uncertainty distribution for VRE from historical data, and adjusted the confidence levels according to estimation uncertainties to ensure constraint satisfaction within predefined confidence levels.

None of the works [26, 27, 28, 29, 30, 31, 32, 33, 34] considered demand charges in their electricity cost (see significance of demand charges in footnote 1). The work in [26] required extra steps to generate scenarios of uncertainty at every time-step for the MPC prediction horizon and considered the scenarios to be Gaussian. The works [27, 29, 30, 32, 33] considered the uncertainties to be Gaussian or other commonly known distributions, which significantly limits the practical application of these studies. Additionally, the approaches in [28, 31, 34] are data-intensive and the performance is substantially influenced by the quality and volume of historical data available.

To tackle the aforementioned problems, [35] presented an online adaptive SMPC model inspired by [21]. The authors in [35] minimized the VRES integrated MG operating cost, and satisfied chance constraints on states (BESS SOC) in closed-loop without making any assumption about the probability distribution or statistics of the uncertainty. To further reduce over-conservativeness, [35] employed online adaptive constraint relaxation in the nominal MPC. However, the online adaptive constraint relaxation rules used in [35] are based on intuition having no convergence guarantees or theoretical analyses, and both the works are application specific. From an economic MG dispatch perspective, [35] did not include demand charges. The authors in [35] used sample historical data of uncertainties for initial constraint relaxation which is an added requirement. Additionally, [35] considered aggregate constraint violations, without any preference for the time when violations should occur. For economic MG dispatch with demand charges, it becomes critical, if necessary, to preferentially be able to violate BESS state constraints during a predefined on-peak period from 16:00 to 21:00 h, to reduce grid import power peaks, as OPDC are charged on top of NCDC.

1.2.3 Deterministic EMPC with a reference trajectory

EMPC has recently gained popularity in real-time optimal control of MGs with high penetration of VRE. Instead of stabilizing a reference trajectory/state in the objective function like a Tracking MPC, EMPC optimizes the actual economic performance over the prediction horizon. As MG operating costs, i.e., electricity costs paid by the MG to the utility, is one of the primary control objectives of MG operators, EMPC is particularly attractive. However, the electricity cost function is generally complex involving both time-of-use energy and demand charge terms [44].

Demand charges can cause a considerable discrepancy between the predicted open-loop solutions in MPC and the actual closed-loop outcomes, even under nominal conditions. This occurs because naively incorporating the demand charge term into the objective function violates the principle of optimality, as noted in [45]. The reason is, once the peak demand has passed, the optimizer may significantly adjust its plan to accommodate for what has now become the new peak. Remembering the previously reached closed-loop peak demand by augmenting the state variables in future open-loop predictions will restore the principle of optimality [46].

The prediction horizon of EMPC is typically $24-48$ h because load and VRE generation forecasts are only accurate one or two days ahead. However, demand charges are applied on a monthly basis. Due to this mismatch in timescales, there can be a significant difference between the performance of an infinite-horizon optimal control problem[3] and closed-loop EMPC, when the objective function is the exact monthly electricity cost (for the infinite horizon control problem), or some approximation of it (for the finite horizon EMPC). This is because an infinite horizon optimal control problem will adjust its prior grid import to incorporate future (unavoidable) demand peaks, which the finite horizon EMPC problem would be oblivious to, suggesting a possible scope for performance improvement

[3]In this case, the infinite horizon optimal control problem would be a one-shot optimization of monthly electricity cost using perfect forecast data over the entire month.

during real-time operation. Demand charge rates are also typically $200 - 300$ times per unit than energy charge rates [44]. Thus, MG operators with dispatchable resources like battery energy storage systems (BESS) and electric vehicles (EVs) can leverage smart charging/discharging to substantially reduce their monthly electricity cost, for which EMPC algorithms with performance guarantees are of paramount importance. Of particular importance to MG operators is the possible performance improvement over any arbitrary non-fixed (i.e., online) reference trajectory[4] known to the MG operator. Development of EMPC methods with such performance guarantees is the primary motivation for our study.

The recent literature on EMPC methods is extensive, and focuses both on asymptotic performance and stability guarantees, generally with respect to an optimal economic steady state [43, 47, 48]. Studies such as [43, 47] have also looked into asymptotic stability with respect to an a-priori known optimal periodic trajectory. However, asymptotic stability guarantees require strict dissipativity assumptions (see Definitions 2.6 and 2.7) with respect to an optimal economic steady state/trajectory [43, 47, 48, 49], which is difficult to satisfy in practice, and is of less importance than economic performance [50, 51], especially for MG operators.

Thus, in our work we focus solely on studies with asymptotic performance guarantees for various EMPC formulations, as assumptions required for asymptotic performance guarantees are mild, and are more useful for MG operators as it can be practically guaranteed in a wide range of situations. The asymptotic performance guarantees for EMPC with the existence of an optimal economic steady state or optimal periodic trajectory as explored in [43, 47, 48], cannot be straightforwardly extended to EMPC for MGs because of: (i) difficulty of expressing the demand charge term in the electricity cost of MGs

[4]A non-fixed reference trajectory as opposed to a fixed trajectory [45], is one which is not known a-priori for all times under consideration, but is continuously regenerated at each time-step by the means of some rule-of-thumb method or online optimization method, and thus is only known until the current time-step.

in additive stage cost terms, which is a prerequisite for the theoretical guarantee; (ii) non-usefulness and moreover, possible non-existence of an optimal economic steady state and optimal periodic trajectory respectively in MG dispatch, and more generally for generic time-varying non-linear systems. An optimal economic steady state is not useful for MG dispatch as directly minimizing economics usually leads to non-steady operating regimes. For example, in a MG, the BESS (where BESS SOC is the state) is expected to operate in a non-steady region, constantly charging and discharging to reduce costs. Having better economic performance with respect to a case where the state is steady [43, 47, 48] is trivial, and thus not useful for BESS dispatch. The existence and a-priori knowledge of an optimal periodic trajectory for a MG is impractical with high temporal (i.e., daily or seasonal) variability of load and VRE, where forecasts are known typically only 24 h ahead [44].

While the studies [43, 47, 48] considered stage costs that are time-invariant, the authors in [52, 53] extended the former works to prove asymptotic performance guarantees for stage costs that are time varying but are either periodic or fulfills certain average assumptions. Stage cost functions that are periodic or the existence and a-priori knowledge of an averaged stage cost function are not guaranteed and are likely to be violated for MGs, especially in the case of temporal variability of energy and demand charge rates which are becoming more prevalent in VRE-dominated grids with real-time electricity tariffs which are non-periodic, and typically known only 24 h ahead [54]. In addition, the studies [52, 53] like [43, 47, 48] still prove asymptotic performance guarantees with respect to an a-priori known optimal periodic reference trajectory, retaining its restrictiveness.

Grüne [50] provided approximate optimal performance guarantees for both the infinite-horizon and transient (i.e., finite-time) closed-loop operation of a receding horizon EMPC. The result is powerful and is achieved without setting a terminal constraint to the EMPC contrary to [43, 47, 48, 52, 53], which may increase the feasible region of operation of the controller. However, the sufficient conditions provided in [50] for ensuring the performance guarantees require strict dissipativity assumptions and controllability conditions implying optimal steady state operation (which further implies the turnpike property), which as discussed before is unrealistic for MGs and economically oriented non-linear systems in general.

None of the above works [43, 47, 48, 50, 52, 53] consider the system dynamics to be time-varying making it unsuitable for handling demand charges in MGs, as certain demand charges are based on the time-of-day when peaks are reached. The authors in [55] extended the work in [50] to encompass time-varying system dynamics. The authors used the notion of time-varying turnpike property and continuity of value function to provide a bound of the deviation of the closed-loop cost of the finite horizon EMPC from the infinite horizon optimal trajectory which is assumed to exist but is unknown. The time-varying turnpike property assumption guaranteed that the open-loop solution of the finite horizon EMPC is close to the optimal trajectory most of the time, which the authors conjectured would arise from restrictive dissipativity and controllability conditions. For MGs with demand charges, an infinite horizon optimal trajectory can be significantly different from the finite horizon open-loop EMPC trajectory which is blind to any information about the optimal trajectory, as the optimal trajectory will adjust the BESS dispatch to the demand peak (to be reached) later, which the finite horizon EMPC would not be aware of, and is thus likely to violate the turnpike property.

More recently, the authors in [45] provided performance guarantees for a generic determinsitic non-linear time-varying system with respect to an arbitrary reference trajectory known a-priori for all times under consideration. The authors also showed the efficacy of their method for optimal BESS dispatch for demand charge reduction in an MG through a case study where an optimal periodic reference trajectory was assumed. However, a-priori knowledge of a reference trajectory for all times is impractical for most realistic systems involving forecasts. This is because a MG always needs to have power balance with the main grid, for which forecasted load and VRE generation (if applicable) is necessary, which generally is known only $24-48$ h ahead. Also, while the case study provided deep insights into the method's efficacy, the demand charge structure (assumed as the maximum energy charge rate of the month, where in general it is $200-300$ times the energy charge rate) underpredicts the penalty for peak demand, requiring further realistic analyses and case studies to encourage implementation by MG operators.

1.3 Work objectives and contributions of the dissertation

1.3.1 Effects of EV charging/discharging on commercial building electricity costs

In Chapter 3, we analyze workplace V2B, V1G, and V0G charging with real load profiles from 14 commercial buildings, by leveraging an economic optimization model. The objective function minimizes the building monthly electricity bill consisting of time-of-use energy and demand charges. One objective of this study is to report the optimal number of V2B charging stations to be installed at a particular building such that the original (pre-EV) operating electricity bill is not exceeded. This study also compares the electricity costs for 14 buildings under V0G, V1G, and V2B charging strategies. Sensitivity analyses elucidate the effects of varying arrival and final SOCs on the total electricity bill. EV charging stations at commercial buildings are generally added "behind the meter" such that the energy consumed is lumped with the building energy consumption and adds to the commercial building owners' electricity costs. Commercial building owners typically either provide free charging to their employees or they contract with a third-party operator who collects charging fees from the EV owners. Charging fees can be structured such that charging (and discharging) flexibility is rewarded. Therefore, while the total electricity costs analyzed in this work only directly apply to commercial building owners, some of the savings can be passed on to EV owners.

The contributions of our work are as follows:

1. Realistic demand charges, which vary according to the time of the day and summer/winter season have been considered in the electricity bill. Zhang et al. [17] considers demand charges whose rate varies according to the tier of demand (first 35 kW costs \$0/kW, next 115 kW costs \$5.72/kW and the remaining costs \$10.97/kW), but not according to time-of-day or season-wise. Zhang et al. [17] also only considers V1G smart charging (no V2G/V2B analysis), and only for one EV demand penetration level.

2. Two case studies are presented to quantify the electricity bill savings obtained by using V2G/V2B over V1G/V0G charging at commercial buildings: (i) A year-long case study, with variable number of EVs, using two daily EV layover intervals that are realistic, but uniform across the fleet; (ii) A 5 day case study which is representative of a monthly analysis, based on historical EV charging data. The works in [7, 15] are the only other similar studies that considers similar (or longer) time duration. Huda et al. [7] presents a year-long analysis of only V2G EV charging to show its effect on electricity cost reduction, but for a predefined fixed number (1 million) of V2G EVs. Li et al. [15] presents a ten year analysis but also only considering V2G EVs. The motivation of [15] is also different, where V2G user and power grid company economic benefits (cost savings) are analyzed solely as a function of discharging power of the V2G EVs at the peaks (peak shaving load). Our study evaluates the electricity bill savings for commercial buildings incorporating V2B charging as a function of number of EV charging stations, and additionally compares the V2B electricity costs to V1G and V0G charging electricity costs.

3. The year-long analysis predicts the optimum number of V2B charging stations to be installed at a building, so as not to exceed the original (pre-EV) electricity bill.

4. We derived and validated approximate analytical expressions for the total electricity costs (original building + optimal EV charging) as a function of (pre-EV) original

building load data, typical EV charging session data, and electricity tariff data. This is the first time that such equations have been derived. The equations allow for quick and accurate estimation of optimal EV charging behavior and benefits worldwide.

1.3.2 Nonconservative chance constrained SMPC

In Chapter 4, we extend the work in [21, 35] to present an online adaptive relaxation-based nonconservative SMPC framework in a generic discrete LTI setting with additional convergence properties and proofs, related theoretical analyses, and additional case studies. The proposed online adaptive SMPC (OA-SMPC) minimizes a generic convex cost function over a finite receding horizon, subject to hard input constraints and chance constraints on states. After presenting the theoretical results of the OA-SMPC, a case study is presented for a grid-connected MG operation with PV, load, and BESS using realistic data for a full year of operation in an economic MPC (EMPC) framework. The performance of the OA-SMPC is compared with a traditional EMPC without chance constraints, and a state-of-the-art approach from the literature with chance constraints having similar computational cost [21]. Simulations performed on realistic load, PV and tariff forecasts, and actual data an at the Port of San Diego MG for the year 2019 show that the proposed OA-SMPC outperforms both the traditional and literature inspired SMPC with respect to yearly electricity costs.

The contributions of the present work are as follows:

1. To the best of the author's knowledge, our work's adaptive state constraint relaxation framework is limited in the literature as compared to the more common adaptive state constraint tightening. Under the novel adaptive relaxation rule of our work, it is proven that the time-average of the constraint violations asymptotically converges to the maximum allowable violation probability under an ideal control policy assumption similar to [21]. However, a rigorous proof is provided here which was not provided in [21]. Also, for practical implementation (i.e., without the simplifying ideal control

policy assumption), while the proposed method cannot guarantee the aforementioned convergence, it still encourages it.

2. We also prove that the the time-average of the constraint violations exhibits martingale-like behavior asymptotically for practical implementation.

3. Our work does not require either any a-priori assumption about the probability distribution of the uncertainty set or its statistics, or sample uncertainties from historical data. Our work is also robust to significant violation of chance constraints under time-varying uncertainty distribution for practical implementation, provided an additional post-processing step is incorporated.

4. Our work incorporates operational adjustments in the online adaptive relaxation rule to account for temporal preference in state constraint violation, which is critical for economic MG dispatch. Additionally, unlike the methods in [21, 35], our method prevents excessive overcharging/overdischarging of the BESS to correct for large forecast uncertainties in real-time by the post-processing step, which otherwise might harm the BESS and leave the MG vulnerable for future demand peaks.

5. The majority of the earlier works for chance constrained SMPC based economic MG dispatch [27, 28, 29, 31, 32, 33, 34] presented results over a short time (24 h), or one or two months [30]. However, for MG operators, it is important to have at-least year-long studies to determine how the algorithm performs under realistic seasonal variations in loads, VRES generation, and forecasts, a gap which our work fills.

1.3.3 Deterministic EMPC with a reference trajectory

In Chapter 5, we generalize the result in [45] by proposing an EMPC framework for a generic deterministic non-linear time-varying system with asymptotic average performance (i.e., cost) guarantee of doing no-worse than any arbitrary reference trajectory which is known only until the current time-step. The proposed EMPC framework is then leveraged to solve an optimal MG dispatch problem with both energy and demand charges incorporating BESS losses. Simulations performed on realistic load, PV and tariff data at the Port of San Diego MG showed that even under finite-time (i.e., a month), the electricity costs for our proposed method is better than reference trajectories generated in a receding-horizon fashion by: (i) directly minimizing the electricity costs over the prediction horizon (usually $24-48$ h, being much smaller than a month); (ii) ideal reference tracking, which is developed from intuitive insights into the demand charge rate structure for MGs.

The contributions of our work are as follows:

1. The asymptotic average performance guarantee with respect to the arbitrary reference trajectory in our proposed work is proven under milder assumptions as opposed to [45], without a-priori knowledge of the reference trajectory for all times under consideration.

2. We converted the one-time demand charge component of MG monthly electricity costs into the additive stage cost structure of the proposed EMPC framework, and provided a generalized non-restrictive method (i.e., one that does not unnecessarily reduce the feasible state-control input set for the problem) to construct terminal regions, control laws and terminal cost functions under mild operational assumptions. The proposed method can be used to generate other variations of terminal regions, control laws and cost functions, which makes further improvement in finite-time performance possible while still retaining the same asymptotic guarantees.

3. With insights from realistic demand charge rate structure in MGs, we also proposed a framework to generate reference trajectories by using methods other than directly minimizing the economic costs over the prediction horizon (standard reference), which can lead to superior economic performance as compared to the standard reference in closed-loop. Thus, this work paves a possible pathway for further investigation into

methods which would lead to reduced MG monthly electricity costs, yet where the prediction horizon is much smaller than a month, with the goal being to get as close as possible to the (best-case) closed-loop electricity cost as (would be) derived from the infinite horizon optimal control problem.

1.3.4 Summary of major contributions

There are three works stemming out of this dissertation and their major contributions are summarized in Table 1.2.

Table 1.2. Summary of major contributions of the works stemming from this dissertation

Work	Major Contribution
Effects of number of EV charging/discharging on total electricity costs in commercial buildings with time-of-use energy and demand charges (Chapter 3)	Developed an accurate analytical framework to quantify optimal EV smart charging benefits without economic optimization using only exogenous inputs.
Adaptive relaxation-based nonconservative chance constrained SMPC (Chapter 4)	Developed a computationally inexpensive, real-time, adaptive relaxation-based provably nonconservative chance constrained SMPC algorithm for a generic discrete LTI system.
Deterministic EMPC with an online reference trajectory (Chapter 5)	Developed a computationally inexpensive, real-time EMPC formulation for a generic deterministic discrete non-linear time varying system with provably no-worse asymptotic economic cost guarantees with respect to any arbitrary reference trajectory known only until the current time-step.

Acknowledgements

This chapter, in part, is a reprint of the material as it appears in 'Effects of number of electric vehicles charging/discharging on total electricity costs in commercial buildings

with time-of-use energy and demand charges' authored by Avik Ghosh, Monica Zamora Zapata, Sushil Silwal, Adil Khurram, and Jan Kleissl, in the Journal of Renewable and Sustainable Energy, 2022; and 'Adaptive Chance Constrained MPC under Load and PV Forecast Uncertainties' authored by Avik Ghosh, Cristian Cortes-Aguirre, Yi-An Chen, Adil Khurram, and Jan Kleissl, in the 2023 IEEE PES Grid Edge Technologies Conference & Exposition; and 'Adaptive Relaxation-Based Nonconservative Chance Constrained Stochastic MPC' authored by Avik Ghosh, Cristian Cortes-Aguirre, Yi-An Chen, Adil Khurram, and Jan Kleissl, in the IEEE Transactions on Control Systems Technology, 2025; as well as 'Economic Model Predictive Control with a Non-Fixed Reference Trajectory for Optimal Microgrid Dispatch' authored by Avik Ghosh, Adil Khurram, Jan Kleissl, and Sonia Martínez, which is currently being prepared for submission for publication in Automatica. The dissertation author was the primary investigator and author of these papers.

Chapter 2

Mathematical preliminaries

In this chapter, we present the standard notations that are common to all the works unless mentioned otherwise in a specific chapter, and review some standard definitions from probability theory, real analysis and control theory that are employed in the dissertation.

2.1 Notations

The set of n-tuple of real numbers is denoted by $\mathbb{R}^n$. Positive and negative real number sets are denoted by $\mathbb{R}_{0+}$ and $\mathbb{R}_{0-}$, respectively. The set of natural numbers including 0 is denoted by $\mathbb{N}$. A set of consecutive natural numbers $\{i, i+1, \dots, j\}$ is denoted by $\mathbb{N}_i^j$. The n-tuple of zeros and ones is denoted by $\mathbb{0}^n$ and $\mathbb{1}^n$, respectively. States, control inputs and uncertainties are denoted by $x \in \mathbb{X} \subseteq R^n$, $u \in \mathbb{U} \subset \mathbb{R}^m$, and $w \in \mathbb{W} \subset \mathbb{R}^p$ respectively. The prediction horizon of the MPC is denoted by $N \in \mathbb{N}$. Actual states at time $t \in \mathbb{T} \subseteq \mathbb{N}$ are denoted by $x(t)$, while predicted states, obtained at t by MPC computation $k \in \mathbb{N}_1^N$ time-steps in the future are denoted by $x(t+k|t)$. Similarly, predicted control inputs over the MPC prediction horizon are denoted by $u(t+k|t)$, with $k \in \mathbb{N}_0^{N-1}$. An ordered collection of vectors (such as states) over the MPC prediction horizon obtained at time t is denoted by bold letters, $\mathbf{x}(t+1) := \Big(x(t+1|t), x(t+2|t), \dots, x(t+N|t)\Big)$, unless mentioned otherwise. For matrices A and B of equal dimensions, the operators $\{<, \leq, =, >, \geq\}$ hold component wise. The right inverse of a matrix $A \in \mathbb{R}^{m \times n}$ with rank $m < n$ is denoted by $A^\dagger$. The i^{th} row, and the element from the i^{th} row and j^{th} column of a matrix A is denoted by A_i and A_{ij} respectively, while the i^{th} element of a vector x is denoted by x_i, unless mentioned otherwise. A vector of the first $a \in \mathbb{N}$ elements of a vector x is denoted by $x_{1:a}$. The expected value of a random variable Z is denoted by $\mathbb{E}[Z]$. $|x|$ and $\|x\|$ denote the 1-norm and 2-norm respectively of a vector x. The 'logical NOT', and 'logical AND' operators are denoted by $\neg$ and $\wedge$ respectively. A function $\rho : \mathbb{R}_{\geq 0} \to \mathbb{R}_{\geq 0}$ is class $\mathscr{K}$ if it is continuous, strictly increasing, and zero at zero (i.e., $\rho(0) = 0$), and is class $\mathscr{K}_\infty$ if it is in class $\mathscr{K}$ and unbounded. A function $\rho : \mathbb{X} \to \mathbb{R}_{\geq 0}$ is positive definite with respect to some point $x_s \in \mathbb{X}$, if it is continuous, zero at zero, and $\rho(x) > 0$ for all $x \neq x_s$.

2.2 Standard definitions

Definition 2.1 (**Filtered probability space [56]**)**.** *A filtered probability space is defined by* $(\Omega, \mathscr{F}, \{\mathscr{F}_t\}, \mathbb{P})$*.* $(\Omega, \mathscr{F}, \mathbb{P})$ *is a probability triple with sample space* Ω*,* σ*-algebra (event space)* $\mathscr{F}$*, and probability measure* $\mathbb{P}$ *on* $(\Omega, \mathscr{F})$*.* $\mathscr{F}_t$ *is a filtration, which is an increasing family of sub* σ*-algebras of* $\mathscr{F}$ *such that* $\mathscr{F}_s \subseteq \mathscr{F}_t \subseteq \mathscr{F}$*,* $\forall t \geq s$*, where* $t, s \in \mathbb{T}$*.*

Definition 2.2 (**Almost surely [56]**)**.** *An event* $E \in \mathscr{F}$ *happens almost surely if* $\mathbb{P}(E) = 1$*. It is denoted by a.s.*

Definition 2.3 (**Adapted stochastic process [56]**)**.** *A stochastic process* $Z := (Z(t) : t > 0)$*, is called adapted to the filtration* $\{\mathscr{F}_t\}$ *if* $Z(t)$ *is* $\mathscr{F}_t$ *measurable* $\forall t$*.*

Definition 2.4 (**Supermartingale [56]**)**.** *A stochastic process* Z *is called a discrete-time supermartingale relative to* $(\{\mathscr{F}_t\}, \mathbb{P})$ *if it satisfies the following:*

(a) Z *is an adapted process,*

(b) $\mathbb{E}[|Z(t)|] < \infty$*,* $\forall t$*,*

(c) $\mathbb{E}[Z(t+1)|\mathscr{F}_t] \leq Z(t)$*, a.s.* $\forall t$*.*

A discrete-time martingale Z *relative to* $(\{\mathscr{F}_t\},\mathbb{P})$ *is defined similarly, with (c) replaced by* $\mathbb{E}[Z(t+1)|\mathscr{F}_t] = Z(t)$*, a.s.* $\forall t$*.*

Definition 2.5 (**Monotone convergence theorem for decreasing sequence**[**57**])**.** *Let* $X = (x_n : n \in \mathbb{N})$ *be a sequence of real numbers which is monotonically decreasing in the sense that* $x_{n+1} \leq x_n, \forall n$*, then the sequence converges if and only if it is bounded, and in which case* $\lim_{n\to\infty} x_n = \inf\{x_n\}$*.*

Definition 2.6 (**Dissipativity for time invariant systems** [**43, 47, 48, 49**])**.** *A non-linear discrete time-invariant system* $x^+ = f(x,u)$*, where* $x \in \mathbb{X}$ *is the state,* $u \in \mathbb{U}$ *is the control input and* $f : \mathbb{X}\times\mathbb{U} \to \mathbb{X}$*, is dissipative with respect to a supply rate* $s : \mathbb{X}\times\mathbb{U} \to \mathbb{R}$*, if there exists a storage function* $\lambda : \mathbb{X} \to \mathbb{R}$*, such that* $\lambda\left(f(x,u)\right) - \lambda(x) \leq s(x,u)$*,* $\forall (x,u) \in \mathbb{X}\times\mathbb{U}$ *[49]. The system is strictly dissipative with respect to the supply rate* s *and a steady state* $x_s \in \mathbb{X}$*, if in addition to the above there exists another* $\mathscr{K}_\infty$ *function* $\rho(\cdot)$*, such that* $\lambda\left(f(x,u)\right) - \lambda(x) \leq -\rho(|x-x_s|) + s(x,u)$*,* $\forall (x,u) \in \mathbb{X}\times\mathbb{U}$ *[49]. Sometimes,* $\rho(\cdot)$ *is also assumed to be a positive definite function [43, 48, 47]. Here,* $x^+ = f(x,u)$ *is equivalent to* $x(t+1) = f(x(t),u(t))$*.*

Definition 2.7 (**Dissipativity for time varying systems** [**45**])**.** *A non-linear discrete time varying system* $x(t+1) = f(x(t),u(t),t)$*, where* $x(t) \in \mathbb{X}(t)$ *is the state,* $u(t) \in \mathbb{U}(t)$ *is the control input and* $f : \mathbb{X}(t)\times\mathbb{U}(t)\times\mathbb{T} \to \mathbb{X}(t+1)$*, is dissipative with respect to a supply rate* $s : \mathbb{X}(t)\times\mathbb{U}(t)\times\mathbb{T} \to \mathbb{R}$*, and a reference trajectory given by* $x^r(t+1) = f(x^r(t),u^r(t),t)$*, where* $x^r(t) \in \mathbb{X}(t)$ *and* $u^r(t) \in \mathbb{U}(t)$*, if there exists a storage function* $\lambda : \mathbb{X}(t)\times\mathbb{T} \to \mathbb{R}$*, such that* $\lambda(x^r(t),t) = 0$*, and* $\lambda\left(f(x(t),u(t),t),t+1\right) - \lambda(x(t),t) \leq s(x(t),u(t),t)$*,* $\forall (x(t),u(t),t) \in \mathbb{X}(t)\times\mathbb{U}(t)\times\mathbb{T}$*. The system is strictly dissipative with respect to the supply rate* s *and reference trajectory given by* $x^r(t+1) = f(x^r(t),u^r(t),t)$*, if in addition to the above there exists another* $\mathscr{K}_\infty$ *function* $\rho(\cdot)$*, such that* $\lambda\left(f(x(t),u(t),t+1)\right) - \lambda(x(t),t) \leq -\rho(|x - x^r(t)|) + s(x(t),u(t),t)$*,* $\forall (x(t),u(t),t) \in \mathbb{X}(t)\times\mathbb{U}(t)\times\mathbb{T}$*.*

Part I

Appropriate sizing of EV charging infrastructure

Chapter 3

Effects of number of EV charging/discharging on total electricity costs in commercial buildings with time-of-use energy and demand charges

3.1 Problem statement

In this chapter, we aim to minimize the building electricity costs following the installation of a variable number of EV charging stations at commercial MGs/buildings by leveraging an economic optimization model. We also seek to develop accurate analytical expressions to quantify the optimal EV smart (V1G or V2G) charging benefits even with the economic optimization using only exogenous model inputs.

To obtain representative savings, the analysis covers EV charging on all weekdays in 2019, while the weekend EV load is assumed to be zero. Weekends are excluded from EV charging as smaller building loads and less workplace charging preclude demand charge events, and time-of-use energy rate differences are smaller. Therefore, weekend EV charging does not materially impact the annual utility bill savings.

3.2 Overview of the EV fleet and charging scenarios

Two case studies (i) and (ii) are considered. Case study (i) consists of an idealized uniform commuter fleet, where all EVs have the same battery, and arrive and depart daily at the same time, with the same initial and final SOC, respectively. The assumption of EVs arriving and departing at the same time daily is valid for certain type of buildings, such as hospitals and corporate buildings. Case study (i) is carried out for 14 commercial buildings located on the University of California (UC) San Diego campus, whose original load data can be found in [58]. The buildings' primary functions are diverse and include classrooms, libraries, office spaces, and research laboratories. The load characteristics of the buildings for the analysis period (year 2019), along with their floor areas and year of construction are given in Table 3.1. Case study (ii) considers a realistic case using historical EV charging data for a parking structure with 16 EV charging stations for 5 weekdays in February 2020, with the EV load being mapped to a building having 0 original load (the EV load thus becomes the net load of the building). The historical EV charging dataset contains the time of EV connection, disconnection and end of charging time, the amount of energy charged, the port type (Level 2 or Direct Current Fast Charger), and the initial and final SOC.

For V0G charging, the EVs charge at their maximum battery power, starting from the time the EVs are plugged in until meeting the charging energy demand, without any regard for the original building load. However, V1G and V2B EVs charge smartly to optimize the electricity costs, with V2B EVs having the additional capability to discharge back to the grid. Case studies (i) and (ii) cover the application of the model for a uniform EV fleet, and non-uniform realistic scenario based on historical EV charging data respectively. The uniform EV fleet was motivated by a real situation (a hospital with defined employee shifts), but a controlled setup that allows identifying patterns in charging schedules and generalizing results.

Table 3.1. Mean original real load for all weekdays, mean of original monthly non-coincident demand peak and on-peak period demand peak, floor areas, number of floors, and year constructed of the buildings analyzed for the year 2019.

Building name (Building number)	Mean original real load (kW)	Mean original NCDP (kW)	Mean original OPDP (kW)	Floor area (ft^2)	No. of floors	Year
Mandeville Center (I)	32.2	60.1	56.9	131,365	4	1974
Police Department (II)	38.1	59.9	54.3	14,567	1	1991
Hopkins Parking Structure (III)	57.6	99.4	78.6	446,095	7	2006
Rady (Wells Fargo) Hall (IV)	60.3	103.1	98.8	93,440	4	2012
Pepper Canyon Hall (V)	62.0	102.4	91.5	85,985	4	2004
Otterson Hall (VI)	90.9	133.6	131.6	104,363	4	2007
Music Center (VII)	91.9	137.5	132.1	91,957	4	2008
Robinson Hall - 3 buildings (VIII)	95.0	134.7	129.9	32,932 + 5,142 + 29,618 = 67,724	4, 1, 2	1990
East Campus Office (IX)	118.3	156.4	146.4	77,164	3	2011
Center Hall (X)	122.8	194.4	186.2	83,288	4	1995
Student Services Center (XI)	140.5	242.9	202.1	135,085	4	2007
Social Sciences Building (XII)	146.5	200.0	184.5	84,386	5	1995
Galbraith Hall (XIII)	196.0	307.4	301.7	127,979	4	1965
Geisel Library (XIV)	532.0	649.2	644.0	416,509	10	1970

3.3 Optimization algorithm

3.3.1 Objective function

The objective function to be minimized is the total electricity charges of the building plus a regularization term. The objective function is

$$\min\left[R_{\mathrm{NC}}(t)\mathrm{NCDP}+R_{\mathrm{OP}}(t)\mathrm{OPDP}+\sum_{d=1}^{m}\sum_{t=0}^{24\ \mathrm{h}-\Delta t}\left(R_{\mathrm{EC}}(t)\mathrm{NL}_{\mathrm{opt}}(d,t)\Delta t\right)+\mathrm{OC}+\mathrm{RT}\right], \tag{3.1}$$

where R_{NC} is the non-coincident demand charge rate, NCDP is the non-coincident demand peak which is the maximum load demand from the grid at any 15 min interval of the month, R_{OP} is the on-peak demand charge rate, OPDP is the on-peak period demand peak which is the maximum load demand from the grid at any 15 min interval between 16:00 and 21:00 h of all days of the month, R_{EC} is the time-of-use energy charge rate, $\mathrm{NL}_{\mathrm{opt}}$ is the building optimized net load demand from the grid, d is the index of the day of the month, m is the number of days of the month, t is the time of the day in hours (note that in this chapter, the variable t is not the time-index as described in Section 2.1), Δt is the time resolution which is chosen as 15 minutes (0.25 h), consistent with the real load input data from the buildings, OC is other charges,[1] and RT is a regularization term which guarantees a unique solution of (3.1). The first term in (3.1) is the NCDC, the second term is the OPDC, and the third term covers the off-peak and on-peak period energy costs over the entire month. The third term in (3.1) shows that for each day, the energy costs are covered from $t=0$ to $t=24\ \mathrm{h}-\Delta t$. $t=0$ corresponds to the time

[1] Other charges are the DWR Bond Charge (\$0.00580 $\cdot$Total energy usage in a month), the City of San Diego Franchisee fee (\$0.0578 $\cdot\left[R_{\mathrm{NC}}(t)\mathrm{NCDP}+R_{\mathrm{OP}}(t)\mathrm{OPDP}+\sum_{d=1}^{m}\sum_{t=0}^{24\ \mathrm{h}-\Delta t}\left(R_{\mathrm{EC}}(t)\mathrm{NL}_{\mathrm{opt}}(d,t)\Delta t\right)+\mathrm{OC}+\mathrm{RT}\right]$), the DWR Bond franchisee fee ((\$0.0688 $\cdot$ DWR Bond Charge), the CA State Surcharge ((\$0.00030 $\cdot$ Total energy usage in a month), and the CA State Regulatory charge (\$0.00058 $\cdot$ Total energy usage in a month). The total energy usage in a month is simply $\sum_{d=1}^{m}\sum_{t=0}^{24\ \mathrm{h}-\Delta t}\left(\mathrm{NL}_{\mathrm{opt}}(d,t)\Delta t\right)$.

period from 00:00 to 00:15 h, while $t = 24h - \Delta t$ corresponds to the time period from 23:45 to 24:00 h, thus covering the entire day. RT aims to prevent non-unique solutions by minimizing the deviation of the optimized net load from the original load (which indirectly avoids unnecessary charging/discharging cycles of the EV which can occur due to the assumption of 100% charging/discharging efficiency in Section 3.3.2), and is formulated as $\mathrm{RT} = w_f \sum_{d=1}^{m} \sum_{t=0}^{24\ \mathrm{h}-\Delta t} \left\| \mathrm{NL}_{\mathrm{opt}}(d,t) - L_{\mathrm{org}}(d,t) \right\|$, where w_f is a weighting factor which is set as 0.01, and L_{org} is the original baseline building load.

3.3.2 Constraints

In this Section, for simplicity, d is dropped from the variable argument, with only t being retained, as the constraints are presented for one day. For example, $\mathrm{NL}_{\mathrm{opt}}(d,t)$ is written as $\mathrm{NL}_{\mathrm{opt}}(t)$. The power balance equation is formulated as:

$$\mathrm{NL}_{\mathrm{opt}}(t) = L_{\mathrm{org}}(t) + \sum_{j=1}^{n} \mathrm{EV}^j(t), \tag{3.2}$$

where n is the number of EVs, and $\mathrm{EV}^j(t)$ is the charging rate of the j^{th} electric vehicle. Power flow from the grid to the EV (charging) is considered positive.

The EV charging rate is constrained as

$$\min \mathrm{EV}^j \leq \mathrm{EV}^j(t) \leq \max \mathrm{EV}^j, \tag{3.3}$$

where the maximum and minimum EV charging rates depend on the charging technology used (V0G/V1G/V2G/V2B). For V0G and V1G, $\min \mathrm{EV}^j = 0$, whereas for V2G/V2B, $\min \mathrm{EV}^j = -\max EV^j$.

The EV battery energy constraints are formulated as

$$\min \mathrm{BE}^j \leq \mathrm{BE}^j(t) \leq \max \mathrm{BE}^j, \tag{3.4}$$

where $\mathrm{BE}^j(t)$ is the battery energy of the j^{th} EV. The minimum and maximum state of charge (SOC) of the battery are inputs, which, in turn, predefine the minimum and maximum battery energy limits.

The initial battery energy of the EV at the time of connection is formulated as

$$\mathrm{BE}^j(t=t_i^j) = \mathrm{SOC}_i^j \mathrm{BC}^j, \tag{3.5}$$

where SOC_i^j is the initial state of charge of the j^{th} EV, t_i^j is the time the j^{th} EV is connected to the charging station, 'i' stands for 'initial', and BC^j is the battery capacity of the j^{th} EV.

The battery energy variation with time is

$$\mathrm{BE}^j(t+\Delta t) = \mathrm{BE}^j(t) + \mathrm{EV}^j(t)\Delta t. \tag{3.6}$$

The total energy demand of the j^{th} EV (ED^j) is known beforehand as we use perfect forecasts. The final EV battery energy is constrained as

$$\mathrm{BE}^j(t=t_f^j) = \mathrm{BE}^j(t=t_i^j) + \mathrm{ED}^j, \tag{3.7}$$

where t_f^j is the disconnection time of the j^{th} EV, and 'f' stands for 'final'. Furthermore, the total energy demand of the EV is formulated as

$$\mathrm{ED}^j = (\mathrm{SOC}_f^j - \mathrm{SOC}_i^j)\mathrm{BC}^j. \tag{3.8}$$

In case study (ii), if (3.8), gives an infeasible energy demand (ED^j greater than the charging ability of the battery given the layover time), then the energy demand is corrected ($\mathrm{ED}^j_{\mathrm{cor}}$) as

$$\mathrm{ED}^j_{\mathrm{cor}} = \min\left[(t_f^j - t_i^j)\max \mathrm{EV}^j,\, \mathrm{ED}^j\right], \tag{3.9}$$

where $(t_f^j - t_i^j)$ is the layover time.

Charging/discharging takes place within the layover period only and is constrained as

$$\mathrm{EV}^j(t) = 0, \quad 0 \leq t < t_i^j \tag{3.10a}$$

$$\mathrm{EV}^j(t) = 0, \quad t_f^j \leq t < t_{\mathrm{end}}^j \tag{3.10b}$$

where $t = 0$ and $t = t_{\mathrm{end}}^j$ correspond to the times at the start and end of the simulation.

3.3.3 Optimization algorithm

The optimization is carried out in CVX, a package for specifying and solving convex programs [59, 60] in the MATLAB environment. A flowchart of the optimization algorithm is shown in Fig. 3.1.

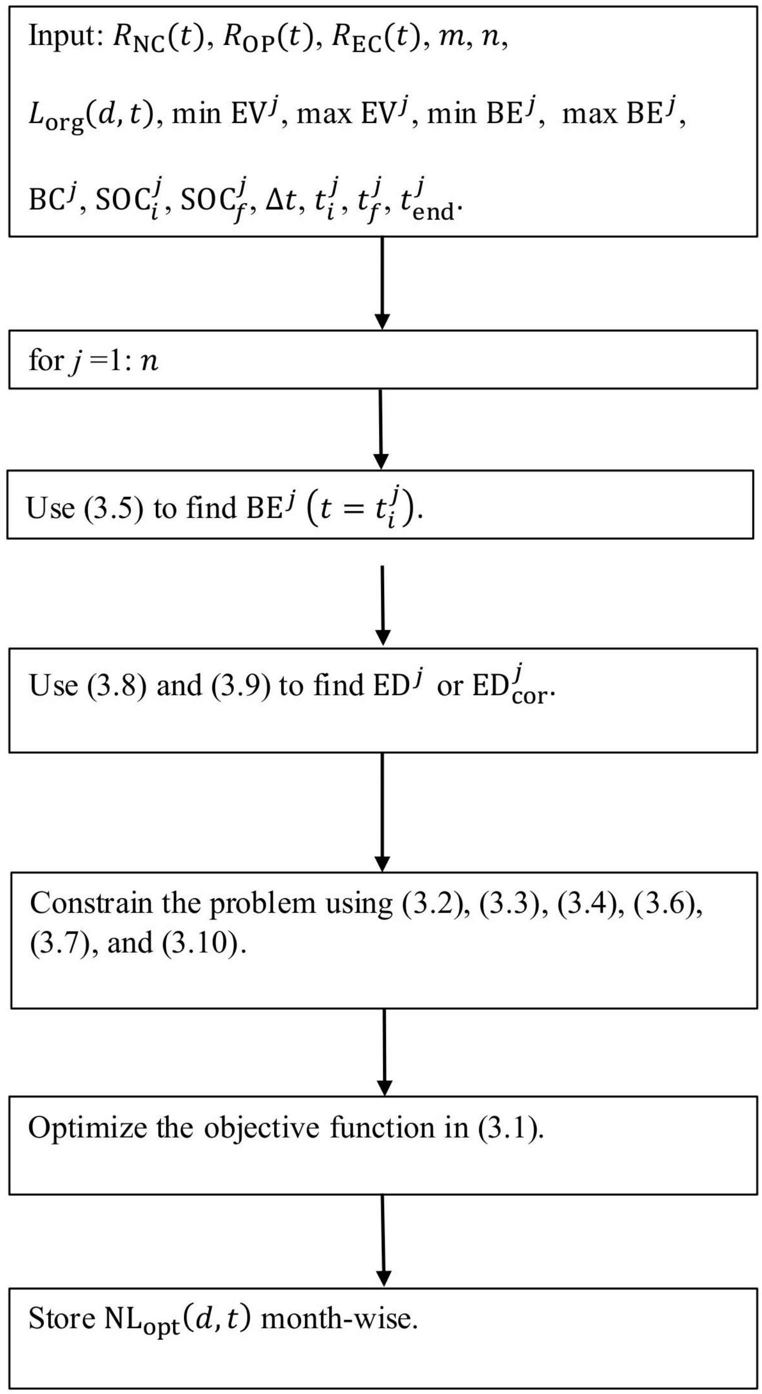

Figure 3.1. Flowchart of the optimization algorithm.

3.3.4 Input data for case studies (i) and (ii)

Case study (i) is carried out for 14 metered UC San Diego buildings without EVs. The Case study (i) is further subdivided into two layover periods, a) 07:45 h to 16:45 h, which is representative of a typical office employee layover consisting of 8 hours of work-time, a 30 min lunch break and 30 mins for travel from the parking lot to the office and vice versa; and b) 06:30 h to 19:30 h, which is representative of a typical medical worker shift, consisting of 12 hours of work-time, a 30 min lunch break and 30 mins for travel from the parking lot to the medical center and vice versa. For Case study (i), the input variables that stay constant throughout the analysis are as follows. The battery capacity of all EVs (for $j = 1$ through n) is chosen as $\mathrm{BC}^j = 60$ kWh which is representative of a typical EV [61]. The minimum and maximum SOC of the EVs are fixed at 20% and 90% respectively, to limit battery degradation during extreme charging states. The maximum charging rate of the EVs are $\max \mathrm{EV}^j$=6.6 kW, which is a typical value for a Level 2 charger, which is the most prevalent type of EV charger in the United States [62]. For Case study (ii), the minimum and maximum SOC of the EVs are fixed at 0 and 100% respectively, with variable EV battery capacity and initial and final SOCs per the real charging dataset. Furthermore, in Case study (ii), the maximum charging and discharging rate of the EVs depends on the type of EV charging port they are plugged into (see Table 3.6). Case Study (ii) uses real data from ChargePoint at UC San Diego, where the initial and final SOC is given for a subset of charging events. For these subsets of EV charging events, initial and final SOC varied between 0-100%. Thus, to impute the missing data consistent with the original data, the SOC range for Case study (ii) is fixed between 0-100%.

The break-down of the electricity bill components levied by San Diego Gas & Electric are shown in Table 3.2. The NCDC rates are constant throughout the year and are higher than the OPDC rates in winter, but lower than the OPDC rates in summer.

The on-peak period energy charge rates are higher than the off-peak period energy charge rates throughout the year.

Table 3.2. Breakdown of electricity bill components — SDG&E AL-TOU tariff. The on-peak period is 16:00 – 21:00 h, with the remaining hours being off-peak. June 1 to October 31 are summer months with the rest of the year being winter.

Cost Component	**Symbol**	**Value**
NCDC rate (summer and winter)	$R_{\mathrm{NC}}(t)$	\$24.48/kW
OPDC rate (summer)	$R_{\mathrm{OP}}(t)$	\$28.92/kW
OPDC rate (winter)	—	\$19.23/kW
Off-peak period energy charge rate (summer)	$R_{\mathrm{EC}}(t)$	\$0.10679/kWh
Off-peak period energy charge rate (winter)	—	\$0.09506/kWh
On-peak period energy charge rate (summer)	—	\$0.12628/kWh
On-peak period energy charge rate (winter)	—	\$0.10626/kWh

3.3.5 Input data for sensitivity analysis

A sensitivity analysis based on Case study (i) is carried out to study the effect of varying the initial and final SOC of the EVs in Section 3.4.6. Initial and final SOC combinations of 40-80%, 45-85% and 50-90% are analyzed to study the effect of changing the initial and final SOCs while keeping the energy demand of the EVs constant. Energy demand sensitivity analyses are also carried out for initial and final SOC combinations of 50-85% and 50-80% to elucidate the effects of changing the final SOC while keeping the initial SOC constant.

3.4 Results and discussions

3.4.1 Idealized uniform commuter EV fleet case study

The results for building V (randomly selected) for initial and final EV SOC of 50% and 90% respectively for Jan (January) 2019 and the entire year 2019 are presented here and summarized in Table 3.3. The $\mathrm{BC}^j = 60$ kWh, and the initial and final SOC of 50 and 90% respectively correspond to a daily charging demand of 24 kWh per EV. Thus, the charging demand is increased in multiples of 24 kWh with each additional charging station / EV (see legend of figures in Section 3.4.2). The analyses are carried out up to 432 kWh charging demand (18 EV charging stations) as the changes in electricity costs per EV thereafter become independent of charging demand. The layover periods shown in the graphical analysis are 06:30 h to 19:30 h and 07:45 h to 16:45 h.

Figure 3.2 shows the original (pre-EV) load for building V for Jan 2019. The electricity load is low on holidays (Jan 1) and weekends (Jan 5, 6, 12, 13, 19, 20, 26, 27) when the building occupancy is low. The original non-coincident (NC) and on-peak (OP) period demand peaks occur on Jan 31 at 14:00 h at 109.0 kW and Jan 16 at 16:00 h at 96.5 kW, respectively.

Table 3.3 shows the NC and OP demand peaks for Jan 2019 for building V for selected EV charging demand scenarios for both the layover periods.

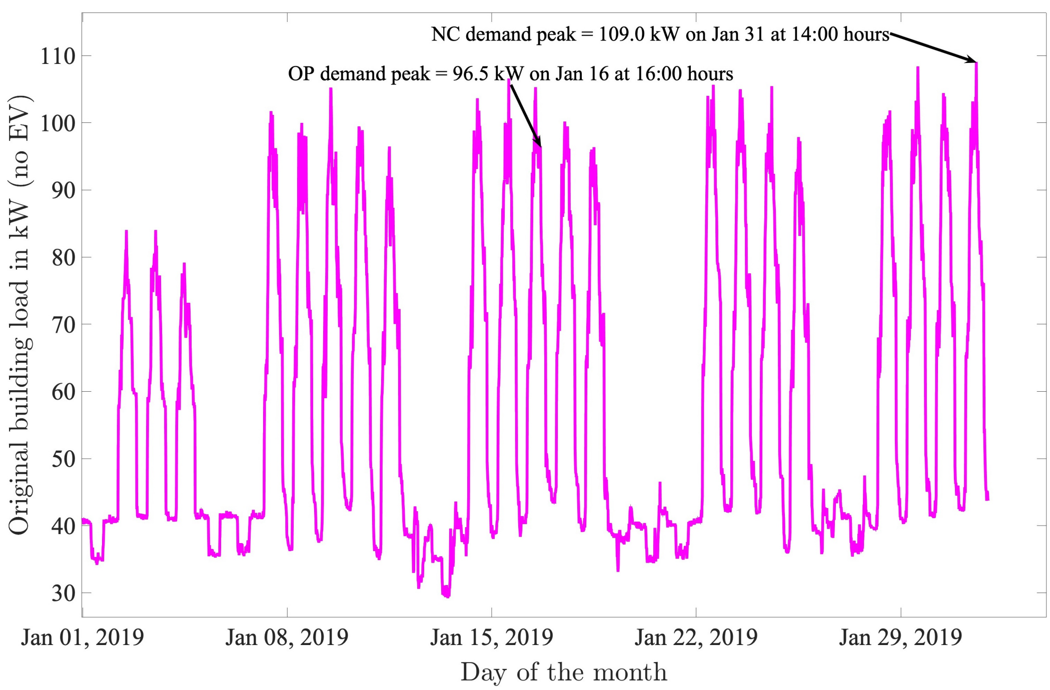

Figure 3.2. Original building V load for Jan 2019.

Table 3.3. Summary of the NC and OP demand peaks for all charging strategies for Jan 2019 for Building V. The original NC and OP demand peaks are 109.0 and 96.5 kW, respectively. The peak values (with EV charging) which are larger/smaller than the original are marked in red/green font.

Daily EV charging demand (kWh) (No. of EVs/ (charging stations)	**Layover 06:30 – 19:30 h**						**Layover 07:45 – 16:45 h**					
	NC demand peak (kW)			OP demand peak (kW)			NC demand peak (kW)			OP demand peak (kW)		
	V0G	V1G	V2B	V0G	V1G	V2B	V0G	V1G	V2B	V0G	V1G	V2B
24 (1)	110.6	109.0	102.4	96.5	96.5	89.9	111.0	109.0	102.4	96.5	96.5	91.0
48 (2)	117.2	109.0	99.5	96.5	96.5	83.5	117.6	109.0	102.6	96.5	96.5	91.0
72 (3)	123.8	109.0	101.5	96.5	96.5	82.4	124.2	109.0	105.0	96.5	96.5	91.0
96 (4)	130.4	109.0	103.1	96.5	96.5	82.4	130.8	109.0	107.6	96.5	96.5	91.0
120 (5)	137.0	109.0	105.0	96.5	96.5	82.4	137.4	109.8	110.3	96.5	96.5	91.0
144 (6)	143.6	109.0	107.1	96.5	96.5	82.4	144.0	112.7	113.2	96.5	96.5	91.0
168 (7)	150.2	109.0	109.6	96.5	96.5	82.4	150.6	115.6	116.1	96.5	96.5	91.0
192 (8)	156.8	109.0	112.1	96.5	96.5	82.4	157.2	118.5	119.0	96.5	96.5	91.0
216 (9)	163.4	109.5	114.7	96.5	96.5	82.4	163.8	121.4	121.9	96.5	96.5	91.0
240 (10)	170.0	112.0	117.2	96.5	96.5	82.4	170.4	124.3	124.8	96.5	96.5	91.0
432 (18)	222.8	132.2	137.4	96.5	96.5	82.4	223.2	147.6	148.1	96.5	96.5	91.0

3.4.2 Layover 06:30 h to 19:30 h – medical worker shift

V0G charging

The V0G EVs start charging the moment they are plugged in (06:30 h) at the highest possible EV battery power rate (6.6 kW), resulting in charging terminating by 10:15 h. The highest original load in the 06:30 – 10:15 h period occurs on Jan 22 at 09:30 h and is 104.0 kW. Therefore, on Jan 22 the net load (with V0G EVs) at 09:30 h for 24 kWh (1 EV) of charging demand, which contributes 6.6 kW of charging load, becomes the V0G NC monthly demand peak at 110.6 kW (see Table 3.3). The V0G monthly demand peak increases with further increasing charging demand by 6.6 kW per EV. As all charging occurs before the on-peak period, the OP demand peak remains the same as the original at 96.5 kW. Refer to Fig. 3.3 for a graphical representation.

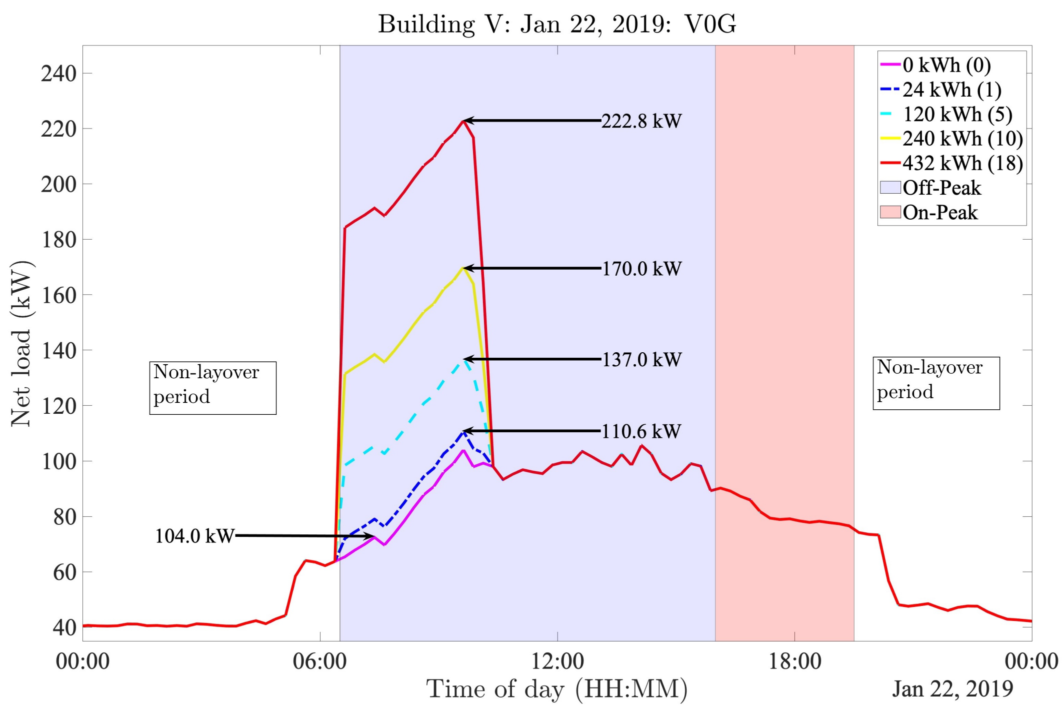

Figure 3.3. V0G charging for the 06:30 – 19:30 h layover: NC demand peak on Jan 22, 2019. The legend shows total daily EV charging demand and the number in brackets in the legend correspond to the number of EVs/charging stations. The blue shading denotes the off-peak layover period, the red shading denotes the on-peak layover period, while the unshaded area denotes the non-layover period. The original NC and OP demand peaks are 109.0 kW and 96.5 kW, respectively.

V1G charging

V1G chargers cannot discharge back into the grid, and hence the optimized net load (with EV charging) cannot be smaller than the original load. Figure 3.4(a) shows that on Jan 31, with up to 192 kWh of charging demand, the NC demand peak remains the same as the original at 109.0 kW. Increasing the charging demand to 216 kWh increases the NC demand peak to 109.5 kW, which exceeds the original NC demand peak. With the addition of more V1G EV charging demand (above 216 kWh charging demand), the optimal NC peak demand increases by 2.5 kW per EV because the increasing charging demand (of 24 kWh per EV) is uniformly spread out over the 9.5 hour off-peak layover period from 06:30 – 16:00 h (see Section 3.4.4 for a detailed explanation).

Figure 3.4(b) shows that the OP demand peak remains the same as the original at 96.5 kW for all charging demands. Because of the higher energy and demand charges applicable in the on-peak period as compared to the off-peak period, all charging will take place in the off-peak layover period before 16:00 h if feasible. A complete charging before 16:00 h occur on some days (e.g. Figure 3.4(b) for 1 or 2 EVs) when accommodating all the charging demand within the off-peak layover period does not lead to an increase of the NC demand peak beyond the original. However, complete charging before 16:00 h is not optimal on days when the original off-peak load curve during the layover period cannot accommodate the charging demand without increasing the NC demand peak. Therefore, charging during the off-peak layover period (from 06:30 – 16:00 h) takes place until the optimized load becomes constant at the original NC demand peak. A further increase in the charging demand results in EVs being charged during the on-peak layover period (16:00 – 19:30 h) until the optimized on-peak layover period load becomes constant at the original OP demand peak. With further increasing the charging demand, charging occurs again exclusively in the off-peak layover period (06:30 – 16:00 h), leading to increasing NC demand peak beyond the original demand peak (see Fig. 3.4(c)). Specifically, the additional charging demand is spread out uniformly over the off-peak layover period. The reasoning for the optimized charging strategy is given in Section 3.4.4.[2]

Figure 3.4(c) shows the V1G timeseries analysis on Jan 22 to elucidate the optimized charging strategy. For a charging demand of 24 kWh, the entire charging takes place in the off-peak layover period. With further increasing charging demand (192 kWh), charging continues to occur in the off-peak layover period until the off-peak layover period load becomes constant at the original NC demand peak (109.0 kW), with the rest of the charging occurring in the on-peak period without increasing the OP demand peak (96.5 kW). For a charging demand of 216 kWh, additional charging occurs initially in the on-peak period until the on-peak layover period load becomes constant at the OP demand peak, with the rest of the additional charging demand being uniformly accommodated in the off-peak layover period increasing the NC demand peak to 109.5 kW. With further increasing charging demand (above 216 kWh), additional charging occurs exclusively in the off-peak layover period, with the additional charging demand spread out uniformly, leading to an increase in the NC demand peak by 2.5 kW per EV (see Table 3.3). Comparing Figs. 3.4(a) and 3.4(c) show that for some charging demands, the optimized NC and OP demand peaks are reached on multiple days.

[2]Note that in rare cases the maximum EV charging rate can restrict the maximum charging such that charging deviates slightly from the strategy described above. But most of the results relevant to this work can be explained by the optimized charging strategy discussed above.

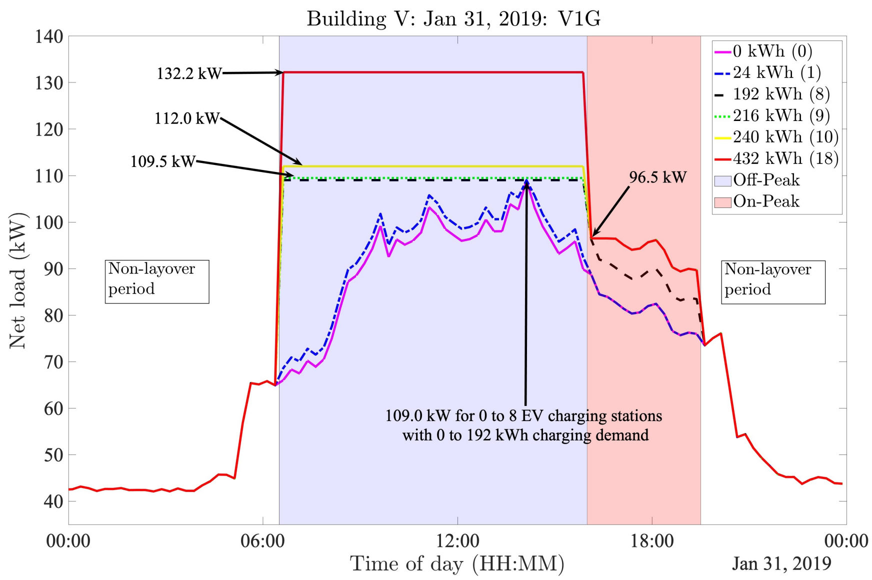

(a)

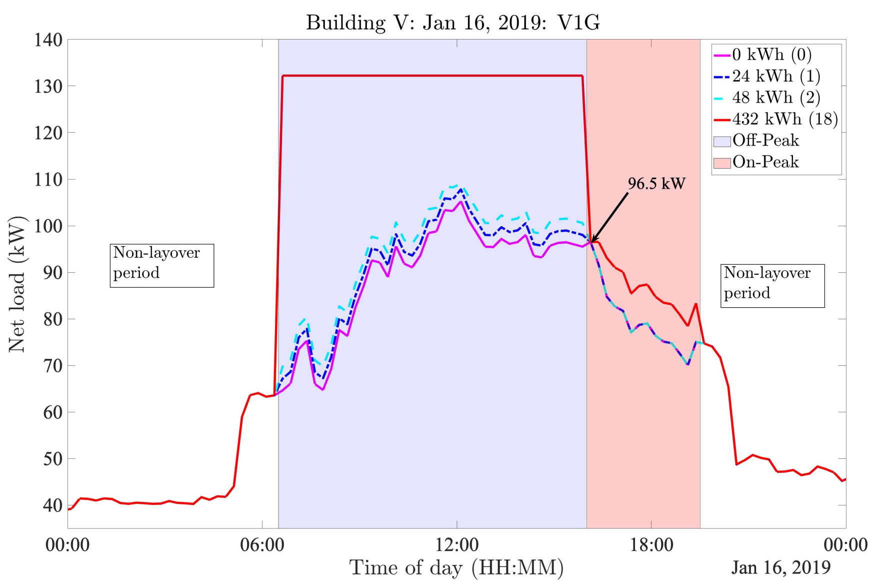

(b)

Figure 3.4. V1G charging for the 06:30 – 19:30 h layover: (a) NC demand peak for Jan 31 2019, when the original NC demand peak also occurs, (b) OP demand peak for Jan 16 2019, when the original OP demand peak also occurs, and (c) NC and OP demand peak for Jan 22 2019, which provides the greatest limitation for accommodating OP EV charging. The legend shows total daily EV charging demand and the number in brackets in the legend correspond to the number of EVs/charging stations. The blue shading denotes the off-peak layover period, the red shading denotes the on-peak layover period, while the unshaded area denotes the non-layover period. The original NC and OP demand peaks are 109.0 and 96.5 kW, respectively.

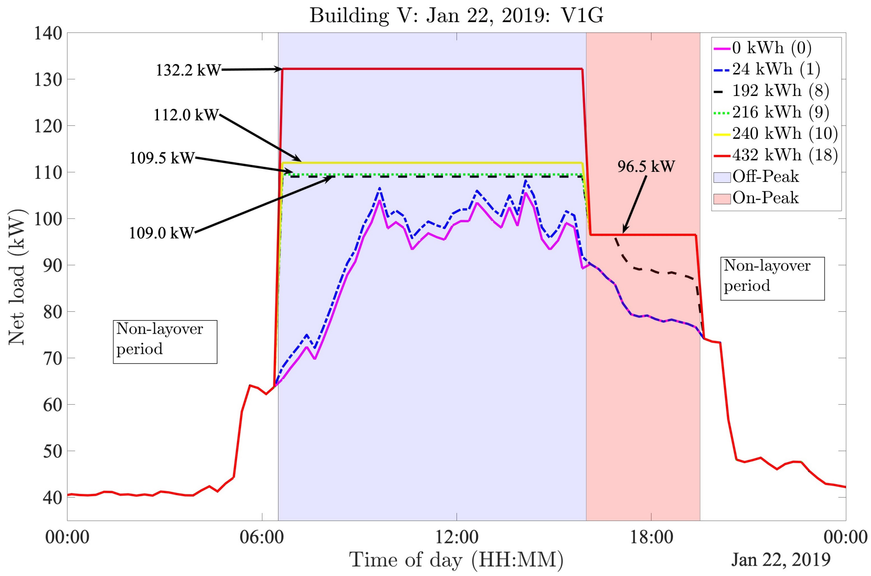

(c)

Figure 3.4. V1G charging for the 06:30 – 19:30 h layover: (a) NC demand peak for Jan 31 2019, when the original NC demand peak also occurs, (b) OP demand peak for Jan 16 2019, when the original OP demand peak also occurs, and (c) NC and OP demand peak for Jan 22 2019, which provides the greatest limitation for accommodating OP EV charging. The legend shows total daily EV charging demand and the number in brackets in the legend correspond to the number of EVs/charging stations. The blue shading denotes the off-peak layover period, the red shading denotes the on-peak layover period, while the unshaded area denotes the non-layover period. The original NC and OP demand peaks are 109.0 and 96.5 kW, respectively.(Continued)

V2B charging

Figure 3.5(a) shows that the V2B chargers can discharge and decrease the optimized net load below the original load. For example, the NC demand peak decreases from 109.0 kW to 102.4 kW and then to 99.5 kW as the charging demand increases from 0 kWh to 24 kWh and then to 48 kWh respectively. This occurs because as the number of EVs increases, the total discharge power also increases. However, from a charging demand of 72 kWh, we see a monotonous increase in the NC demand peak, and starting at 168 kWh the optimized NC demand peak exceeds the original NC demand peak. Above a charging demand of 168 kWh, the NC demand peak increases by 2.5 kW per EV (see Table 3.3), as the additional charging demand (over 168 kWh) is spread out uniformly over the entire off-peak layover period. The reasoning for this optimized V2B charging strategy is elucidated in Section 3.4.4.

Figure 3.5(a) also shows that for Jan 31, the optimized net load varies around 07:00 h for all energy demands. This is because the optimized NC demand peak threshold is reached on multiple days, as we carry out a monthly optimization. For example, for 432 kWh of charging demand, Jan 22 (see Fig. 3.5(b)) determines the off-peak period optimized load curve peak. From Fig. 3.5(b), we see that for 432 kWh of charging demand, the off-peak layover period load is constant at 137.4 kW. Once the 137.4 kW off-peak layover period load threshold is reached on Jan 22, on other days such as Jan 31, it is optimal to charge up to an optimized net load of 137.4 kW as long as possible in the off-peak layover period as we pay no extra non-coincident demand charges (NCDC), and the energy rates are lower in the off-peak period as compared to the on-peak period. In Fig. 3.5(a), for the 432 kWh of charging demand, it is possible to reach the SOC at 16:00 h with some constant net load lower than 137.4 kW. However, the regularization term, which minimizes the deviation of the optimized load curve from the original load curve and guarantees a unique solution, results in variable charging around 07:00 h following the trend of the original load on Jan 31.

Figure 3.5(c) shows the on-peak period on Jan 16 which is the day with the original OP demand peak. With increasing charging demand from 24 kWh to 72 kWh, the OP demand peak decreases. The increased discharging capacity with the addition of more EVs is responsible for the reduction of the OP demand peak. With further increasing charging demand, the OP demand peak remains constant at 82.4 kW. The NC and OP demand thresholds for Jan are decided by different days depending on charging demand. Jan 16 decides the demand thresholds for 1 EV (for 24 kWh daily charging demand). Then, Jan 22 (see Fig. 3.5(b)) decides the demand thresholds for 2 or more EVs as shown by flat lines at 83.5 kW (2 EVs, 48 kWh) and 82.4 kW (3 or more EVs, 72 kWh or more).

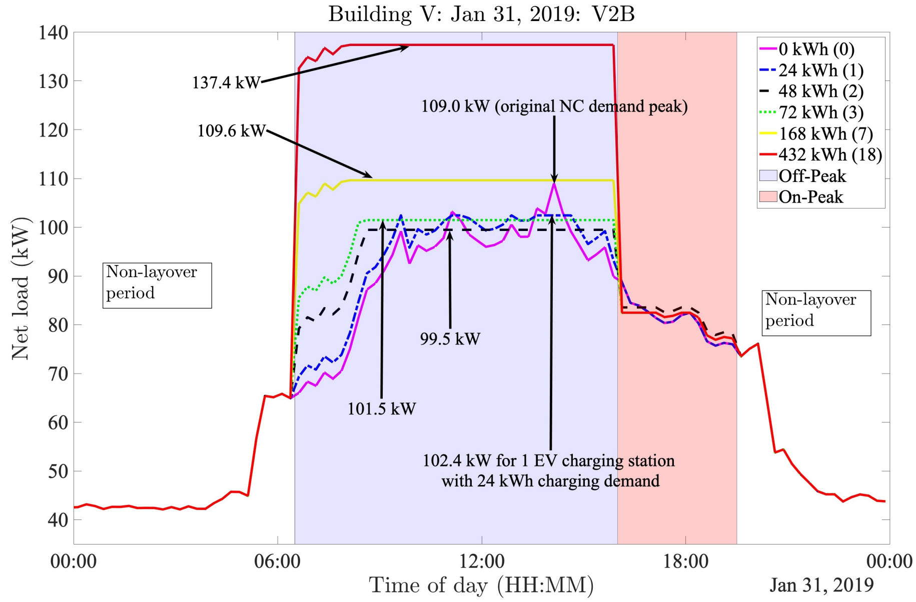

(a)

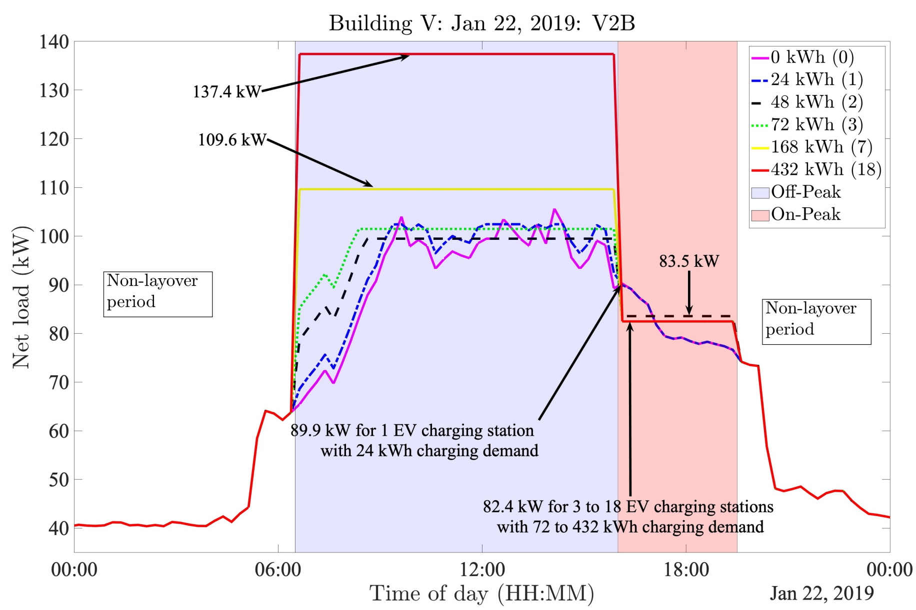

(b)

Figure 3.5. V2B charging for the 06:30 – 19:30 h layover: (a) NC demand peak for Jan 31, 2019, when the original NC demand peak also occurs, (b) NC and OP demand peak for Jan 22, 2019, and (c) OP demand peak for Jan 16, 2019 when the original OP demand peak also occurs. The original NC and OP demand peaks are 109.0 and 96.5 kW, respectively.

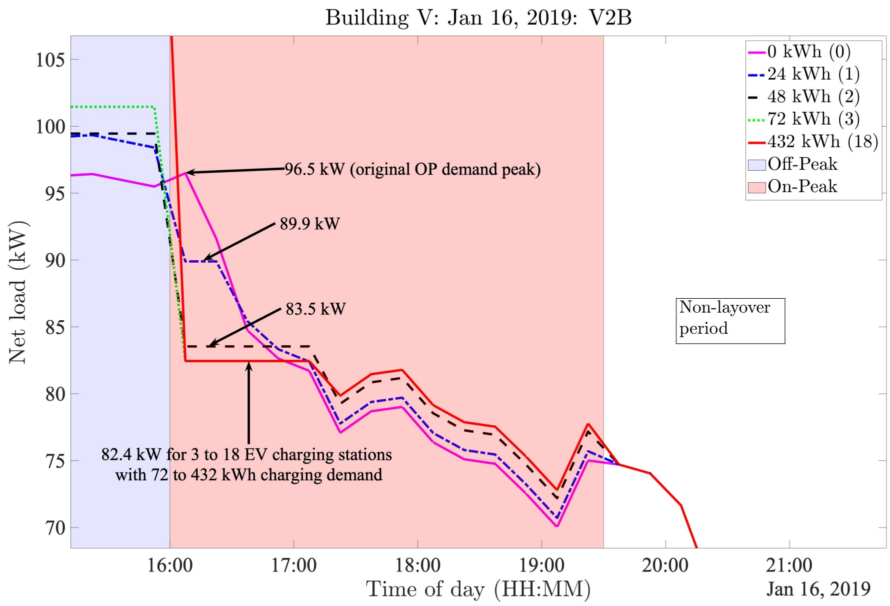

(c)

Figure 3.5. V2B charging for the 06:30 – 19:30 h layover: (a) NC demand peak for Jan 31, 2019, when the original NC demand peak also occurs, (b) NC and OP demand peak for Jan 22, 2019, and (c) OP demand peak for Jan 16, 2019 when the original OP demand peak also occurs. The original NC and OP demand peaks are 109.0 and 96.5 kW, respectively.(Continued)

3.4.3 Layover 07:45 h to 16:45 h – typical office worker shift

V0G charging

The V0G charging analysis for the 07:45 to 16:45 h layover period (not shown graphically) is similar to the one described in Section 3.4.2 for the 06:30 to 19:30 h layover period. The V0G NC demand peaks (see Table 3.3) are slightly higher in the 07:45 – 16:45 h layover period as compared to 06:30 to 19:30 h layover period, because the peaks are reached on Jan 30 at 11:00 h, which has an original load of 104.4 kW (as compared to 104.0 kW at 09:30 h when NC demand peaks are reached in 06:30 – 19:30 h layover period), which is the highest load in the 07:45 – 11:30 h time period during which the charging takes place. The V0G NC demand peak increases above the original NC demand peak, starting from 24 kWh of charging demand and increases thereafter. All charging takes place before the on-peak period, and hence the OP demand peaks remain the same as the original load.

V1G charging

Figure 3.6 shows that the NC demand peak remains the same as the original at 109.0 kW until 96 kWh of charging demand. The NC demand peak increases thereafter with further increasing charging demand. Comparing Figs. 3.6 and 3.4(a) and as documented in Table 3.3, we observe that the shorter 07:45 – 16:45 h layover period leads to greater NC demand peaks as compared to 06:30 -19:30 h, because the original load during the 06:30 – 07:45 h period is less than the original NC demand peak, and therefore provides additional opportunities for charging without increasing the NC demand peak. The optimized NC demand peaks increase by 2.9 kW per EV above 144 kWh of charging demand.

The OP demand peak remains the same as the original at 96.5 kW for the entire analysis (not shown graphically). This is similar to the results observed in Fig. 3.4(b) of the main text for the layover period 06:30 -19:30 h.

V2B charging

Comparing Figs. 3.7 and 3.5(a), the NC demand peak is greater in the 07:45 – 16:45 h layover for the same charging demand as compared to the 06:30 – 19:30 h layover for the same reason as in the V1G charging. The optimized NC demand peaks increase by 2.9 kW per EV above 144 kWh charging demand.

The OP demand peak (not shown graphically) is also greater for the 07:45 – 16:45 h layover (91.1 kW for all charging demands from 24 to 432 kWh) as compared to the 06:30 – 19:30 h layover (varies from 89.9 to 82.4 kW, as shown in Fig. 3.5(c)). The shorter layover time gives the V2B EVs less time to charge up again to 90% SOC before leaving (after discharging during the on-peak period) and thus, the discharging is less in the shorter layover period leading to greater OP demand peaks as compared to the longer layover

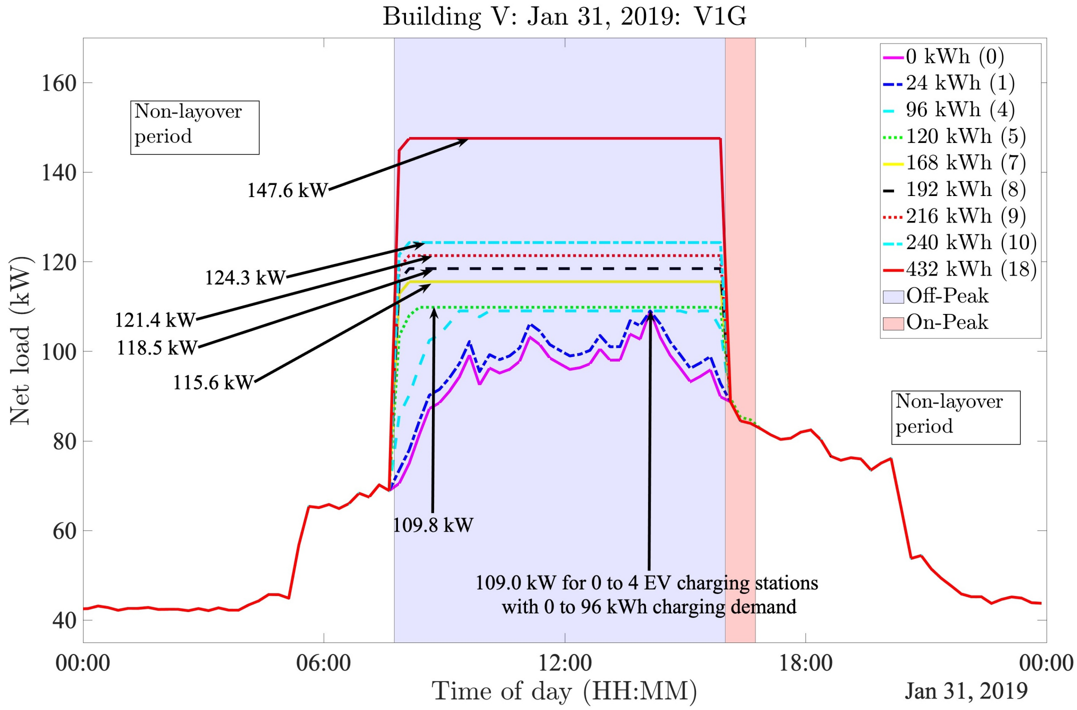

Figure 3.6. V1G charging for the 07:45 – 16:45 h layover: NC demand peak on Jan 31, 2019, when the original NC demand peak (109.0 kW) also occurs.

period.

3.4.4 Dependence of the total electricity cost on charging type, load shape and layover period

In this section, we compare the performance between V0G, V1G and V2B charging strategies in terms of total electricity costs for Jan and the entire year 2019. We also derive general mathematical expressions for the slopes (once they become constant) of the V0G, V1G and V2B total electricity charges versus daily energy demand curves month-wise, daily charging demand when the V1G and V2B curves transition to constant slope, and final offset between V1G and V2B total electricity charges. Although, we mostly present results from building V in this work for the 06:30 – 19:30 h layover, the mathematical expressions are applicable to all the other buildings and for other layover periods.

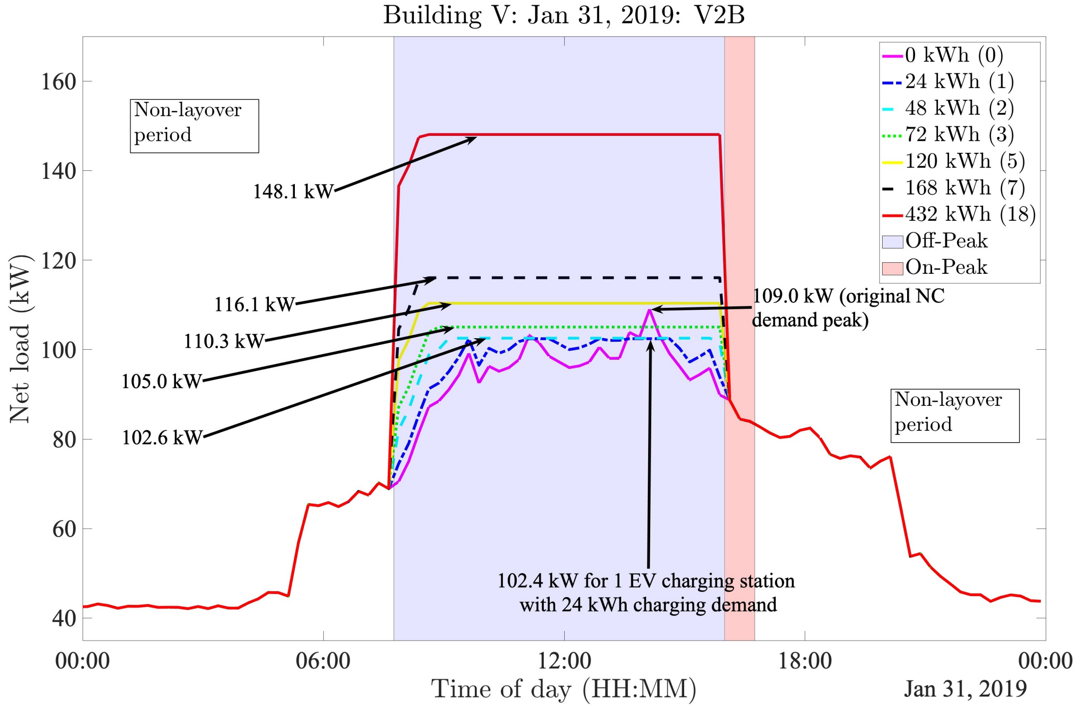

Figure 3.7. V2B charging for the 07:45 – 16:45 h layover: NC demand peak on Jan 31, 2019, when the original NC demand peak (109.0 kW) also occurs.

Cumulative results: 06:30 – 19:30 h layover

Figure 3.8 shows that for both Jan (Fig. 3.8(a)) and the entire year 2019 (Fig. 3.8(b)), the total electricity costs with V2B are lower than the original building costs for charging capacities up to 120 kWh (or 5 V2B charging stations), making 5 the optimal number of V2B charging station installations for building V for the layover period 06:30 – 19:30 h.

Figure 3.8 also shows that V0G charging incurs the highest electricity costs, followed by V1G and V2B respectively. This is expected as V0G cannot time-shift load demand from the grid and charges at the maximum charger power of 6.6 kW, while for V1G and V2B, charging is spread out smartly to optimize electricity costs. V2B reduces the electricity costs compared to V1G because the V2B discharging capability reduces the demand peak costs. The net summation of NC and OP demand peak charges are less for V2B than V1G which results from a greater reduction in OP demand peak charges

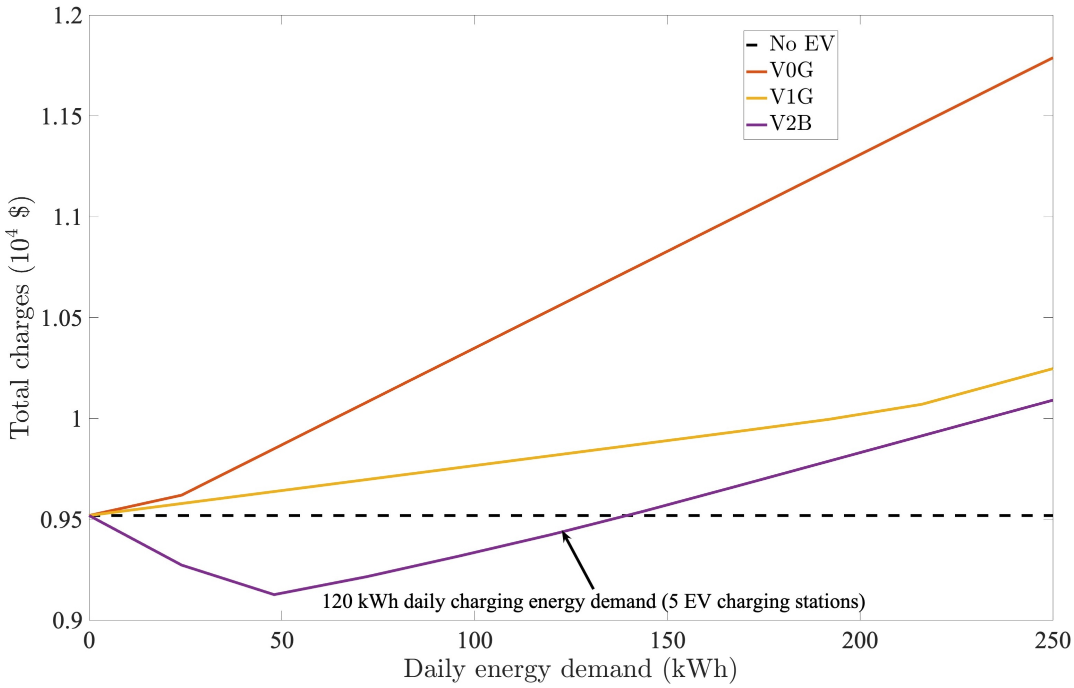

(a)

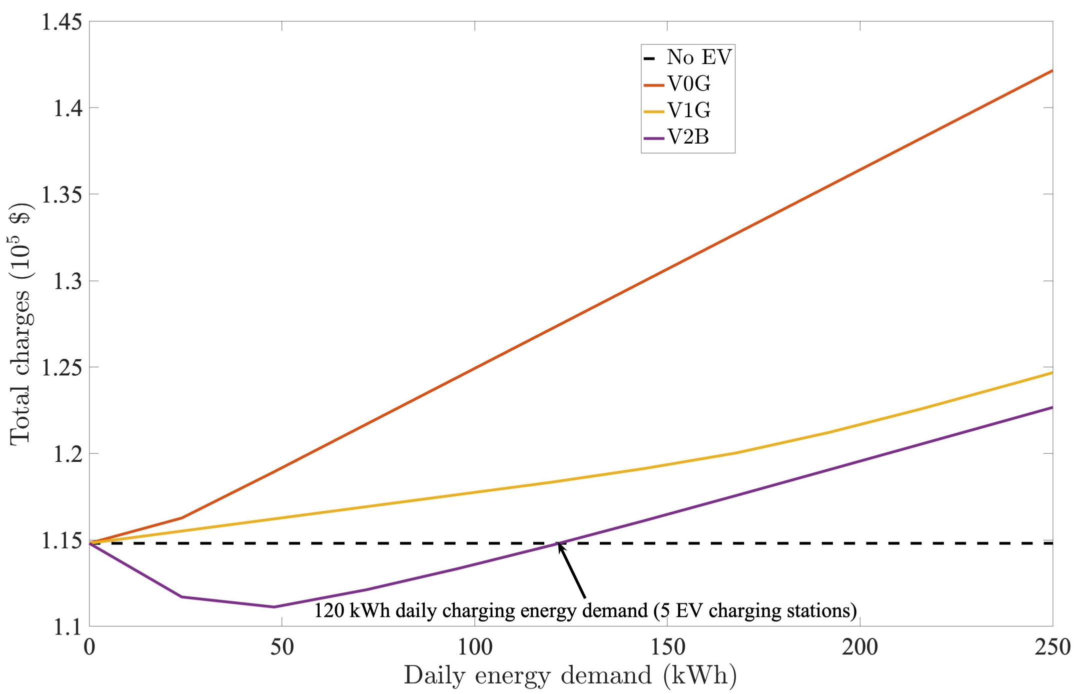

(b)

Figure 3.8. Total electricity charges versus total daily EV energy demand for (a) Jan 2019 and (b) the entire year 2019 for the layover period 06:30 – 19:30 h at building V.

compared to the increase in NC demand charges (Table 3.3). The net cost savings as a result of shifting demand from the on-peak to off-peak layover period of V2G/V2B EVs are demonstrated for a hypothetical case study in Section 3.4.4.

Initially the V2B and V1G electricity costs diverge because with an increasing number of EVs, the V2B EVs can discharge during the non-coincident and on-peak period peaks, while charging at other times, which leads to reduced costs. However, after a certain energy demand, Figs. 3.8(a) and 3.8(b) show that the V1G and V2B cost curves become parallel to each other.

For V1G, as described in Section 3.4.2, after both the off-peak and on-peak layover period loads become constant (at their respective original peaks), additional charging demand is accommodated in the off-peak layover period only. Accommodating the additional charging demand exclusively in the off-peak layover period leads to an increase of the non-coincident demand peak as, $\Delta\text{NCDP} = \frac{\Delta\text{CD}_{\text{day}}}{16\text{ h} - t_i^j}$, where ΔNCDP is the increase of the NC demand peak, $\Delta\text{CD}_{\text{day}}$ is the daily increase in the charging demand and $(16\text{ h} - t_i^j)$ is the off-peak layover which is 9.5 h (06:30 – 16:00 h) for the 06:30 – 19:30 h layover. Accommodating the daily increase in charging demand exclusively in the on-peak layover period would increase the on-peak period demand peak as, $\Delta\text{OPDP} = \frac{\Delta\text{CD}_{\text{day}}}{t_f^j - 16\text{ h}}$, where ΔOPDP is the increase of the OP demand peak and $(t_f^j - 16\text{ h})$ is the on-peak layover which is 3.5 h (16:00 – 19:30 h) for the 06:30 – 19:30 h layover. Therefore, after the net loads are flat, V1G charging only occurs in the off-peak layover period if $R_{\text{NC}}(t)\Delta\text{NCDP} - R_{\text{OP}}(t)\Delta\text{OPDP} < 0$, which is the case as $\frac{R_{\text{NC}}(t)}{R_{\text{OP}}(t)} < \frac{(16\text{ h} - t_i^j)}{t_f^j - 16\text{ h}}$ for both summer and winter. Table 3.2 shows that the ratio of R_{NC} to $R_{\text{OP}}(t)$ is 1.27 for winter and 0.85 for summer. For the 06:30 – 19:30 h layover, the ratio of off-peak (9.5 hours) to on-peak (3.5 hours) layover duration is 2.7. Table 3.2 also shows that the OP energy charges are higher than the off-peak period energy charges for both summer and winter. Thus, after the net loads are flat, accommodating the additional charging demand uniformly in the off-peak layover period is most economical from both the energy and demand charges point of view.

For V2B, with a small charging demand it is economical to discharge during the off and on-peak period peaks, and charge at other times such that the off and on-peak layover period loads become constant, since a constant net load by definition has the smallest peak. The divergence of V2B and V1G electricity costs for a small number of EVs occurs as the V2B EVs – unlike V1G – can discharge during the original off-peak and on-peak period peaks, reducing the NC and OP demand peaks. With further increasing charging demand, once the off peak and on peak period loads are constant, it is most economical to spread out the additional charging demand exclusively over the off-peak layover period, keeping the OP load constant (as shown in Fig. 3.7 above 168 kWh charging demand) for the same reason discussed above for V1G charging. When additional charging demand is accommodated by charging in the off-peak layover period only, V2B offers no further economic advantages over V1G. If the V2B EVs were to discharge at a given time, the same amount of energy would have to be charged at another time and therefore introduce a new peak. Thus, the V1G and V2B electricity costs become parallel after a certain energy demand as the additional energy and demand charges per added vehicle is identical. The trends of the total electricity charges versus the total daily EV energy demand curve for electricity tariff structures other than those in this work are similar to Fig. 3.8 and is discussed in detail in the general applicability of the electricity costs trend, later in Section 3.4.4.

Final slope of total electricity charges versus daily EV charging demand curve

For V0G charging in Jan 2019 and daily charging/energy demand over 24 kWh (see Table 3.3), when the slope of the V0G total electricity charges versus charging demand curve becomes constant (see Fig. 3.8(a)), with every 24 kWh of daily additional EV charging demand ($\Delta\mathrm{CD}_{\mathrm{day}}$), the $\Delta\mathrm{NCDP}$ is 6.6 kW while the $\Delta\mathrm{OPDP}$ is 0, which leads to an increase in the NCDC as $\Delta\mathrm{NCDC} = R_{\mathrm{NC}}(t)\Delta\mathrm{NCDP}$, where $R_{\mathrm{NC}}(t)$ is \$ 24.48/kW. The total charging demand increase in the month is $\Delta\mathrm{CD}_{\mathrm{month}} = \mathrm{Weekdays}\Delta\mathrm{CD}_{\mathrm{day}}$, where

Weekdays=23 for Jan 2019. The entire charging demand is added in the off-peak layover period which leads to increasing monthly energy charges as $\Delta\mathrm{EC}_{\mathrm{month}} = R_{\mathrm{EC}}(t)\Delta\mathrm{CD}_{\mathrm{month}}$, where $R_{\mathrm{EC}}(t)$ is \$0.09506/kWh. Due to the increase in NCDC and energy charges, there is a corresponding increase in other charges as $\Delta\mathrm{OC} = [0.00580 + 0.00030 + 0.00058 + (0.0688 \cdot 0.00580)]\Delta\mathrm{CD}_{\mathrm{month}} + 0.0578(\Delta\mathrm{NCDC} + \Delta\mathrm{EC}_{\mathrm{month}})$.

For the V1G and V2B charging, when the final slopes of their total electricity charges versus daily energy demand curves become constant for a month, further increasing daily charging demand ($\Delta\mathrm{CD}_{\mathrm{day}}$) is accommodated and spread out uniformly over the off-peak layover period. This leads to $\Delta\mathrm{NCDP} = \frac{\Delta\mathrm{CD}_{\mathrm{day}}}{(16\ \mathrm{h} - t_i^j)}$, while the equations governing $\Delta\mathrm{NCDC}$, $\Delta\mathrm{CD}_{\mathrm{month}}$, $\Delta\mathrm{EC}_{\mathrm{month}}$ and $\Delta\mathrm{OC}$ remain the same as those of V0G. The final slope of the V0G, V1G and V2B total electricity charges versus energy daily demand curves, once they become constant for the month, is governed by

$$\mathrm{Slope}_{\mathrm{V0G/V1G/V2B}} = \frac{\Delta\mathrm{NCDC} + \Delta\mathrm{EC}_{\mathrm{month}} + \Delta\mathrm{OC}}{\Delta\mathrm{CD}_{\mathrm{day}}}, \tag{3.11}$$

where the difference between the slopes of V0G and V1G/V2B, once they become constant, is determined by $\Delta\mathrm{NCDP}$ (and hence $\Delta\mathrm{NCDC}$), which are different for V0G and V1G/V2B charging.

Daily EV charging demand when the V1G and V2B total electricity cost versus daily EV charging demand curve transitions to constant slope

The daily V1G charging demand above which the final slope of the total electricity charges versus daily energy demand becomes constant for a month is approximated by calculating the V1G threshold daily charging demand ($\mathrm{CD}_{\mathrm{day,thr,V1G}}$) above which charging takes place in the off-peak layover period only.

For any weekday of the month, for daily charging demands ($\mathrm{CD}_{\mathrm{day}}$) for (and above) which V1G charging takes place in the off-peak layover period only satisfies

$$\mathrm{ED_{org}}(d) + \mathrm{CD_{day}} \geq \mathrm{NCDP_{org}}(16\,\mathrm{h} - t_i^j) + \mathrm{OPDP_{org}}(t_f^j - 16\,\mathrm{h}), \tag{3.12a}$$

where $\mathrm{NCDP_{org}}$ and $\mathrm{OPDP_{org}}$ are the original NCDP and OPDP, respectively. Furthermore, $\mathrm{ED_{org}}(d)$ is the original energy demand during the EV layover period on 'd' day of the month, formulated as $\mathrm{ED_{org}}(d) = \sum_{t_i^j}^{t_f^j - \Delta t} \left(L_{\mathrm{org}}(d,t)\Delta t\right)$.

The V1G threshold daily charging demand is calculated by using an equality operator in (3.12a), for the day of the month when the original energy demand during the layover period is maximum, and is formulated as

$$\mathrm{CD_{day,thr,V1G}} = \mathrm{NCDP_{org}}(16\,\mathrm{h} - t_i^j) + \mathrm{OPDP_{org}}(t_f^j - 16\,\mathrm{h}) - \max \mathrm{ED_{org}}, \tag{3.12b}$$

where $\max \mathrm{ED_{org}}$ is the maximum of $\mathrm{ED_{org}}(d)$ of all weekdays of the month.

If there are no limitations on the optimized charging due to maximum power constraints (as is the case for the 06:30 – 19:30 h EV layover at building V, discussed in Section 3.4.2), (3.12b) accurately predicts the daily V1G charging demand above which the final slope of the total electricity charges versus daily energy demand becomes constant. Otherwise, (3.12b) yields a lower bound.

Ideally, the V2B EVs would discharge at their maximum power back to the grid at the original NC and OP demand peak times resulting in the off-peak and on-peak period loads becoming constant at the reduced off-peak and on-peak demand peaks. After that, charging should take place in the off-peak layover period only. The V2B threshold daily charging demand ($\mathrm{CD_{day,thr,V2B}}$) above which charging takes place in the off-peak layover period only is approximated as

$$\mathrm{CD}_{\mathrm{day,thr,V2B}} = \left[\mathrm{NCDP}_{\mathrm{org}} - p \max \mathrm{EV}^j\right](16\,\mathrm{h} - t_i^j) + \left[\mathrm{OPDP}_{\mathrm{org}} - p \max \mathrm{EV}^j\right](t_f^j - 16\,\mathrm{h}) - \max \mathrm{ED}_{\mathrm{org}}, \tag{3.13a}$$

where p is the number of EVs corresponding to $\mathrm{CD}_{\mathrm{day,thr,V2B}}$.

$$p = \frac{\mathrm{CD}_{\mathrm{day,thr,V2B}}}{\mathrm{CD}_{\mathrm{EV}}}, \tag{3.13b}$$

where $\mathrm{CD}_{\mathrm{EV}}$ is the daily charging demand of one EV.

Combining (3.13a) and (3.13b), we get

$$\mathrm{CD}_{\mathrm{day,thr,V2B}} = \frac{\mathrm{NCDP}_{\mathrm{org}}(16\,\mathrm{h} - t_i^j) + \mathrm{OPDP}_{\mathrm{org}}(t_f^j - 16\,\mathrm{h}) - \max \mathrm{ED}_{\mathrm{org}}}{1 + \frac{\max \mathrm{EV}^j(16\,\mathrm{h} - t_i^j)}{\mathrm{CD}_{\mathrm{EV}}} + \frac{\max \mathrm{EV}^j(t_f^j - 16\,\mathrm{h})}{\mathrm{CD}_{\mathrm{EV}}}} \tag{3.13c}$$

$\mathrm{CD}_{\mathrm{day,thr,V2B}}$ is a lower bound for the daily V2B charging demand above which the final slope of the total electricity charges versus daily energy demand becomes constant. This is because V2B EVs do not discharge at the maximum power at the original NC and OP demand peak times as (3.13c) does not take into account if the EV charging demand is met or not at the time of the EV departure.

$\mathrm{CD}_{\mathrm{day,thr,V2B}} \leq \mathrm{CD}_{\mathrm{day,thr,V1G}}$ because of V2B EV's ability to discharge (V1G is the limiting worst case of V2B). Thus, the threshold daily charging demand above which charging takes place in the off-peak layover period only for both V1G and V2B is decided by $\mathrm{CD}_{\mathrm{day,thr,V1G}}$ calculated from (3.12b).

Final monthly offset between the V1G and V2B total electricity charges

The final monthly offset between V1G and V2B (the difference between the V1G and V2B total electricity charges) once the final slopes of both V1G and V2B total electricity charges versus daily energy demand curves become constant can be approximated for any $\mathrm{CD}_{\mathrm{day}} \geq \mathrm{CD}_{\mathrm{day,thr,V1G}}$. Choosing a $\mathrm{CD}_{\mathrm{day}}$ corresponding to p number of EVs where $\mathrm{CD}_{\mathrm{day}} \geq \mathrm{CD}_{\mathrm{day,thr,V1G}}$, the final monthly offset between V1G and V2B is

$$\begin{aligned}\text{Offset} = {} & R_{\mathrm{NC}}(t)(\mathrm{NCDP}_{\mathrm{V1G}} - \mathrm{NCDP}_{\mathrm{V2B}}) + R_{\mathrm{OP}}(t)(\mathrm{OPDP}_{\mathrm{V1G}} - \mathrm{OPDP}_{\mathrm{V2B}}) \\ & + \left[\sum_{\text{Weekdays}} \left(\mathrm{EC}_{\mathrm{day,V1G}} - \mathrm{EC}_{\mathrm{day,V2B}}\right)\right] + (\mathrm{OC}_{\mathrm{V1G}} - \mathrm{OC}_{\mathrm{V2B}}),\end{aligned} \tag{3.14}$$

where the energy charges (EC) and the OC are calculated for the EV layover period times on weekdays only. Outside the EV layover times, the electricity charges for V1G and V2B are identical and equal to the original electricity charges.

For V1G charging, for the $\mathrm{CD}_{\mathrm{day}}$ above which charging takes place in the off-peak layover period only, $\mathrm{OPDP}_{\mathrm{V1G}}$ is

$$\mathrm{OPDP}_{\mathrm{V1G}} = \mathrm{OPDP}_{\mathrm{org}}. \tag{3.15a}$$

$\mathrm{NCDP}_{\mathrm{V1G}}$ is calculated based on the day of the month when the original energy demand during the layover period is maximum, and is formulated as

$$\mathrm{NCDP}_{\mathrm{V1G}} = \frac{\max \mathrm{ED}_{\mathrm{org}} + \mathrm{CD}_{\mathrm{day}} - \mathrm{OPDP}_{\mathrm{V1G}}(t_f^j - 16\,\mathrm{h})}{16\,\mathrm{h} - t_i^j.} \tag{3.15b}$$

The total daily energy charges are formulated as

$$\mathrm{EC}_{\mathrm{day,V1G}} = \mathrm{EC}_{\mathrm{day,off,V1G}} + \mathrm{EC}_{\mathrm{day,on,V1G}}, \tag{3.15c}$$

where $\mathrm{EC}_{\mathrm{day,V1G}}$, $\mathrm{EC}_{\mathrm{day,off,V1G}}$, and $\mathrm{EC}_{\mathrm{day,on,V1G}}$ are the daily V1G total, off-peak, and on-peak layover energy charges, respectively.

For one weekday, $\mathrm{EC}_{\mathrm{day,off,V1G}}$ and $\mathrm{EC}_{\mathrm{day,on,V1G}}$ are approximated as

$$\mathrm{EC}_{\mathrm{day,off,V1G}} = \sum_{t_i^j}^{16\,\mathrm{h}-\Delta t} \min\left[(L_{\mathrm{org}}(t) + p\max \mathrm{EV}^j),\ \mathrm{NCDP}_{\mathrm{V1G}}\right] R_{\mathrm{EC}}(t)\Delta t, \tag{3.15d}$$

$$\begin{aligned}\mathrm{EC}_{\mathrm{day,on,V1G}} = \Bigg(&\left\{ \sum_{t_i^j}^{t_f^j-\Delta t} L_{\mathrm{org}}(t) \right\} + \frac{\mathrm{CD}_{\mathrm{day}}}{\Delta t} \\ &- \sum_{t_i^j}^{16\,\mathrm{h}-\Delta t} \min\left[(L_{\mathrm{org}}(t) + p\max \mathrm{EV}^j),\ \mathrm{NCDP}_{\mathrm{V1G}}\right] \Bigg) R_{\mathrm{EC}}(t)\Delta t.\end{aligned} \tag{3.15e}$$

For V2B charging, on the day which determines the $\mathrm{OPDP}_{\mathrm{V2B}}$, the EVs charge to their maximum SOC during the off-peak layover to have maximum discharging capability during the on-peak layover. The on-peak layover energy demand ($\mathrm{ED}_{\mathrm{on}}$) on the day which determines the $\mathrm{OPDP}_{\mathrm{V2B}}$ is formulated as

$$\mathrm{ED}_{\mathrm{on}} = p\left\{ \mathrm{BE}^j(t = t_f^j) - \max BE^j \right\}. \tag{3.16a}$$

The $\mathrm{OPDP}_{\mathrm{V2B}}$ is calculated based on the day of the month when the original energy demand during the on-peak layover period is maximum. Let $\mathrm{ED}_{\mathrm{org,on}}(d) = \sum_{16\,\mathrm{h}}^{t_f^j-\Delta t} (L_{\mathrm{org}}(d,t)\Delta t)$ be the original energy demand during the on-peak EV layover period on 'd' day of the month and $\max \mathrm{ED}_{\mathrm{org,on}}$ be the maximum $\mathrm{ED}_{\mathrm{org,on}}(d)$ of all weekdays of the month, then the $\mathrm{OPDP}_{\mathrm{V2B}}$ is formulated as

$$\mathrm{OPDP}_{\mathrm{V2B}} = \frac{\max \mathrm{ED}_{\mathrm{org,on}} + \mathrm{ED}_{\mathrm{on}}}{t_f^j - 16\,\mathrm{h}}. \tag{3.16b}$$

$\mathrm{NCDP}_{\mathrm{V2B}}$ is calculated based on the day of the month when the original energy demand during the layover period is maximum, and is formulated as

$$\mathrm{NCDP}_{\mathrm{V2B}} = \frac{\max \mathrm{ED}_{\mathrm{org}} + \mathrm{CD}_{\mathrm{day}} - \mathrm{OPDP}_{\mathrm{V2B}}(t_f^j - 16\,\mathrm{h})}{16\,\mathrm{h} - t_i^j}. \tag{3.16c}$$

The energy charges for V2B are formulated similar to (3.15c), (3.15d) and (3.15e), with 'V1G' subscripts being replaced by 'V2B'.

Validation of the mathematical approximations for Jan 2019

Table 3.4 shows a comparison between the optimization and analytically derived V0G, V1G and V2B metrics in (3.11) through (3.16) for the 06:30 – 19:30 h layover in Jan 2019. The final V0G, V1G and V2B slopes are predicted without error by the analytical method in (3.11), because charging takes place exactly according to the strategy described in the cumulative results in Section 3.4.4. The $\mathbf{CD}_{\text{day,thr,V1G}}$ is predicted accurately analytically, and the difference between the optimization and analytical values occurs primarily because we increase the daily charging demand in multiples of 24 kWh for the optimization (see discussion of Fig. 3.4(c), where increasing the $\mathbf{CD}_{\text{day}}$ from 192 to 216 kWh changes the off-peak layover period load from 109.0 to 109.5 kW and makes the on-peak period layover load constant at 96.5 kW). If the $\mathbf{CD}_{\text{day}}$ were 211 kWh, both the off-peak and on-peak period layover loads would have been constant at 109.0 and 96.5 kW respectively, after which the excess charging demand is accommodated uniformly in the off-peak layover period). $\mathbf{CD}_{\text{day,thr,V2B}}$ is underpredicted by the analytical method and gives only a lower bound of the actual daily threshold charging demand. $\mathbf{CD}_{\text{day,thr,V2B}}$ is underpredicted because according to (3.13), the V2B EVs are assumed to discharge at their maximum capacity during the original NC and OP demand peaks, resulting in the off-peak and on-peak loads becoming constant at their reduced peaks, without regard for the EV final SOC constraints. The Offset is calculated analytically with high accuracy with the maximum error being less than 6% with respect to the optimization value. The error is caused due to the approximate energy charges in (3.15)(d) and (3.15)(e), and other charges, as the NC and OP demand charges are calculated accurately (not shown in Table 3.4).

For the layover period of 07:45 – 16:45 h, Table 3.4 shows that for Jan 2019, the final V0G, V1G and V2B slopes are predicted exactly by the analytical method. The $\mathbf{CD}_{\text{day,thr,V1G}}$ is underpredicted analytically, and the difference between the optimization and analytical values occurs primarily because above 114 kWh of daily charging demand, additional charging takes place exclusively in the off-peak period, but the charging is non-uniform; only at approximately 144 kWh of daily charging demand, the additional charging demand is spread out uniformly over the off-peak period leading to a constant slope. Like the 06:30 – 19:30 h layover, the Offset is calculated analytically with high accuracy with maximum error being about 1.2%.

Interpretation of the total electricity charges versus daily EV charging demand curve: 06:30 – 19:30 h layover

Figure 3.8(a) shows that for Jan 2019 V0G charging for the 06:30 – 19:30 h layover, the slope becomes constant at $9.6/kWh/day with increasing daily charging demand above 24 kWh. These costs should not be confused with electricity (energy) costs per kWh charged. Since there are 23 weekdays in the month when EV charging occurs, $9.6/kWh/day = $0.42/kWh/month; in other words, the average electricity cost per kWh charged is 42 cents. Since all graphs are presented in kWh of daily EV charging (energy) demand, we chose to continue to report results using the $/kWh/day metric.

For V1G charging, the slope is initially constant at $2.5/kWh/day until 144 kWh of daily charging demand, because charging takes place in the off-peak layover period only, without increasing the NC demand peak over the original. The slope until 144 kWh of daily charging demand can be found from (3.11), with $\Delta\mathbf{NCDC} = 0$. Finally, the V1G slope becomes constant at $5.2/kWh/day with additional daily charging demand above 216 kWh. For V2B charging, the slope is negative initially, then becomes positive and increases to $5.1/kWh/day with increasing daily charging demand up to 168 kWh. With additional charging daily demand above 168 kWh, the slope becomes constant at $5.2/kWh/day,

Table 3.4. Comparison of analytical and optimization results for the two layover periods.

Metric	Symbol	Layover 06:30 – 19:30 h		Layover 07:45 – 16:45 h	
		Optimization	Analytical	Optimization	Analytical
Final V0G slope ($/kWh/day)	$\mathrm{Slope}_{\mathrm{V0G}}$	9.6	9.6	9.6	9.6
Final V1G slope ($/kWh/day)	$\mathrm{Slope}_{\mathrm{V1G}}$	5.2	5.2	5.6	5.6
Final V2B slope ($/kWh/day)	$\mathrm{Slope}_{\mathrm{V2B}}$	5.2	5.2	5.6	5.6
V1G threshold daily charging demand (kWh)	$\mathrm{CD}_{\mathrm{day,thr,V1G}}$	216	211	144	114
V2B threshold daily charging demand (kWh)	$\mathrm{CD}_{\mathrm{day,thr,V2B}}$	168	46	144	33
Final monthly offset ($) between V1G and V2B	Offset	156.4	164.6	97.9	99.0

resulting in parallel V2B and V1G curves above 216 kWh of daily charging demand. The slope of the V2B electricity charges curve increases faster than V1G from 48 to 216 kWh of daily charging demand because the addition of daily charging demand (from 48 kWh to 216 kWh) results in a greater increase of the NC demand peak for V2B as compared to V1G (see Table 3.3 for the V1G and V2B NC and OP demand peaks for the 06:30 – 19:30 h layover). For example, for 72 to 216 kWh of daily charging demand, the OP demand peak remains constant for V1G at 96.5 kW and at 82.4 kW for V2B and does not affect the slope of electricity costs versus daily energy demand curve. On the other hand, the NC demand peak costs increase faster for V2B resulting in a faster increasing slope of electricity costs versus daily energy demand for V2B compared to V1G.

Figure 3.8(b) shows that for the entire year 2019, the slope of V0G charging for the 06:30 – 19:30 h layover, becomes constant at \$114.9/kWh/day above 48 kWh of daily charging demand. For V1G charging, the slope is \$29.4/kWh/day until 120 kWh of daily charging demand, then increases, and becomes constant at \$62.2/kWh/day with daily charging demands above 240 kWh. For V2B charging, the slope is negative up to a daily charging demand of 48 kWh, then becomes positive and increases, and finally becomes constant at \$62.2/kWh/day above 216 kWh of daily charging demand, resulting in parallel V2B and V1G curves above 240 kWh of daily charging demand.

Interpretation of the total electricity charges versus daily EV charging demand curve: 07:45 – 16:45 h layover

Figure 3.9(a) shows that for Jan 2019, until the installation of 72 kWh of V2B charging capacity (or 3 V2B charging stations), the total electricity costs with V2B are lower than the original cost. Figure 3.9(b) shows that for the entire year 2019, until the installation of 48 kWh of V2B charging capacity (or 2 V2B charging stations), the V2B costs are lower than the original costs, making 2 the optimal number of V2B charging station installations for building V as per the yearly analysis for the layover period 07:45 – 16:45

h. In both Figs. 3.9(a) and 3.9(b), similar trends of V2B electricity costs first diverging and then becoming parallel to V1G is seen, as discussed for Figs. 3.8(a) and 3.8(b).

Comparing Fig. 3.9 with Fig. 3.8 shows that less V2B charging stations can be installed for the original electricity costs not to be exceeded for the 07:45 – 16:45 h layover period than the 06:30 – 19:30 h layover period. The shorter layover period provides less opportunities for the V2B EVs to shift demand to times which have low original load, resulting in smaller economic benefits of using V2B for shorter layover periods as compared to longer layover periods.

Figure 3.9(a) shows that for Jan 2019 V0G charging for 07:45 – 16:45 h layover, the slope is \$9.6/kWh/day with increasing daily charging demand above 24 kWh. For V1G charging, the slope is \$2.5/kWh/day until 96 kWh daily charging demand, then increases thereafter, and then becomes constant at \$5.6/kWh/day with the increase of daily charging demand above 144 kWh. For V2B charging, the slope is negative initially up to daily charging demand of 24 kWh, then becomes positive and increases, and becomes constant at \$5.6/kWh/day above 144 kWh, resulting in parallel V2B and V1G curves above 144 kWh daily charging demand.

For the entire year 2019 (see Fig. 3.9(b)) the same trends are observed with final slopes of \$114.9/kWh/day for V0G and \$67.1/kWh/day for V1G and V2B. The V1G and V2B curves become parallel above 216 kWh daily charging demand.

Hypothetical case on the capability of V2G/V2B EVs to shift load from the on to off peak layover period

Here, a hypothetical case of shifting 1.65 kWh of load during the original OP demand peak time in a month, by one V2B/V2G EV (i.e., maximum possible discharging of 6.6 kW at original OP demand peak time) to the entire off-peak layover uniformly is examined. It is assumed that the nature of the original load curve is such that the original and new NC and OP demand peak times are the same, and the V2B/V2G EV's initial

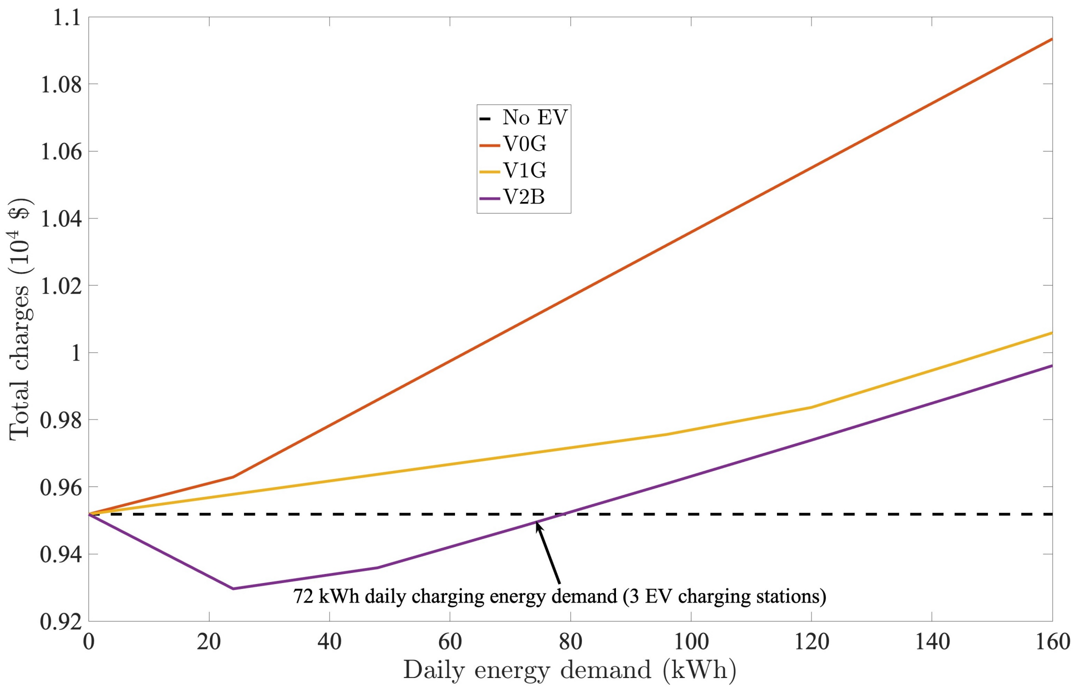

(a)

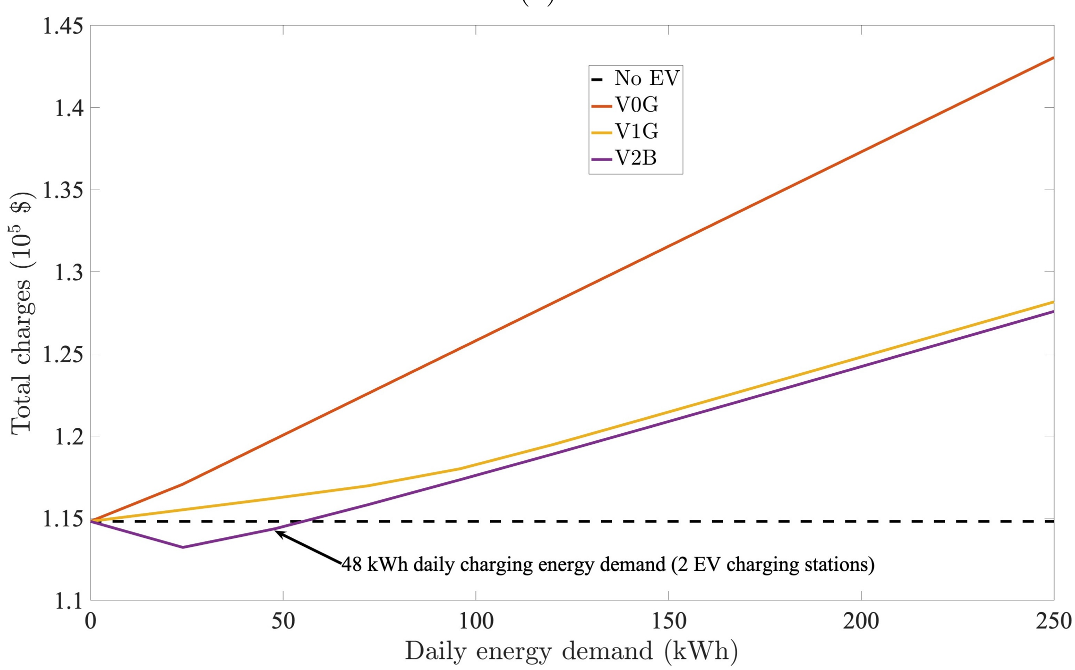

(b)

Figure 3.9. Total electricity charges versus total daily EV energy demand for (a) Jan 2019 and (b) the entire year 2019 for the layover period 07:45 – 16:45 h at building V.

and final SOC is 50 and 90% respectively with $\mathrm{BC} = 60$ kWh. The purpose of this case study is to demonstrate the ability of V2B/V2G charging to decrease on-peak demand and energy charges while increasing non-coincident demand and off-peak energy charges resulting in net cost savings.

The net load reduction of 1.65 kWh during the original OP demand peak time, reduces the OPDP by 6.6 kW ($\frac{1.65}{\Delta t}$), leading to change in OPDC as $\Delta\mathrm{OPDC} = -6.6R_{\mathrm{OP}}(t)$.

The 1.65 kWh load is spread out uniformly in the off-peak layover leading to change in NCDC as $\Delta\mathrm{NCDC} = \frac{1.65}{16\ \mathrm{h} - t_i^j} R_{\mathrm{NC}}(t)$.

The on-peak energy rate is higher than off-peak energy rate and the net EV charging takes place in the off-peak period, leading to change in energy cost, $\Delta\mathrm{EC}$ as $\Delta\mathrm{EC} = \mathrm{CD}_{\mathrm{EV}} R_{\mathrm{EC}}(t)\mathrm{Weekdays} - 1.65\Delta R_{\mathrm{EC}}(t)$, where $\Delta R_{\mathrm{EC}}(t)$ is the difference between the on and off-peak energy rates.

The other charges would also change as $\Delta\mathrm{OC} = \Big(0.00580(1 + 0.0688) + 0.00030 + 0.00058\Big)\mathrm{CD}_{\mathrm{EV}}\mathrm{Weekdays} + 0.0578(\Delta\mathrm{NCDC} + \Delta\mathrm{OPDC} + \Delta\mathrm{EC})$.

The total electricity cost savings are formulated as, $\mathrm{Savings} = -(\Delta\mathrm{NCDC} + \Delta\mathrm{OPDC} + \Delta\mathrm{EC} + \Delta\mathrm{OC})$.

For the rates given in Table 3.2, for the 06:30 – 19:30 h layover in Jan 2019, Savings for this hypothetical case study is $70.4.

General applicability of the optimization model and the trend of the total electricity charges versus total daily EV energy demand curve

Demand charge rates ($/kW) are generally orders of magnitude higher than energy charges ($/kWh) and thus have the most significant impact on the optimized net load. In the tariff structure for our work, we consider off-peak and on-peak energy charges, and NC and OP demand charges. However, the trend of the total electricity charges versus total daily EV energy demand, we have discussed so far (see Fig. 3.8 and Fig. 3.9) applies to a broad range of other utility tariff structures.

Some other typical utility tariffs in the United States are:

(a) off-peak and on-peak energy charges with only NC demand charge.

(b) flat energy charges with only NC demand charge.

(c) flat energy charges with NC and OP demand charge.

The V0G EVs charge at the maximum possible battery power rate irrespective of the pricing model, i.e., Cases (a), (b) or (c).

For Case (a), the V1G EVs initially charge during the off-peak period until the off-peak net load becomes equal to the original NC demand peak. Thereafter, the V1G EVs charge during the on-peak period until the on-peak net load also becomes equal to the original NC demand peak. Thereafter charging takes place by distributing the additional charging demand uniformly over the entire layover period.

For Case (b), the V1G EVs initially charge during the entire layover period until the net load during the entire layover period becomes equal to the original NC demand peak. Thereafter, similar to Case (a), additional charging takes place by distributing the additional charging demand uniformly over the entire layover period.

For Case (c), the V1G EVs initially charge until the net load in the off and on-peak periods become constant at the original NC and OP demand peaks respectively. Thereafter, additional charging takes place by distributing the additional charging demand uniformly over the off-peak layover period, leading to an increasing NC demand peak (with the OP demand peak remaining the same as original).

Thus, the general charging strategy of the V1G EVs, for the tariff structure followed in this work, to charge initially during a period of low energy charge rate without increasing the demand charges, and finally resorting to increasing both demand and energy charges (by distributing the additional charging energy uniformly) once the load is constant in both the off and on-peak periods is applicable for all Cases (a), (b) and (c).

For the V2B charging strategies in Case (a) and Case (b), the V2B EVs discharge during the original NC demand peak and charge at other times until the net load in the entire layover period becomes constant. Thereafter charging takes place by distributing the additional charging demand uniformly over the entire layover period like for V1G.

For Case (c), the V2B EVs initially discharge during the original NC and OP demand peaks, and charge at other times, such that the off and on-peak layover period net loads become constant. Thereafter, additional charging takes place by distributing the additional charging demand uniformly over the off-peak layover period, leading to an increasing NC demand peak, just like V1G.

Thus, the general V2B charging strategy for the pricing model followed in this work, of discharging during the demand peaks, and charging at other times to achieve constant load and then resorting to increasing both demand and energy charges (by distributing the additional charging energy uniformly) similar to V1G is generally applicable.

3.4.5 Overall results for all buildings

To explain the building-to-building differences in the electricity charges associated with EV charging, in this Section we discuss the results for all buildings for one sample initial and final SOC combination (50 and 90% respectively) and one layover period (06:30 – 19:30 h). The initial and final SOC combination is chosen as 50 and 90% respectively to be consistent with the rest of the work.

Figure 3.10 shows that for all buildings, V0G incurs the highest EV charging costs (the difference between post and pre-EV charging building electricity costs), followed by V1G and V2B. For V0G charging, all charging takes place between 06:30 – 10:15 h (see Section 3.4.2). The difference between the V0G EV charging costs from building-to-building is driven by differences in the NCDC. The monthly increase in the NCDC for a building depends on two factors: (a) The intersection of the original NC demand peak time with the time of V0G charging. If the original NC demand peak falls within the

V0G charging time, the post-EV charging new NC demand peak increases at the charging power of the EV; (b) If there is no intersection in (a), the difference between the original NC demand peak and the maximum original load in the month during the V0G charging time. If the original NC demand peak time falls outside the V0G charging time, and the lower the difference between the original NCDP and the maximum original load in the month in the V0G charging time, the higher the chance that a particular number of EV will increase the NCDP. For V0G, most buildings show EV charging cost increases consistent with 6.6 kW per EV of increased NCDP for daily EV energy demand over 100 kWh, but building XIII shows smaller cost increases as the original NC demand peak is much larger than the maximum load during the EV charging time.

Building XIII is also the main outlier for V1G and V2B as the charging can be spread over the layover period such that the building load stays below the original peak demand even for 432 kWh of daily EV charging demand. Therefore, electricity cost increases for building XIII reflect only the additional energy charges and there is no demand charge contribution. For V1G and V2B charging at the other buildings, the variation between the EV charging costs from building-to-building is driven by NCDC, OPDC (only for V2B), and off and on-peak energy costs. For V1G, the electricity costs initially increase with a slope that is consistent with only energy charges from off-peak charging, but eventually transition to a slope consistent with energy and demand charges from constant charging during the off-peak period. The transition occurs mostly between 100 to 400 kWh of charging demand, depending on the building. The smaller the difference between the original demand peaks and the off and on-peak layover period mean loads, the higher the chance that a particular number of EVs will increase the peak demand charges.

For V2B, the final slopes are consistent with the V1G slopes and the ordering of the EV charging costs for high daily EV energy demand is also consistent with V1G. The lower envelope of the initial decrease in V2B electricity costs is consistent with a decrease of 6.6 kW in both NC and OP demand charges, i.e. EVs discharging at full power. Depending on the building, the slope is maintained for up to 3 EVs (72 kWh of charging demand), is followed by a slower decrease (less than 6.6 kW decreases in NC and OP demand charges), and eventually becomes positive as demand charge reductions become infeasible and the energy costs increase, and eventually the demand charge increases dominate. The intersection of the original demand peak times along with the layover period plays a large role for V2B. Specifically, if the original demand peak times do not fall within EV layover time, V2B charging cannot reduce costs.

The results for the total electricity charges (not shown graphically) elucidate that for all three charging strategies, generally, as the mean original real load (proxy for the original load of the buildings) of the buildings increase (see Table 3.1), the total electricity charges also increase, as the demand and energy charges are higher for a building with higher original load.

Table 3.5 shows the optimal number of V2B EV charging stations to be installed at a building such that the original (pre-EV) electricity costs are not exceeded. Generally, for a given month, the larger the difference between the original NCDP and the mean load in the off-peak period, and the original OPDP and the mean load in the on-peak period (as quantified in (3.17)), the more V2B EV charging reduces the NCDC and OPDC. It then follows that the greater the NCDC and OPDC savings, the higher the number of optimal V2B charging stations for a building. Hence, in Table 3.5, we present the optimal number of V2B charging stations as a function of a metric w_{site}, which weights the difference in original peak and mean loads by the off and on-peak layover times averaged over the 12 months in 2019. w_{site} is formulated as

$$
\begin{aligned}
w_{\text{site}} = \text{mean}\Bigg[\Bigg(&\mathbf{NCDP}_{\text{org}}(m') - \text{mean}\Bigg\{\sum_{\substack{d=1\\ d\neq\text{Weekend}}}^{m}\ \sum_{t=0}^{16\,\text{h}-\Delta t} L_{\text{org}}(d,t,m') \\
&+ \sum_{\substack{d=1\\ d\neq\text{Weekend}}}^{m}\ \sum_{t=21\,\text{h}}^{24\,\text{h}-\Delta t} L_{\text{org}}(d,t,m')\Bigg\}\Bigg)\frac{16\,\text{h} - t_i^j}{t_f^j - t_i^j} \\
&+ \Bigg(\mathbf{OPDP}_{\text{org}}(m') - \text{mean}\Bigg\{\sum_{\substack{d=1\\ d\neq\text{Weekend}}}^{m}\ \sum_{t=16\,\text{h}}^{21\,\text{h}-\Delta t} L_{\text{org}}(d,t,m')\Bigg\}\Bigg)\frac{t_f^j - 16\,\text{h}}{t_f^j - t_i^j}\Bigg]
\end{aligned}
\tag{3.17}
$$

where d takes the value of the date index of the month for only weekdays (when EV charging occurs). The month argument is represented by m' in (3.17).

Table 3.5 shows that generally as w_{site} increases, the optimal number of V2B charging stations also increases. The optimal number of V2B charging stations for building XIII is an outlier because, for the EV layover period (06:30 – 19:30 h) considered, for most of the months (9 out of 12) its $\mathbf{NCDP}_{\text{org}}$ occurred outside the layover period and for the remaining 3 months it occurred in the OP period, giving the V2B EVs little chance to reduce the NCDP. For some of the months, the $\mathbf{OPDP}_{\text{org}}$ of building XIII also occurred out of the layover period, further preventing load shifting and electricity cost reduction by V2B.

3.4.6 Sensitivity analyses

In this section, we carry out sensitivity analyses based on the initial and final SOCs of 45 and 85%, 40 and 80%, 50 and 85%, and 50 and 80%, to present the effect of varying the initial and final SOCs on the NC and OP demand charges, energy costs, and total electricity costs for both layover periods for the year 2019. The effect of varying initial and final SOCs on total electricity costs is presented graphically for building V for 2019 in this Section (consistent with the rest of the work), while the variation of all metrics (NC and OP demand charges, energy costs and total electricity costs) for the SOC combinations

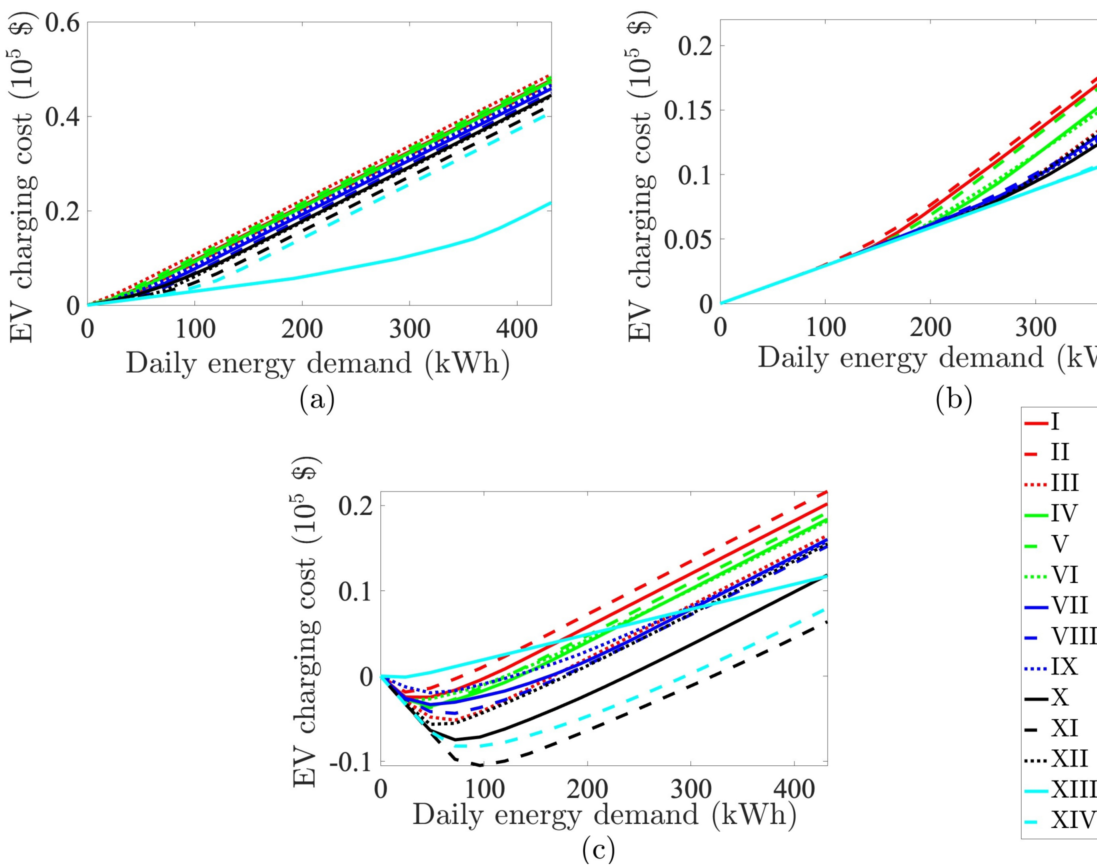

Figure 3.10. EV charging cost versus total daily EV energy demand for all buildings for the 06:30 – 19:30 h layover for the entire year 2019 for initial and final SOC of 50 and 90% respectively for (a) V0G charging, (b) V1G charging, and (c) V2B charging. The legend represents the building number.

Table 3.5. Optimal number of V2B EV charging stations by building. Buildings are arranged in increasing order of w_{site} (3.17).

Building	w_{site}	**Optimal Number of V2B Charging Stations**
II	20.8	3
I	29.2	4
III	38.2	6
VII	40.6	6
IX	42.4	5
V	44.0	5
IV	44.7	5
VII	44.9	6
VI	48.0	5
XII	53.6	7
X	81.6	9
XI	104.0	13
XIII	114.4	1
XIV	134.2	12

with the same daily charging energy demand, for all buildings for both the layover periods are presented in the supplemental tables.

If the final SOC is reduced below 90% (note that for our analyses the maximum and minimum SOC of the EV battery is 20 and 90% respectively), it is possible for the V2B EVs to discharge immediately before disconnecting and therefore further discharge during the on-peak period. In Section 3.4.2, typically the net V2B charging demand during the on-peak period was zero or positive (if charging up to 90% during the off-peak period was not optimal, resulting in net charging during the on-peak period), while in this Section (for final SOCs below 90%) the net V2B charging demand during the on-peak period is expected to be negative (net discharging).

Figures 3.11(a) and 3.11(c) show results for EVs having different initial and final SOCs but the same daily charging energy demand for the 06:30 – 19:30 h and 07:45 – 16:45 h layover, respectively. For a particular layover period, the V0G and V1G total electricity charges are the same if the daily charging energy demand of the EVs is the same, as the

V0G and V1G EV charging costs do not depend on the final SOC because they do not have the ability to discharge. V2B EVs make use of the lower final SOC, to shift demand from the on-peak period to the off-peak period resulting in cost savings, as the on-peak period has higher energy charge rates and additional demand charges over the off-peak period. The V2B total electricity costs decrease for both layover periods as the final SOC decreases from 90 to 80% (with initial SOC decreasing from 50 to 40%) because the smaller the final SOC the more flexibility for discharging during the on-peak period. The strategy of V2B EVs to discharge more during the on-peak period as final SOC decreases from 90 to 80% is accompanied by more charging during the off-peak period, which ultimately leads to net total electricity cost savings, i.e., the decrease in the on-peak periods costs is greater than the increase in the off-peak period costs.

Figures 3.11(b) and 3.11(d) correspond to EVs having different final SOCs (with initial SOC fixed at 50%) and thus different daily charging energy demand for the 06:30 – 19:30 h and 07:45 – 16:45 h layovers, respectively. The total electricity charges for both layover periods for all charging strategies are smallest for a final SOC of 80% and increase as the final SOC increases to 85 to 90%. The smaller cost for V0G and V1G, for lower final SOCs is due to the smaller total charging energy demand (as initial SOC is fixed at 50%). The V1G costs decrease more than V0G because, as the final SOC (and thus charging demand) decreases, the V1G average load (and therefore incremental NCDC) is proportional to the charging demand per (3.15b), as opposed to V0G which charges without regard for the original load curve and costs. For V2B, in addition to the former point, there is an added benefit of more discharging potential during the on-peak period when the final SOC is lower than 90%. The sensitivity analyses (comparison between Figs. 3.11(a) & 3.11(c), and 3.11(b) & 3.11(d)) also show that the shorter layover period of 07:45 – 16:45 h leads to higher total electricity charges compared to the longer layover period of 06:30 – 19:30 h for all charging strategies for any particular initial and final SOC combination.

The three supplemental tables present the results with initial and final SOC of 50 and 90%, 45 and 85%, and 40 and 80%, respectively.

3.4.7 A realistic case using historical data

A realistic case study is carried out using historical EV data of charging records available from ChargePoint at UC San Diego. The relevant historical data used in this analysis are the time of EV connection and disconnection, end of charging, charging demand, initial and final SOC (for a subset of events only), EVSE IDs, and port type (Level 2 (L2) and Direct Current Fast Chargers (DCFC)). For a data sample, see [58]. Originally the EVs were charged with the V0G charging strategy, which did not make use of the flexibility afforded by the complete layover time, i.e., originally the EVs charged too quickly when more suitable later times were available for charging.

The EV battery capacity is required to understand the EV discharging or delayed charging opportunities. The ChargePoint data does not (directly) contain the EV (rated) battery capacity data, but the initial and final SOCs are given for 5,754 out of the total of 168,122 charging events that occurred between March 15, 2016 and August 4, 2020. For the 5,754 events, EV battery capacity is calculated as $\mathbf{BC}^j = \frac{\mathrm{ED}^j}{(\mathrm{SOC}_f^j - \mathrm{SOC}_i^j)}$. We observe an anomaly for five charging events, for which the calculated battery capacity is above 200 kWh. We remove these five datapoints from our analysis as most EVs have a battery capacity below 200 kWh [63]. To impute the missing EV battery capacity for the remaining 162,368 charging events, we randomly draw data from the calculated battery capacity (5,749 events).

Following these calculations, we set the following charging constraints: (i) The missing final SOC is initially imputed by randomly drawing from the given 'valid' final SOCs. (ii) The missing initial SOC is calculated from the final SOC, energy demand, and the EV battery capacity data as $\mathbf{SOC}_i^j = \mathbf{SOC}_f^j - \frac{\mathrm{ED}^j}{\mathrm{BC}^j}$. (iii) If the $\mathbf{SOC}_i^j$ is calculated as less than 0% by (ii), it is corrected and fixed at 0% as the SOC range for the analyses

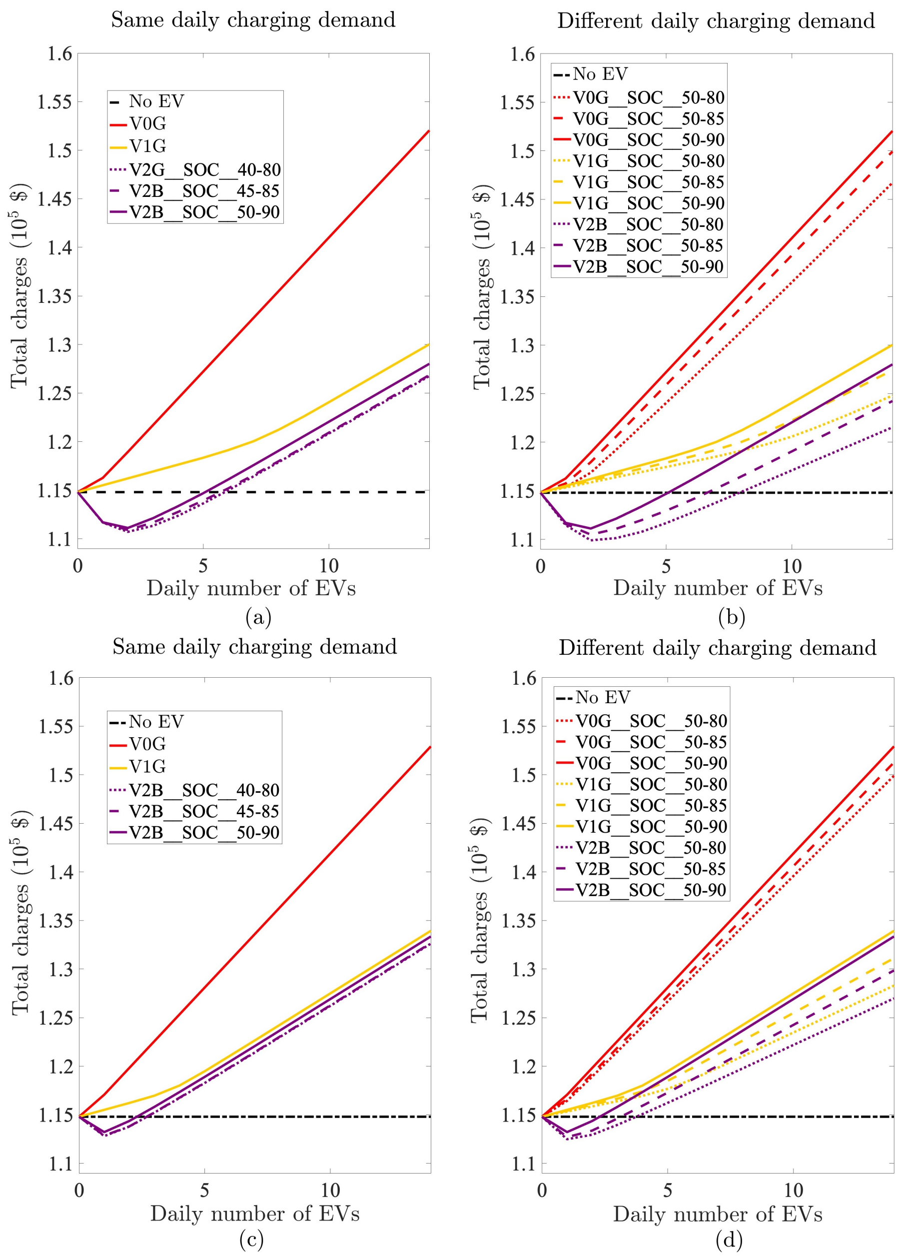

Figure 3.11. Total electricity charges versus daily number of EVs for the for the entire year 2019 for the layover period (a, b) 06:30 – 19:30 h, and (c, d) 07:45 – 16:45 h, at building V for (a, c) same daily charging demand with initial and final SOCs being 40 and 80%, 45 and 85%, and 50 and 90%, respectively, and (b, d) different daily charging demand with initial and final SOCs being 50 and 80%, 50 and 85%, and 50 and 90%, respectively. The legends in the figure correspond to the charging strategies along with their initial and final SOCs. For example, V0G_ SOC_50-80 indicates V0G charging with initial and final SOC of 50 and 80% respectively.

is 0 – 100%. Correspondingly the battery capacity is again updated for that EV as $\mathrm{BC}^j = \frac{\mathrm{ED}^j}{(\mathrm{SOC}_f^j - \mathrm{SOC}_i^j)}$, for which $\mathrm{SOC}_i^j = 0$. (iv) The maximum charging and discharging rate of EVs is 7.2 kW for L2 and 50 kW for DCFC. The input variables for the realistic analysis are shown in Table 3.6.

Table 3.6 shows that the data sampling interval is chosen as 1 hour instead of 15 minutes as for the uniform fleet Case study (i), because of unreasonably long run-times for 15-minute timesteps in the realistic case study. The actual time of EV connection and disconnection is mapped onto the hourly scale, depending on the minute of the hour of the connection or disconnection from the charging station. Initially the EV connection and disconnection time is rounded up to the nearest hour. For example, if an EV originally connects at 00:29 h and disconnects at 1:35 h on the same day, it is assumed in our algorithm that the EV connects at 00:00 h and disconnects at 02:00 h on that day. After the initial rounding to the nearest hour, a correction is implemented for the EVs that have the same connection and disconnection time. In these cases, the connection time is assumed to be the beginning of the hour and the disconnection time is assumed to be the end of the hour. For example, if an EV originally connects at 16:45 h and disconnects at 16:59 h on the same day, rounding to the nearest hours would cause both the connection and disconnection time to be 17:00 h on that day. The correction assumes that the EV connects at 16:00 h and disconnects at 17:00 h.

Our analysis is carried out for 5 weekdays of February 2020. The EV charging stations are located in the Osler Parking Structure. The Osler Parking Structure is chosen for the analysis as it consists of 16 L2 (with 14 being in use for this analysis) and 2 DCFC fast chargers which is representative of an EV charging station installation infrastructure at a single location [64]. The total load of the Osler Parking Structure EV charging stations is mapped to a single building having 0 original load, i.e. the optimized EV load is assumed to equal the final building net load. As per the original V0G charging schedule the NC demand peak occurs on Feb 14, 2020, we choose the weekdays Feb 10 to Feb 14, 2020 for the analyses, so that the NC demand peak is representative for the entire month of February 2020. 338 charging events occur from Feb 10 through 14, 2020, with average layover, charging time, and energy demand of 3 h 29 minutes, 1 h 38 minutes, and 9.8 kWh respectively, with 256 events occurring at L2 chargers and 82 events occurring at DCFC chargers. 251 charging events at L2 chargers have charging flexibility, whereas all the events at DCFC chargers have charging flexibility (i.e. $(t_f^j - t_i^j)\max \mathrm{EV}^j > \mathrm{ED}^j$). Since there are some inconsistencies in the dataset, the final EV energy demand is corrected for 5 L2 charging events by charging at maximum power during the entire layover period (refer to (3.9)). The objective function minimized is (3.1), with the cost components (NC and OP demand charges, energy charges, and other charges) being adjusted for 5 days instead of the entire month.

Figure 3.12(a) shows the timeseries for February 10 through February 14, 2020 for all 3 charging strategies. Figure 3.12(b) shows the NC and PP demand charges along with the total electricity costs for our analysis. The total electricity costs incurred by the EVs based on the original V0G charging, and the optimized V1G and V2G charging are \$5,694, \$3,402, and \$2,598 respectively. The results show that the V2G and V1G charging strategies results in 54.4% and 40.3% total electricity cost savings, respectively over the original V0G charging schedule.

Table 3.6. Inputs for the realistic case study

Metric	**Symbol**	**Value**
Maximum charging rate of L2 chargers	$\max \mathrm{EV}_{\mathrm{L2}}^j$	7.2 kW
Maximum charging rate of DCFC chargers	$\max \mathrm{EV}_{\mathrm{DCFC}}^j$	50 kW
Data sampling interval	Δt	1 hour

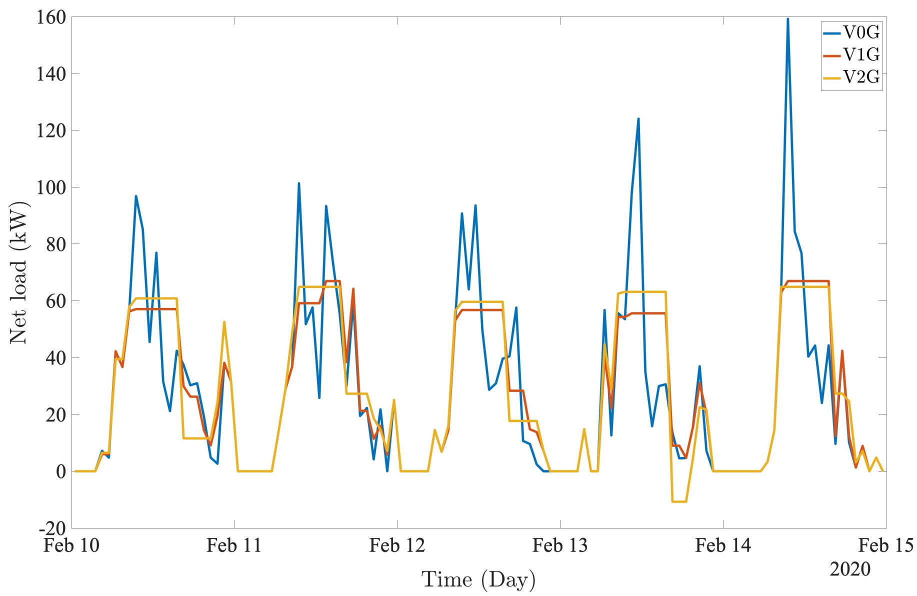

(a)

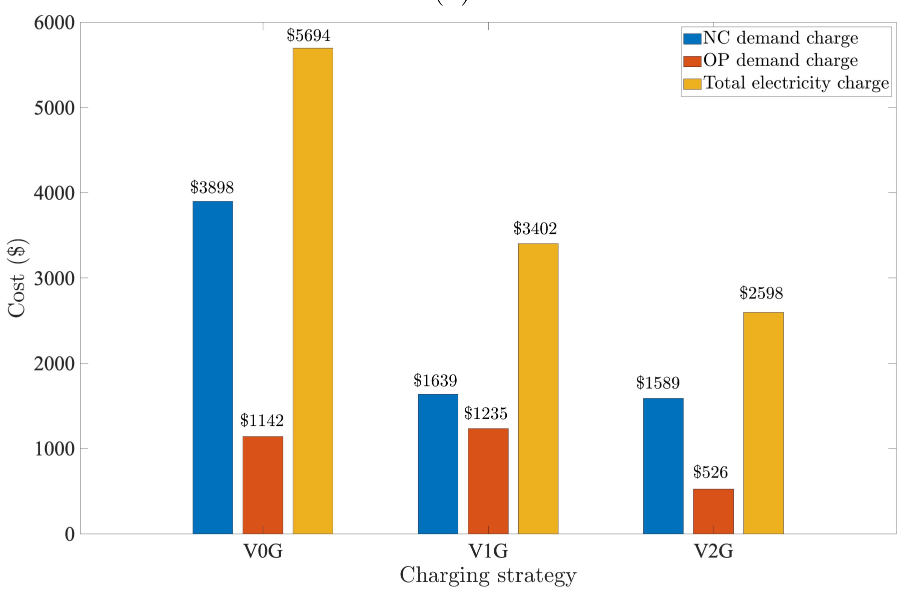

(b)

Figure 3.12. (a) Original (V0G) and optimized net load (= EV charging) timeseries analysis, and (b) Electricity cost components for the 3 charging strategies, for the realistic case study from February 10 through 14, 2020. The total electricity charges in (b) differ from the sum of the NC and OP demand charges because they also include energy charges.

Acknowledgements

This chapter, in full, is a reprint of the material as it appears in ‘Effects of number of electric vehicles charging/discharging on total electricity costs in commercial buildings with time-of-use energy and demand charges’ authored by Avik Ghosh, Monica Zamora Zapata, Sushil Silwal, Adil Khurram, and Jan Kleissl, in the Journal of Renewable and Sustainable Energy, 2022. The dissertation author was the primary investigator and author of this paper.

Part II

Computationally inexpensive real-time MPC algorithms

Chapter 4

Adaptive relaxation-based nonconservative chance constrained SMPC

4.1 Problem statement

Chance constrained SMPCs trade-off full constraint satisfaction for economical plant performance under uncertainty, making it particularly attractive for reducing monthly electricity costs of MGs. However, over-conservativeness in constraint violations can result in less-than-desired cost savings. Most past works mitigate this over-conservativeness by leveraging a-priori information about the uncertainty set, limiting their application. In this chapter, inspired by economical BESS dispatch, we seek to develop a computationally inexpensive adaptive relaxation-based SMPC framework for generic discrete LTI systems with unknown uncertainty distribution, statistics, or samples — for provable nonconservative chance constraint satisfaction in closed-loop.

4.2 Problem formulation

4.2.1 System description

The dynamics of the discrete LTI system are governed by

$$x(t+1) = Ax(t) + Bu(t) + Ew(t), \qquad \forall t, \tag{4.1}$$

where $A \in \mathbb{R}^{n \times n}$, $B \in \mathbb{R}^{n \times m}$, and $E \in \mathbb{R}^{n \times p}$.

Assumption 4.1 (**System**). *(a) At each time t, a measurement of the state is available. (b) The set of admissible control inputs $\mathbb{U}$ and states $\mathbb{X}$ are polytopes containing the origin.*

Assumption 4.2 (**Uncertainties**). *The set of uncertainties $\mathbb{W}$ is bounded and contains the origin.*

In this setup, $\mathscr{F} = \sigma(\{w : w(t) \in \mathbb{W}\} : t \in \mathbb{T})$, and $\mathscr{F}_t = \sigma(\{w(s) : w(s) \in \mathbb{W}\} : s < t)$. The system is subject to hard control input constraints and chance constraints on states. The control input constraints are formulated as,

$$Su(t) \leq s, \qquad \forall t, \tag{4.2}$$

where $S \in \mathbb{R}^{q \times m}$, $s \in \mathbb{R}^q$. The time-varying equality constraints coupling the control inputs are formulated as,

$$Mu(t) = c(t) + Fw(t), \qquad \forall t, \tag{4.3}$$

where $M \in \mathbb{R}^{d \times m}$, $c \in \mathbb{R}^d$, and $F \in \mathbb{R}^{d \times p}$. In previous works like [21], (4.3) is not considered but for applications such as economic MG dispatch, (4.3) is important for incorporating physical constraints such as power balance of the MG with the main grid (discussed in detail in Section 4.2.6). However, if (4.3) is considered in the problem formulation, the $Ew(t)$ term in the RHS of (4.1) is dropped as the $Fw(t)$ term in the RHS of (4.3) accommodates the uncertainty.[1] Additionally, note that constraint (4.3) is application specific and is independent of the method and theoretical results presented in this work. The chance constraints on the states are formulated as,

$$\mathbb{P}[Gx(t) \leq g] \geq \bar{1} - \bar{\alpha}, \qquad \forall t, \tag{4.4}$$

[1] The E matrix is still required for assigning a unique control input after accommodating the uncertainty in closed-loop for multi-input systems. See details in Section 4.2.6.

where $G \in \mathbb{R}^{r\times n}$, $g \in \mathbb{R}^r$ and $\bar{1} = \mathbb{1}^r$ for individual chance constraints. $\bar{\alpha} = [\alpha_1, \ldots, \alpha_r]^\top$ is the vector of the pointwise-in-time maximum probability of constraint violation, where $\alpha_i \in (0, 0.5)$ $\forall i \in \mathbb{N}_1^r$. In the individual chance constraint form, (4.4) can be expressed as, $\mathbb{P}[G_i x \leq g_i] \geq 1-\alpha_i, \quad \forall i \in \mathbb{N}_1^r$. In the joint chance constraint (JCC) form, a single violation probability denoted by $\alpha \in (0, 0.5)$ can be defined for simultaneous satisfaction of all state constraints as,

$$\mathbb{P}[G_1 x \leq g_1 \wedge G_2 x \leq g_2 \wedge \cdots \wedge G_r x \leq g_r] \geq 1-\alpha.$$

Note that in this work, we re-interpret the maximum probability of violation of state constraints pointwise-in-time given by the chance constraints (4.4) as the maximum time-average of state constraint violations in closed-loop similar to [21, 22, 24, 41, 42]. $Gx(t) \leq g$ is referred to as the original constraint with respect to which violations are measured.

4.2.2 Online Adaptive SMPC (OA-SMPC)

Over the MPC prediction horizon N, computed from time t, we define the ordered collection of states, control inputs, uncertainties and coupling vectors as,

$$\begin{aligned}
\mathbf{x}(t+1) &:= \Big(x(t+1|t), x(t+2|t), \ldots, x(t+N|t)\Big)^\top \in \mathbb{R}^{Nn}, \\
\mathbf{u}(t) &:= \Big(u(t|t), u(t+1|t), \ldots, u(t+N-1|t)\Big)^\top \in \mathbb{R}^{Nm}, \\
\mathbf{w}(t) &:= \Big(w(t|t), w(t+1|t), \ldots, w(t+N-1|t)\Big)^\top \in \mathbb{R}^{Np}, \\
\mathbf{c}(t) &:= \Big(c(t|t), c(t+1|t), \ldots, c(t+N-1|t)\Big)^\top \in \mathbb{R}^{Nd}.
\end{aligned}$$

The system dynamics can be written in expanded form as

$$x(t+k|t) = A^k x(t|t) + \sum_{i=0}^{k-1} A^{k-1-i} B u(t+i|t) + \sum_{i=0}^{k-1} A^{k-1-i} E w(t+i|t), \qquad \forall k \in \mathbb{N}_1^N, \forall t, \tag{4.5}$$

where $x(t|t) = x(t)$. Writing (4.5) in compact form yields,

$$\mathbf{x}(t+1) = \mathbf{A}x(t) + \mathbf{B}\mathbf{u}(t) + \mathbf{E}\mathbf{w}(t), \qquad \forall t, \tag{4.6}$$

where $\mathbf{A} \in \mathbb{R}^{Nn\times n}$, $\mathbf{B} \in \mathbb{R}^{Nn\times Nm}$ and $\mathbf{E} \in \mathbb{R}^{Nn\times Np}$.

The hard control input constraints over the MPC prediction horizon are formulated as,

$$Su(t+k|t) \leq s, \qquad \forall k \in \mathbb{N}_0^{N-1}, \forall t. \tag{4.7}$$

The equality constraints coupling the control inputs over the MPC prediction horizon are formulated as,

$$Mu(t+k|t) = c(t+k|t) + Fw(t+k|t), \qquad \forall k \in \mathbb{N}_0^{N-1}, \forall t. \tag{4.8}$$

Generally, the chance constraints in (4.4) are interpreted for the MPC prediction horizon pointwise-in-time by (4.9a), which is over-conservative in closed-loop (see Remark 4.3). The corresponding relaxed deterministic reformulation of (4.9a) as implemented in the MPC prediction horizon by some previous works [21, 22] is given by (4.9b). The aim of the deterministic reformulation is to tighten the state constraints under nominal MPC computations (resulting from ignoring uncertainties, i.e., $\mathbf{w}(t) = \mathbf{0}$) by an adaptive tightening parameter $\tilde{h} \in \mathbb{R}^r$ given by,

$$\mathbb{P}[Gx(t+k|t) \leq g] \geq \bar{1} - \bar{\alpha}, \qquad \forall k \in \mathbb{N}_1^N, \forall t, \tag{4.9a}$$

$$Gx(t+k|t) \leq g - \tilde{h}(t+k|t), \qquad \forall k \in \mathbb{N}_1^N, \forall t, \mathbf{w}(t) = \mathbf{0}, \tag{4.9b}$$

where $\tilde{h}_i > 0$, $\forall i \in \mathbb{N}_1^r$ and is updated based on the time-average of past state constraint violations in closed-loop. Note that violations of state constraints (i.e., $Gx(t) > g$) can occur in closed-loop, as the uncertainties come into effect. The adaptive constraint tightening in (4.9b) attempts to reduce the conservatism inherent to (4.9a) by incorporating past state constraint violation behavior of the system in closed-loop, but can still be over-conservative (see Remark 4.3).

Remark 4.3 (Over-conservativeness of previous approaches). (4.9a) *approximates* (4.4) *conservatively [22], [24, Sec. II-A], as* (4.9a) *requires the constraint satisfaction conditionally on $x(t)$ (i.e., for $x(t)$ that can be reached at time t by the given control policy under the uncertainty sequence). Equation* (4.4)*, however, requires constraint satisfaction in a more relaxed average sense (i.e., over all realizations of the uncertainty sequence up to t). Moreover,* (4.9a) *does not consider the memory of past state constraint violations which is critical in the present time-average re-interpretation of chance constraints. Incorporating past constraint violations by using the adaptive tightening in* (4.9b) *can still be conservative in satisfying* (4.4) *in closed-loop due to the over-estimation of the tightening parameter $\tilde{h}$ [22]. Additionally, in* (4.9b)*, the nominal MPC solutions never violate the state constraints over the prediction horizon, as a result of restricting the size of the feasible state set (despite a larger feasible state set being available to the controller as compared to the nominal MPC when accommodating for uncertainty), which the MPC optimizer can theoretically exploit to further reduce conservativeness in closed-loop.*

Based on Remark 4.3, which shows that both (4.9a) and (4.9b) can be over-conservative in satisfying (4.4) in closed-loop, we propose to adaptively relax the state constraints in the nominal MPC instead of tightening them. The adaptive relaxation allows for state constraint violations over the nominal MPC prediction horizon ($Gx(t+k|t) > g$ with $\mathbf{w}(t) = \mathbf{0}$), to *push* the system towards reduced conservativeness. We relax the satisfaction of (4.9a) and approximate (4.4) by reformulating the nominal state constraints as,

$$Gx(t+k|t) \leq g - h(t), \qquad \forall k \in \mathbb{N}_1^N, \forall t, \mathbf{w}(t) = \mathbf{0}, \tag{4.10}$$

where $h \in \mathbb{R}^r$ is the adaptive relaxing parameter with $h_i < 0$, $\forall i \in \mathbb{N}_1^r$. It should be noted that the sign of h_i in (4.10) is opposite to $\tilde{h}_i$ in (4.9b). We also observe that decreasing $h(t)$ in (4.10) expands the feasible state set, pushing the system more towards state constraint violations (i.e., $Gx(t+k|t) > g$), while increasing $h(t)$ contracts the feasible state set pulling the system away from state constraint violations.[2] The initial value of h at $t = 0$ can be calculated based on domain knowledge [65], which obviates the requirement of past uncertainty samples, as in [21]. The initial value of h is not important since h gets adapted as the system evolves with time [25]. The ordered collection of adaptive relaxation parameters along the MPC prediction horizon is denoted as,

$$\mathbf{h}(t) := \Big(h(t), h(t), \ldots, h(t)\Big)^\top \in \mathbb{R}^{Nr}.$$

The nominal OA-SMPC, which is assumed to be a convex optimization problem is then formulated as,

$$\mathbf{u}^*(t) = \underset{\mathbf{u}(t) \in \mathbb{R}^{Nm}}{\arg\min}\ J(t, x(t), \mathbf{u}(t), \mathbf{w}(t) = \mathbf{0}), \tag{4.11a}$$

subject to

$$\mathbf{x}(t+1) = \mathbf{A}x(t) + \mathbf{B}\mathbf{u}(t), \tag{4.11b}$$

$$\mathbf{S}\mathbf{u}(t) \leq \mathbf{s}, \tag{4.11c}$$

$$\mathbf{M}\mathbf{u}(t) = \mathbf{c}(t), \tag{4.11d}$$

[2]Note that in economic MG dispatch with BESS in VRE grids, where the objective function is the actual economic cost of system operation like the electricity bill, and not necessarily only a penalty on the control input (BESS dispatch), relaxing the state constraints in the nominal MPC does not automatically lead the system to predicted nominal solutions that violate the (original) state constraints pathologically over the nominal MPC prediction horizon. The state (BESS SOC), in these applications tries to exploit the full feasible state set to best reduce economic cost for the MPC prediction horizon. Nevertheless, the case where the proposed formulation can result in pathological constraint violations is averted in closed-loop by a post-processing step described later in Section 4.2.6 and Remark 4.20.

$$\mathbf{G}\mathbf{x}(t+1) \leq \mathbf{g} - \mathbf{h}(t). \tag{4.11e}$$

where $J : \mathbb{R}^n \times \mathbb{R}^{Nm} \times \mathbb{R}^{Np} \to \mathbb{R}$ is an arbitrary convex function, $\mathbf{S} \in \mathbb{R}^{Nq \times Nm}$, $\mathbf{s} \in \mathbb{R}^{Nq}$, $\mathbf{M} \in \mathbb{R}^{Nd \times Nm}$, $\mathbf{c} \in \mathbb{R}^{Nd}$, $\mathbf{G} \in \mathbb{R}^{Nr \times Nn}$, $\mathbf{g} \in \mathbb{R}^{Nr}$. Note that dropping (4.11d) makes the problem setup similar to [21]. Note that in (4.11e), the MPC state constraints are applied for $x(t+k|t)$, $\forall k \in \mathbb{N}_1^N$, and not for the present state corresponding to $k=0$ to allow for the present state to be outside of the feasible state set of the nominal OA-SMPC. Assumption 4.4, discussed next, ensures recursive feasibility and existence of an ideal control policy (described later in Assumption 4.8).

Assumption 4.4 (**Control inputs [21]**). *(a) The control input constraints* (4.11c) *are such that the system can provide enough control input to bring the predicted state at the next time-step, from any present state $x(t)$, to the feasible region of the nominal OA-SMPC* (4.11e). *Specifically,*

$$\exists\, u(t|t) \;\; s.t. \;\; Su(t|t) \leq s,\, Mu(t|t) = c(t|t),$$
$$G(x(t+1|t)) \leq g - h(t),$$

where $x(t+1|t) = Ax(t) + Bu(t|t)$, for all t. (b) The system is one step controllable.

The condition for testing Assumption 4.4(a) which ensures recursive feasibility (similar to [21, 66]) of the nominal OA-SMPC is given in the Appendix in Section 7.1.1, and is excluded here for brevity. Assumption 4.4(a) ensures that after handling the uncertainty from the previous time step in closed-loop, resulting in the present state $x(t)$, which may be outside the feasible state set of the nominal OA-SMPC (4.11e), the computed control input is strong enough to bring the predicted system state at the next time-step back to the feasible state set.

Assumption 4.4(a), while theoretically can be, is generally not restrictive for practical applications such as MGs or HVAC systems, as these systems are generally designed to be able to have enough control input power to be able to handle uncertainties [21]. Assumption 4.4(b) is more restrictive and is only used for ensuring sufficient conditions for the existence of an ideal control policy at every time step (see Assumption 4.8). Assumption 4.4(b) can be relaxed for practical applications such as the one described in the case study in Section 4.3.

Remark 4.5 (**Structure of the input matrix**). *Note that Assumption 4.4(b) is sufficient for saying that the system has at least as many control inputs as states (i.e., $n \leq m$) and B has full row rank. The assumption implies that if $n = m$, B has an inverse, while if $n < m$, B has a right inverse.*

Assumption 4.6 (**Form of the *h* update rule**). *The online h (adaptive relaxing parameter) update rule can be written as $h_i(t) := h_i(t-1)[1+K_i(t)]$, where $K_i(t) > -1$, $\forall t$ ensures $h_i(t) < 0$, $\forall t$ [65, Eq. (12)].*

Remark 4.7 (**Behavior of the *h* update rule**). *In Assumption 4.6, $K_i(t) > 0$ decreases $h_i(t)$, expanding the state constraints, pushing the system more towards state constraint violations, while $K_i(t) < 0$ increases $h_i(t)$, contracting the state constraints, pulling the system away from state constraint violations.*

4.2.3 Observed violations

In this section, for consistency with earlier works like [21], we drop (4.3) and (4.11d). Thus, the nominal OA-SMPC computed optimal control inputs for the first time-step of the prediction horizon are implemented in closed-loop. The observed states get corrected once the uncertainties are realized, by using (4.1). The case where (4.3) and (4.11d) are considered in the problem formulation is discussed in Section 4.2.6 which additionally post-processes the nominal OA-SMPC computed control inputs to correct for the uncertainty.

Without loss of generality, consider the i^{th} state constraint in (4.4). Let $V_i(t+1) \in \{0,1\}$ track whether the state constraint is violated in closed-loop at time $t+1$, while

$Y_i(t+1) \in [0,1]$ keeps track of the time-average of violations up to time $t+1$. Note that the control input applied at time t (along with the uncertainty realized at t) is manifested with updated system states, which can be observed only at $t+1$, i.e., there is 1 time-step delay in observing violations (or non-violations) from the time when the control inputs and uncertainties are applied.

$$V_i(t+1) := \begin{cases} 1, & G_i(Ax(t)+Bu^*(t|t)+Ew(t)) > g_i, \\ 0, & G_i(Ax(t)+Bu^*(t|t)+Ew(t)) \leq g_i. \end{cases} \tag{4.12a}$$

$$Y_i(t+1) := \frac{\sum_{j=1}^{t+1} V_i(j)}{t+1}. \tag{4.12b}$$

The framework for tracking the state constraint violations and time-average of violations in the case of JCC, is the same as that of the individual chance constraints described in (4.12). The only difference in the case of JCC is that a violation occurs if any one of the constraints (involved in the JCC) violates its specific state constraint bounds in closed-loop.

4.2.4 Convergence properties of $Y(t)$

In this section, like 4.2.3, without loss of generality, we limit our discussion to the i^{th} state constraint in (4.4) with $i \in \mathbb{N}_1^r$, with its corresponding adaptive relaxation parameter $h_i \in \mathbb{R}_{0-}$. The conditions established for ensuring the convergence of the time-average of state constraint violations to the maximum allowable violation probability in this work uses a similar simplifying assumption as in [21]. The simplifying assumption (see Assumption 4.8) allows the controller to apply ideal control inputs at the current time-step leading to a desired probability of violation of state constraints at the next time-step, under unknown bounded uncertainties.

Denote by $Z_i(t) = |\alpha_i - Y_i(t)|$ the absolute difference between the maximum allowable violation probability and time-average of violations of the i^{th} state constraint observed at time t. We have to ensure that Y_i tends to α_i in closed-loop as the system evolves with time for nonconservative chance constraint satisfaction. The nonconservative strategy ideally leads to lower costs without violating the state constraints beyond the maximum allowable violation probability.

As $Z_i(t)$ is non-negative, the convergence of Z_i can be guaranteed a.s., if $Z_i(t)$ is a supermartingale [56]. The three conditions for Z_i being a supermartingale are investigated below:

(a) Let $\mathscr{F}_t = \sigma(\{w(0), w(1), \ldots, w(t-1)\})$ be a σ-algebra on uncertainties realized up to time $t-1$. $Z_i(t)$ depends on $Y_i(t)$, which depends on the realization of all the uncertainties up to time $t-1$. Since $Z_i(t)$ is exactly known with information available up to time $t-1$, $Z_i(t)$ is $\mathscr{F}_t$ measurable $\forall t > 0$, and is thus adapted. Also, since $Z_i(t+1)$ is random with information available in $\mathscr{F}_t$, the process Z_i is stochastic.

(b) As $V_i(t) \in \{0,1\}$, $Y_i(t) \in [0,1]$, and $\alpha_i \in (0, 0.5)$, thus $Z_i(t) = |\alpha_i - Y_i(t)| \in [0,1)$. Thus, $\mathbb{E}[|Z(t)|] < 1 < \infty, \quad \forall t > 0$.

(c) It remains to show $\mathbb{E}[Z_i(t+1)|\mathscr{F}_t] \leq Z_i(t)$ a.s., $\forall t > 0$, which we will show to hold under similar simplifying assumptions as in [21]. The assumption involves replacing the stochastic $Z_i(t+1)|\mathscr{F}_t$ by its ideal surrogate $Z_i^*(t+1)|\mathscr{F}_t$ as explained next.

From (4.12b) $Y_i(t+1)$ can be written as,

$$Y_i(t+1) = \sum_{j=1}^{t+1} \frac{V_i(j)}{t+1} = t\frac{Y_i(t)}{t+1} + \frac{V_i(t+1)}{t+1}. \tag{4.13}$$

Denoting $\mathbb{E}[Z_i(t+1)|\mathscr{F}_t] - Z_i(t)$ by $\Delta_i(t)$ and substituting (4.13) in $\Delta_i(t)$ results in,

$$\Delta_i(t) = \mathbb{E}\left[\left|\alpha_i - t\frac{Y_i(t)}{t+1} - \frac{V_i(t+1)}{t+1}\right| |\mathscr{F}_t\right] - |\alpha_i - Y_i(t)|. \tag{4.14}$$

Let $p_i(t+1) := \mathbb{P}(V_i(t+1) = 1|\mathscr{F}_t)$, which means that $p_i(t+1)$ is the probability of observing a constraint violation at time $t+1$. Similarly, $1-p_i(t+1)=\mathbb{P}(V_i(t+1)=0|\mathscr{F}_t)$ is the probability of not observing a violation at time $t+1$. We notice that the only stochastic part within the expectation in the RHS of (4.14) is $V_i(t+1)$ based on $\mathscr{F}_t$. Therefore, (4.14) can be rewritten in terms of $p_i(t+1)$ to replace the expectation as,

$$\Delta_i(t) = p_i(t+1)\left[\left|\alpha_i - t\frac{Y_i(t)}{t+1} - \frac{1}{t+1}\right|\right] + (1-p_i(t+1))\left[\left|\alpha_i - t\frac{Y_i(t)}{t+1}\right|\right] - |\alpha_i - Y_i(t)|. \tag{4.15}$$

Simplifying yields,

$$\Delta_i(t) = p_i(t+1)\beta_i(t) + \left[\left|\alpha_i - t\frac{Y_i(t)}{t+1}\right| - |\alpha_i - Y_i(t)|\right], \tag{4.16}$$

$$\beta_i(t) = \left|\alpha_i - t\frac{Y_i(t)}{t+1} - \frac{1}{t+1}\right| - \left|\alpha_i - t\frac{Y_i(t)}{t+1}\right|. \tag{4.17}$$

To keep the analysis applicable to any arbitrary probability distribution of $w(t)$, we consider the sign of $\beta_i(t)$ to decide the ideal control policy [21], for which we introduce Assumption 4.8.

Assumption 4.8 (**Ideal control policy**). *(a) There exists an ideal control policy (or ideal control input) at time t, applying which makes $p_i(t+1)=p_i^*(t+1)$, where $p_i^*(t+1)\in\{0,1\}$, $\forall t$. (b) When $\beta_i(t)<0$, we apply ideal control inputs at t leading to $p_i^*(t+1)=1$ whereas, if $\beta_i(t)>0$, we apply ideal control inputs at t leading to $p_i^*(t+1)=0$.*

Definition 4.9 (**Ideal surrogate of a variable**). *The manifestation of a variable under the ideal control policy in Assumption 4.8 is defined as the ideal surrogate of that variable. It is denoted by an asterisk after the variable.*

Assumption 4.8(a) ensures that there exists a control input which causes a constraint violation a.s. at the next time step $t+1$ in closed-loop from any present state $x(t)$, i.e., $p_i^*(t+1)=1$. Similarly, $p_i^*(t+1)=0$ means that the controller can drive the system to prevent a constraint violation a.s. at $t+1$ in closed-loop. $Z_i(t)$ and $\Delta_i(t)$ under the ideal control policy are referred to as $Z_i^*(t)$ and $\Delta_i^*(t)$ respectively,[3] consistent with Definition 4.9. Assumption 4.8(b) ensures that when $\beta_i(t) < 0$, we choose ideal control inputs leading to $p_i^*(t+1) = 1$ so that $\Delta_i^*(t)$ may be ≤ 0 a.s. Similarly, when $\beta_i(t) > 0$, Assumption 4.8(b) ensures that we choose ideal control inputs leading to $p_i^*(t+1) = 0$ so that $\Delta_i^*(t)$ may be ≤ 0 a.s. Note that despite the application of ideal control inputs, the second and third term in the RHS of (4.16) can lead to $\Delta_i^*(t) > 0$, which is used to derive the critical region $\kappa(\alpha_i, t)$, in Theorem 4.10 later. The critical region signifies a region where, if $Y_i(t) \in \kappa(\alpha_i, t)$, then $\Delta_i^*(t) > 0$ a.s.

The case when $\beta_i(t) = 0$ implies $p_i^*(t+1)$ not having an effect on $\Delta_i(t)$, as the first term in the RHS of (4.16) vanishes regardless of the value of $p_i(t+1)$. From (4.17), it can be shown that $\beta_i(t) = 0 \Leftrightarrow Y_i(t) = \frac{\alpha_i - \frac{1}{2(t+1)}}{1 - \frac{1}{(t+1)}}$, and further solving for $\Delta_i(t) > 0$ in (4.16), yields $\alpha_i > \frac{1}{2(t+1)}$, which becomes more likely to be satisfied as t increases. However, the case $\beta_i(t) = 0$ can be avoided by a particular choice of α_i. From (4.17),

$$\beta_i(t) \neq 0 \Leftrightarrow Y_i(t) \neq \frac{\alpha_i - \frac{1}{2(t+1)}}{1 - \frac{1}{(t+1)}}.$$

Since, $Y_i(t) = \frac{\sum_{j=1}^{t} V_i(j)}{t}$, and $\sum_{j=1}^{t} V_i(j) \in \mathbb{N}$, therefore,

$$Y_i(t) \neq \frac{\alpha_i - \frac{1}{2(t+1)}}{1 - \frac{1}{(t+1)}} \iff \sum_{j=1}^{t} V_i(j) \neq (t+1)\alpha_i - \frac{1}{2},$$

which can be ensured by appropriate choice of α_i. Specifically, $(t+1)\alpha_i - \frac{1}{2} \notin \mathbb{N}$, $\forall t$. The online adaptive relaxation rule is introduced next in Section 4.2.4, with its behavior under practical scenarios being discussed in Section 4.2.4.

[3] $Z_i^*(t) = |\alpha_i - Y_i^*(t)|$ and $\Delta_i^*(t) = Z_i^*(t+1) - Z_i(t)$.

h update rule

$\beta_i(t) < 0$ implies $\alpha_i - Y_i(t) + \frac{2Y_i(t)-1}{2(t+1)} > 0$,[4] and is associated with violation of state constraints at $t+1$ which is achieved by expanding the state constraint limits in (4.11e). Similarly $\beta_i(t) > 0$ implies $\alpha_i - Y_i(t) + \frac{2Y_i(t)-1}{2(t+1)} < 0$ and is associated with non-violation of state constraints at $t+1$ which is achieved by contracting the limits in (4.11e). From Assumption 4.6, the h_i update rule can be framed with $K_i(t) \propto \left[\alpha_i - Y_i(t) + \frac{2Y_i(t)-1}{2(t+1)}\right]$ as

$$h_i(t) = h_i(t-1)\left[1 + \frac{\alpha_i - Y_i(t) + \frac{2Y_i(t)-1}{2(t+1)}}{\gamma_i}\right], \tag{4.18}$$

where $\gamma_i \in \mathbb{R}_{0+}$ is a constant of proportionality that adjusts the rate of h_i update ensuring $\frac{\alpha_i - Y_i(t) + \frac{2Y_i(t)-1}{2(t+1)}}{\gamma_i} > -1$, $\forall t$.

Note that Theorem 4.10, discussed next, implicitly assumes that (4.18) is able to enforce Assumption 4.8. However, it may be possible to devise other h update rules enforcing Assumption 4.8, wherein Assumption 4.6 (and consequently, use of (4.18)) can be relaxed. In practical applications, while (4.18) cannot guarantee satisfaction of Assumption 4.8 in closed-loop, it still encourages it (see Section 4.2.4).

Theorem 4.10. *Let Assumptions 4.1, 4.2, 4.4, and 4.8 hold. Given* $\alpha_i > \frac{1}{2(t_0+1)}$*,* $Z_i^*(t)$*, which is the ideal surrogate of the desired supermartingale* $Z_i(t)$*, is monotonically decreasing a.s.* $\forall t \geq t_0$*, if and only if,* $Y_i(t) \notin \kappa(\alpha_i, t)$*,* $\forall t \geq t_0$*, where* $\kappa(\alpha_i, t)$ *is a neighborhood of* α_i *defined as,*

$$\kappa(\alpha_i, t) := \left(\frac{\alpha_i - \frac{1}{2(t+1)}}{1 - \frac{1}{2(t+1)}}, \frac{\alpha_i}{1 - \frac{1}{2(t+1)}} \right).$$

Proof. Theorem 4.10 says that given $\alpha_i > \frac{1}{2(t_0+1)}$, $\mathscr{P} \iff \mathscr{Q}$, where $\mathscr{P}$ is defined as $\Delta_i^*(t) \leq 0$ a.s., $\forall t \geq t_0$, and $\mathscr{Q}$ is defined as $Y_i(t) \notin \kappa(\alpha_i, t)$, $\forall t \geq t_0$. To prove, $\mathscr{P} \iff \mathscr{Q}$,

[4] $\beta_i(t) = |\zeta_i(t) - \frac{1}{t+1}| - |\zeta_i(t)|$, where $\zeta_i(t) = \alpha_i - t\frac{Y_i(t)}{t+1}$. Solving for $\beta_i(t) < 0$ leads to $\zeta_i(t) > \frac{1}{2(t+1)}$, which implies $\alpha_i - Y_i(t) + \frac{2Y_i(t)-1}{2(t+1)} > 0$.

we will first prove the inverse as true, i.e., $\neg\mathscr{P} \implies \neg\mathscr{Q}$, which implies $\mathscr{Q} \implies \mathscr{P}$. Then we will prove the contrapositive as true, i.e., $\neg\mathscr{Q} \implies \neg\mathscr{P}$, which implies $\mathscr{P} \implies \mathscr{Q}$, which will complete the proof.

To prove $\neg\mathscr{P} \implies \neg\mathscr{Q}$, assume $\neg\mathscr{P}$ is true, i.e., $\Delta_i^*(t) > 0$ a.s. To show, $\neg\mathscr{Q}$ holds, we consider Cases 4.1, 4.2 and 4.3 based on the sign of $\beta_i(t)$ below.

Case 4.1.

$$\begin{aligned} &\beta_i(t) < 0 \Leftrightarrow\ p_i^*(t+1) = 1 \\ &\Leftrightarrow\ \alpha_i - Y_i(t) + \frac{2Y_i(t)-1}{2(t+1)} > 0 \Leftrightarrow Y_i(t) < \frac{\alpha_i - \frac{1}{2(t+1)}}{1-\frac{1}{t+1}}. \end{aligned} \tag{4.19a}$$

Solving for $\Delta_i^*(t) > 0$ when $p_i^*(t+1) = 1$ yields

$$Y_i(t) > \frac{\alpha_i - \frac{1}{2(t+1)}}{1-\frac{1}{2(t+1)}}. \tag{4.19b}$$

Equation (4.19) implies the critical region of Case 4.1 is $\kappa_1(\alpha_i,t) = \left(\frac{\alpha_i - \frac{1}{2(t+1)}}{1-\frac{1}{2(t+1)}}, \frac{\alpha_i - \frac{1}{2(t+1)}}{1-\frac{1}{t+1}}\right)$, implying if $Y_i(t) \in \kappa_1(\alpha_i,t)$, despite applying ideal control inputs to the system at t leading to $p_i^*(t+1) = 1$, $\Delta_i^*(t) > 0$ a.s.

Case 4.2.

$$\begin{aligned} &\beta_i(t) > 0 \Leftrightarrow\ p_i^*(t+1) = 0 \\ &\Leftrightarrow\ \alpha_i - Y_i(t) + \frac{2Y_i(t)-1}{2(t+1)} < 0 \Leftrightarrow Y_i(t) > \frac{\alpha_i - \frac{1}{2(t+1)}}{1-\frac{1}{t+1}}. \end{aligned} \tag{4.20a}$$

Solving for $\Delta_i^*(t) > 0$ when $p_i^*(t+1) = 0$ yields

$$Y_i(t) < \frac{\alpha_i}{1-\frac{1}{2(t+1)}}. \tag{4.20b}$$

Equation (4.20) implies the critical region of Case 4.2 is $\kappa_2(\alpha_i,t) = \left(\frac{\alpha_i - \frac{1}{2(t+1)}}{1-\frac{1}{t+1}}, \frac{\alpha_i}{1-\frac{1}{2(t+1)}}\right)$, implying if $Y_i(t) \in \kappa_2(\alpha_i,t)$, despite applying ideal control inputs to the system at t leading to $p_i^*(t+1) = 0$, $\Delta_i^*(t) > 0$ a.s.

Case 4.3. $\beta_i(t) = 0$ leads to $\Delta_i^*(t) > 0$ a.s. because $\alpha_i > \frac{1}{2(t_0+1)} \geq \frac{1}{2(t+1)}$, $\forall t \geq t_0$. Additionally, $\beta_i(t) = 0 \Leftrightarrow Y_i(t) = \frac{\alpha_i - \frac{1}{2(t+1)}}{1-\frac{1}{(t+1)}} = \kappa_3(\alpha_i, t)$.

The total critical region from Cases 4.1, 4.2 and 4.3 yields,

$$\begin{aligned}\kappa(\alpha_i,t) =& \kappa_1(\alpha_i,t) \cup \kappa_2(\alpha_i,t) \cup \kappa_3(\alpha_i,t) \\ =& \left(\frac{\alpha_i - \frac{1}{2(t+1)}}{1 - \frac{1}{2(t+1)}}, \frac{\alpha_i}{1 - \frac{1}{2(t+1)}} \right),\end{aligned}$$

which shows that if $\Delta_i^*(t) > 0$ a.s., then $Y_i(t) \in \kappa(\alpha_i, t)$, which proves $\neg\mathscr{P} \implies \neg\mathscr{Q}$.

To prove $\neg\mathscr{Q} \implies \neg\mathscr{P}$, assume, $\neg\mathscr{Q}$, i.e, $Y_i(t) \in \kappa(\alpha_i,t)$. $\neg\mathscr{Q}$ is subdivided into Cases 4.4, 4.5 and 4.6.

Case 4.4. $\beta_i(t) < 0 \Leftrightarrow p_i^*(t+1) = 1$, which yields (4.19a). (4.19a) and $Y_i(t) \in \kappa(\alpha_i,t)$ yields, $Y_i(t) \in \left(\frac{\alpha_i - \frac{1}{2(t+1)}}{1-\frac{1}{2(t+1)}}, \frac{\alpha_i - \frac{1}{2(t+1)}}{1-\frac{1}{t+1}}\right) = \kappa_1(\alpha_i,t)$. However, from Case 4.1, we know that when $p_i^*(t+1) = 1$ and $Y_i(t) \in \kappa_1(\alpha_i,t)$, then $\Delta_i^*(t) > 0$ a.s.

Case 4.5. $\beta_i(t) > 0 \Leftrightarrow p_i^*(t+1) = 0$, which yields (4.20a). (4.20a) and $Y_i(t) \in \kappa(\alpha_i,t)$ yields, $Y_i(t) \in \left(\frac{\alpha_i - \frac{1}{2(t+1)}}{1-\frac{1}{t+1}}, \frac{\alpha_i}{1-\frac{1}{2(t+1)}}\right) = \kappa_2(\alpha_i,t)$. However, from Case 4.2, we know that when $p_i^*(t+1) = 0$ and $Y_i(t) \in \kappa_2(\alpha_i,t)$, then $\Delta_i^*(t) > 0$ a.s.

Case 4.6. $\beta_i(t) = 0 \Leftrightarrow Y_i(t) = \kappa_3(\alpha_i,t)$ which leads to $\Delta_i^*(t) > 0$ a.s. because $\alpha_i > \frac{1}{2(t+1)}$.

Cases 4.4, 4.5 and 4.6 together prove $\neg\mathscr{Q} \implies \neg\mathscr{P}$, which completes the proof. $\square$

Remark 4.11 (**Extension of Theorem 4.10**). *Theorem 4.10 establishes the conditions necessary and sufficient for $\Delta_i^*(t) \leq 0$ a.s., $\forall t \geq t_0$, which implies that $Z_i^*(t)$ is monotonically decreasing a.s., $\forall t \geq t_0$. From Cases 4.1, 4.4, and Cases 4.2, 4.5, if the critical region is defined by $\kappa'(\alpha_i,t) := \left[\frac{\alpha_i - \frac{1}{2(t+1)}}{1-\frac{1}{2(t+1)}}, \frac{\alpha_i}{1-\frac{1}{2(t+1)}}\right]$, then $\Delta_i^*(t) < 0$ a.s., $\forall t \geq t_0$, which implies that $Z_i^*(t)$ is strictly decreasing a.s., $\forall t \geq t_0$. As $Z_i^*(t)$ is bounded from below by 0, we conclude $\lim_{t\to\infty} Z_i^*(t) = \inf\{Z_i^*(t)\} = 0$ a.s. from the monotone convergence theorem, which* *implies the asymptotic convergence of* Y_i^* *to* α_i *a.s., if* $\alpha_i > \frac{1}{2(t_0+1)}$, $p_i(t+1) = p_i^*(t+1)$, *and* $Y_i(t) \notin \kappa'(\alpha_i, t)$, $\forall t \geq t_0$.[5]

Remark 4.12 (Width of the critical region [21]). *The width of the critical region* $\kappa'(\alpha_i, t)$ *is* $\frac{1}{2t+1}$, *while* $Y_i(t) \in \{0, \frac{1}{t}, \frac{2}{t}, \ldots, 1\}$. *The granularity in possible values of* $Y_i(t)$ *is* $1/t$, $\forall t$. *As* $\frac{1}{2t+1} < \frac{1}{t}$, *there is at most one critical value of* $Y_i(t)$, *such that despite adapting the system to take ideal control inputs leading to* $p_i(t+1) = p_i^*(t+1)$, *it is possible that* $\Delta_i^*(t) \geq 0$ *which can lead to the deviation of* Y_i^* *from* α_i *momentarily. However, the width of the critical region monotonically decreases as* t *increases, therefore, the assumption of* $Y_i(t) \notin \kappa'(\alpha_i, t)$, *is weak and can be easily satisfied as* t *increases. The width of the critical region in the present work is also smaller than [21], implying more relaxed conditions for guaranteeing convergence of* Y_i^* *to* α_i.

Lemma 4.13. *Let Assumptions 4.1, 4.2, 4.4, and 4.8 hold. Given any initial time* t_0, *with* $\alpha_i > \frac{1}{2(t_0+1)}$ *and* $Y_i(t_0) \notin \kappa'(\alpha_i, t_0)$, *there exists some time* $t' = \inf\{t > t_0 \,|\, Y_i^*(t) \in \kappa'(\alpha_i, t)\}$ *a.s.*

Proof. The lemma states that if the initial time-average of violations of state constraints is outside of the critical region, and we apply ideal control inputs from thereon, then at some future time t', the time-average of violations comes inside the critical region a.s. Lemma 4.13 implies the a.s. strict decrease of $Z_i^*(t)$ is violated for $t \geq t'$ (see Remark 4.11). Lemma 4.13 can be proved by showing that when $Z_i^*(t)$ decreases, then $\frac{\delta \hat{w}_i(t)}{\delta t} > \frac{\delta Z_i^*(t)}{\delta t}$, where $\hat{w}(t)$ is the width of the critical region at time t, and δ is the forward finite difference operator.

$\hat{w}_i(t) := \frac{1}{2t+1}$, implying $\delta \hat{w}_i(t) := \hat{w}_i(t+1) - \hat{w}_i(t) = \frac{-2}{(2t+1)(2t+3)}$ where $\delta t := 1$. Thus, $\hat{w}_i(t)$ decreases in the order of $\mathscr{O}(\frac{1}{t^2})$.

Similarly, $\delta Z_i^*(t) := Z_i^*(t+1) - Z_i(t) = \Delta_i^*(t)$. $\Delta_i^*(t)$ can be subdivided into Cases 4.7 and 4.8.

[5]Note that although $Y_i(t_0)$ need not necessarily be $Y_i^*(t_0)$, we abuse the notation to use $Z_i(t_0)$ and $Z_i^*(t_0)$ interchangeably in Theorem 4.10 and Remark 4.11 to aid in a more intuitive explanation.

Case 4.7. When $p_i^*(t+1)=1$, $\Delta_i^*(t) = \left[\left|\alpha_i - t\frac{Y_i(t)}{t+1} - \frac{1}{t+1}\right|\right] - |\alpha_i - Y_i(t)|$.

Case 4.8. When $p_i^*(t+1)=0$, $\Delta_i^*(t) = \left|\alpha_i - t\frac{Y_i(t)}{t+1}\right| - |\alpha_i - Y_i(t)|$.

Substituting $Y_i(t) = \frac{\sum_{j=1}^{t} V_i(j)}{t}$, where $\sum_{j=1}^{t} V_i(j) \leq t$, in both Cases 4.7 and 4.8, we see that when $Z_i^*(t)$ decreases a.s. by virtue of $Y_i(t) \notin \kappa'(\alpha_i,t)$, then $Z_i^*(t)$ decreases most modestly (i.e., with the least magnitude of decrease), in the order of $\mathscr{O}(\frac{1}{t})$, which proves that, $\frac{\delta \hat{w}_i(t)}{\delta t} > \frac{\delta Z_i^*(t)}{\delta t}$, which completes the proof. □

Lemma 4.14. *Let Assumptions 4.1, 4.2, 4.4, and 4.8 hold. Given any initial time* t_0*, with* $\alpha_i > \frac{1}{2(t_0+1)}$ *and* $Y_i(t_0) \in \kappa'(\alpha_i,t_0)$*, there exists some time* $t' = \inf\{t > t_0 \,|\, Y_i^*(t) \notin \kappa'(\alpha_i,t)\}$ *a.s.*

Proof. The lemma states that if the initial time-average of violation of state constraints is inside the critical region, and we apply ideal control inputs from thereon, then at some future time t', the time-average of violation goes outside of the critical region a.s. Lemma 4.14 prevents the monotonic increase of $Z_i^*(t)$ for $t \geq t'$. When $Y_i(t) \in \kappa'(\alpha_i,t)$, $\frac{\delta Z_i^*(t)}{\delta t} \geq 0$, while $\frac{\delta \hat{w}_i(t)}{\delta t} < 0$, thus leading to $\frac{\delta Z_i^*(t)}{\delta t} > \frac{\delta \hat{w}_i(t)}{\delta t}$, which completes the proof. □

Theorem 4.15. *Let Assumptions 4.1, 4.2, 4.4, and 4.8 hold. Given any initial time* t_0 *with* $\alpha_i > \frac{1}{2(t_0+1)}$*, and time-average of violations* $Y_i(t_0)$*,* Y_i^* *asymptotically converges to* α_i *a.s.*

Proof. The theorem states that if ideal control inputs are applied to the system starting from any arbitrary time t_0 with $\alpha_i > \frac{1}{2(t_0+1)}$, then the time-average of violations converges to the maximum probability of violations of state constraints a.s. The proof follows from Theorem 4.10, Remarks 4.11 and 4.12, Lemmas 4.13, 4.14, and relaxes the assumption of $Y_i(t) \notin \kappa'(\alpha_i,t)$, $\forall t \geq t_0$, of Remark 4.11. Theorem 4.15 also rigorously proves the result which was intuitively argued in [21].

From Remark 4.12, the width of the critical region $\hat{w}_i(t)$ is $\frac{1}{2t+1}$, which monotonically decreases with time. As the critical region $\kappa'(\alpha_i,t)$ is a neighborhood of α_i by construction, decrease of $\hat{w}_i(t)$ implies decrease of the width of the neighborhood. $\lim_{t\to\infty} \hat{w}_i(t) = 0$, which implies $\lim_{t\to\infty} \kappa'(\alpha_i, t) = \alpha_i$, i.e., the critical region becomes a point. With $\alpha_i > \frac{1}{2(t_0+1)}$ and $p_i(t+1) = p_i^*(t+1)$, $\forall t \geq t_0$, two cases are possible:

Case 4.9. When $Y_i(t_0) \notin \kappa'(\alpha_i, t)$, Lemma 4.13 concludes that there exists some $t' = \inf\{t > t_0 \,|\, Y_i^*(t) \in \kappa'(\alpha_i, t)\}$ a.s, which implies that $Y_i^*(t')$ is closer to α_i as compared to $Y_i(t_0)$ a.s. (see Remark 4.11). Then, from Lemma 4.14, we can conclude that there exists some $t'' = \inf\{t > t' \,|\, Y_i^*(t) \notin \kappa'(\alpha_i, t)\}$ a.s., which implies that $Y_i^*(t'')$ is no closer to α_i as compared to $Y_i^*(t)'$ a.s. (see Remark 4.11). The process repeats, with Y_i^* coming in and out of the critical region a.s. as time progresses. However, as the width of the critical region vanishes at $t \to \infty$, making the critical region the point α_i, we conclude Y_i^* converges to α_i a.s. as $t \to \infty$.

Case 4.10. When $Y_i(t_0) \in \kappa'(\alpha_i, t)$, a similar argument can be made as in Case 4.9 involving Lemma 4.13 and 4.14, with Y_i^* coming in and out of the critical region a.s. until ultimately converging to α_i a.s. as $t \to \infty$.

Both Cases 4.9 and 4.10 complete the proof. $\square$

Deviation of the practical control policy from the ideal control policy

Remark 4.12 establishes that the assumption of $Y_i(t) \notin \kappa'(\alpha_i, t)$, is weak and can be easily satisfied as t increases. Thus, given $Y_i(t) \notin \kappa'(\alpha_i, t)$, if at some time t $Y_i(t) < \frac{\alpha_i - \frac{1}{2(t+1)}}{1 - \frac{1}{2(t+1)}}$, then $Y_i(t) < \frac{\alpha_i - \frac{1}{2(t+1)}}{1 - \frac{1}{(t+1)}} < \alpha_i$ holds, which results in $h_i(t) < h_i(t-1)$ on applying (4.18). The decrease of h_i expands the feasible state set for $x(t+1)$ in (4.11) and thereby encourages constraint violations at $t+1$ in closed-loop. While under the ideal control policy (Assumption 4.8), $h_i(t) < h_i(t-1)$ would have guaranteed constraint violation at time $t+1$ a.s., in practical scenarios, just the expansion of the feasible state set alone cannot guarantee violation. A similar argument can be made when $Y_i(t) > \frac{\alpha_i}{1 - \frac{1}{2(t+1)}}$, which by virtue of $Y_i(t) > \alpha_i > \frac{\alpha_i - \frac{1}{2(t+1)}}{1 - \frac{1}{(t+1)}}$ and (4.18) leads to $h_i(t) > h_i(t-1)$, contracting the feasible state set for $x(t+1)$ thereby discouraging constraint violations at $t+1$ in closed-loop. Thus under deviation of the practical control policy from the ideal, while asymptotic convergence of Y_i to α_i cannot be guaranteed, it still is encouraged by (4.18).

4.2.5 Asymptotic behavior of the practical system

It is important to determine the asymptotic behavior (i.e., as $t \to \infty$) of the practical system in which the simplifying assumption of applying an ideal control policy referred to in Assumption 4.8 is dropped.

Theorem 4.16. *Let Assumptions 4.1, 4.2, and 4.4(a) hold. The expected value of $Y_i(t+1)|\mathscr{F}_t$ asymptotically converges to $Y_i(t)$.*

Proof. Applying the limit of $t \to \infty$ to (4.16), and rearranging to bypass the indeterminate $\frac{\infty}{\infty}$ form, we get,

$$\lim_{t\to\infty} \Delta_i(t) = \lim_{t\to\infty} \; p_i(t+1)\left[\left|\alpha_i - \frac{Y_i(t)}{1+\frac{1}{t}} - \frac{1}{t+1}\right| - \left|\alpha_i - \frac{Y_i(t)}{1+\frac{1}{t}}\right|\right] + \left|\alpha_i - \frac{Y_i(t)}{1+\frac{1}{t}}\right| - |\alpha_i - Y_i(t)|. \tag{4.21}$$

As $p_i(t+1) \in [0,1]$, substituting $t \to \infty$ in (4.21), yields $\lim_{t\to\infty} \Delta_i(t) = 0$, which implies either:

Case 4.11. $\lim_{t\to\infty} Y_i(t) = \lim_{t\to\infty} \mathbb{E}[Y_i(t+1)|\mathscr{F}_t]$.

Case 4.12. $\lim_{t\to\infty} Y_i(t) = \alpha_i + l$ and $\lim_{t\to\infty} \mathbb{E}[Y_i(t+1)|\mathscr{F}_t] = \alpha_i - l$, where, $l \in [-\alpha_i, \alpha_i]$.

Taking expectation on both sides of (4.13) yields,

$$\mathbb{E}[Y_i(t+1)|\mathscr{F}_t] = t\frac{Y_i(t)}{t+1} + \mathbb{E}\left[\frac{V_i(t+1)|\mathscr{F}_t}{t+1}\right]. \tag{4.22}$$

Taking the limit at $t \to \infty$ in (4.22), and substituting the values of $\lim_{t\to\infty} Y_i(t)$ and

$\lim_{t\to\infty}\mathbb{E}[Y_i(t+1)|\mathscr{F}_t]$ yields,

$$\alpha_i - l = \lim_{t\to\infty}\frac{\alpha_i + l}{1+\frac{1}{t}} + \lim_{t\to\infty}\mathbb{E}\left[\frac{V_i(t+1)|\mathscr{F}_t}{t+1}\right]. \tag{4.23}$$

As $\mathbb{E}[V_i(t+1)|\mathscr{F}_t] = p_i(t+1) \in [0,1]$, hence evaluating the limit in (4.23) yields $l = 0$. Hence Case 4.12 implies Case 4.11 (but not the other way around).

Case 4.11 completes the proof. □

The above proof shows that the time-average of the state constraint violations has a martingale-like behavior asymptotically which may be useful for practical operation of the proposed OA-SMPC to avoid unpredictable violation behavior in the long run as the system evolves.

4.2.6 Post-processing for real-time system operation

In previous works such as [21], after the nominal MPC computed optimal control inputs for the first time-step of the prediction horizon are implemented, the observed states get corrected in closed-loop to account for real-time uncertainties by (4.1). Accommodation of the entire uncertainty (uncertainty in weather forecast) by the state is reasonable for building climate control applications where the state (room temperature) and control input (heating/cooling effect from the air-conditioner) are not coupled to the same physical equipment [21]. However, in certain applications where the states and control inputs are coupled to the same equipment (like BESS, where state of charge (SOC) is the state, and charging/discharging power is a control input), the first time-step optimal control inputs (computed by the nominal MPC) can also be post-processed in real-time to correct for the realized uncertainty. For example, the BESS can alter its nominal MPC computed optimal control inputs and states to correct for the VRES and gross load forecast uncertainty in real-time to maintain power balance of the MG with the main grid.

Assumption 4.17 (Post-processing to correct for uncertainties in real-time). *For each chance constrained state affected by uncertainties: (a) There are two mutually coupled sources of control with one source having the primary responsibility of handling the uncertainties in closed-loop. During correction of the observed states in closed-loop to account for the uncertainty, the feasible altered control input and state set is the same as defined by* $\mathbf{s}_{1:q}$ (4.11c) *and* $\mathbf{g}_{1:r} - \mathbf{h}_{1:r}(t)$ (4.11e) *respectively, which are the time-varying design limitations. The secondary control source always has enough control input available to handle the remaining part of the uncertainty (through satisfaction of* (4.3)*) that cannot be handled by the primary source due to the possibility of violation of the time-varying design limitations by the primary control source in closed-loop, (b) The state transition is not dependent on the secondary control source, (c) The primary and secondary control sources are coupled only to each other, (d) The state transition is not dependent on the control sources associated with other states.*

$\mathbf{s}_{1:q}$ is a hard constraint and does not vary with time, but as $\mathbf{h}_{1:r}(t)$ is time-varying, we refer to these design limitations as time-varying, when considered together. After updating the states and control inputs, $h(t+1)$ is updated by (4.18), and the optimization in (4.11) is repeated. The schematic diagram of the complete OA-SMPC operational framework with post-processing is shown in Fig. 4.1, with the algorithm presented in Algorithm 1. The results from Theorems 4.10, 4.15 and 4.16 are independent of the post-processing framework, and still hold with post-processing. Additionally, the restrictive one step controllability in Assumption 4.4(b) can be relaxed for practical systems while still maintaining the structure of the input matrix in Remark 4.5 due to Assumption 4.17.

Note that the computational cost of the proposed OA-SMPC is same as that of a nominal MPC, with the h update happening outside of the MPC framework which makes the present method extremely scalable for practical implementation. Also, similar to [21, Sec. VII], as the linear structure of the system is not leveraged for Theorems 4.10, 4.15

and 4.16, the results hold for nonlinear systems too provided the relevant assumptions hold.

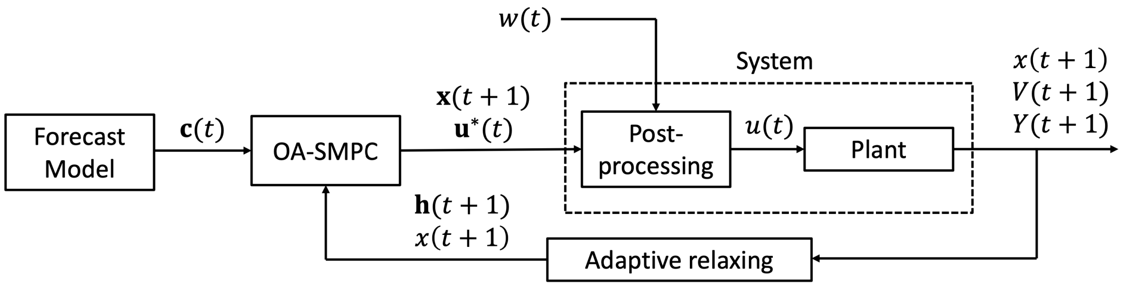

Figure 4.1. OA-SMPC operational framework with post-processing.

Example 4.18. To demonstrate the post-processing, consider a simple system with $x(t) = [x_1(t)]$ as the state subjected to chance constraints, control inputs $u(t) = \begin{bmatrix} u_1(t) & u_2(t) \end{bmatrix}^\top$, where u_1 and u_2 are the primary and secondary control sources respectively, and the uncertainty is denoted by $w(t)$. The system matrices are A, $B = \begin{bmatrix} B_{11} & 0 \end{bmatrix}$ and E. The structure of B follows from Assumption 4.17(b). $u_1(t)$ and $u_2(t)$ are coupled by (4.3), following Assumption 4.17(c). Let $\tilde{x}_1(t+1)$ and $\tilde{u}_1$ be the state and primary control upper limits based on the time-varying design limitations following Assumption 4.17(a). The system described is similar to a MG with BESS, VRE, local load demand and grid connectivity, where the BESS SOC is the state, BESS charging/discharging power is the primary control source, and the grid import power is the secondary control source. Both the control sources are coupled by the grid power balance equation, while the uncertainty is the real-time VRES and load forecast error.

When correcting for the uncertainties in closed-loop, first it is ensured that the primary control source handles only the part of the uncertainty that still keeps it within the feasible set. The altered primary control input can be formulated as,

$$u_1(t) := \min\Big(u_1^*(t|t) + D_1 w(t), \tilde{u}_1\Big), \tag{4.24a}$$

where $D = B^{\dagger}E$, and $u_1^*(t|t)$ is the optimal MPC computed primary control input. The state update equation using Assumptions 4.17(a) and 4.17(b) is formulated as

$$x_1(t+1) = \min\Big(Ax_1(t) + B_{11}u_1(t), \tilde{x}_1(t+1)\Big). \tag{4.24b}$$

If from (4.24b), $x_1(t+1) = \tilde{x}_1(t+1)$, we re-compute, $u_1(t) = (B_{11})^{-1}(\tilde{x}_1(t+1) - Ax_1(t))$. Finally, the altered secondary control input $u_2(t)$ is computed by satisfying (4.3). In the case of the time-varying design limitations giving the lower limits of the state and primary controls, $\underset{\sim}{x}_1(t+1)$ and $\underset{\sim}{u}_1$ respectively, (4.24a) and (4.24b) are modified by replacing the $\min$ by the $\max$ function. Assumptions 4.17(a) and 4.17(b) ensure that the post-processing steps give unique solutions, and Assumptions 4.17(c) and 4.17(d) ensure that the correction for uncertainties affecting a chance constrained state and related control inputs does not unnecessarily affect other states and control inputs which may lead to inconsistency in the post-processed solutions. After post-processing, the state constraint violations in closed-loop are tracked as (4.25) with time-average of violations calculated similar to (4.12b).

$$V_1(t+1) := \begin{cases} 1, & G_1x(t+1) > g_1, \\ 0, & G_1x(t+1) \leq g_1. \end{cases} \tag{4.25}$$

Remark 4.19 (**Significance of the post-processing framework**). *In related previous works with two mutually coupled sources of control to handle uncertainties on chance constrained states such as [35], the time-varying design limitations as that of Assumption 4.17(a) are not considered. Large primary control inputs to handle large uncertainties can, thus, potentially lead to damaging the primary controller in [35]. In other works like [21], MPC computed control inputs are not altered to account for uncertainties, making the state handle the entire uncertainty in closed-loop. Large uncertainties can thus steer the system away from the OA-SMPC feasible region, which due to Assumption 4.4(a) can lead to the application of expensive control input at the next time-step to bring the system back* *to feasibility. Such an expensive control input can lead to high economic cost, a problem not considered in both [21] and [35].*

Remark 4.20 (**Nonconservative chance constraint satisfaction in a 'practical sense' in closed-loop even under time-varying uncertainty distribution, and repeated large uncertainties**). *As the nominal OA-SMPC always has access to relaxed feasible states, it is possible for the predicted nominal solutions to always violate the (original) state constraints $\forall k, t$ (as satisfaction of* (4.9a) *is not mandatory in our formulation). In closed-loop, thus, if solutions are continuously violated more than the maximum prescribed level, h_i increases until $h_i \to 0^-$ according to* (4.18)*. Mathematical violations can still persist in $V_i(t+1)$ after $h_i \to 0^-$ which fails to give the benefit of adaptive relaxation. These violations can be ignored during practical implementation, by adding a small $\varepsilon > 0$ to g_i resulting in considering violations only if $G_i x(t+1) > g_i + \varepsilon$. The consideration of ε in tracking violations is an operational step and can be removed by the user when h_i decreases sufficiently to relax the state constraint and reduce conservatism. This adaptive behavior of our system along with post-processing ensures that the chance constraints in* (4.4) *are satisfied in a 'practical sense' in closed-loop, which previous works [21, 35, 42] may not be able to satisfy under repeated large uncertainties when the mixed worst-case disturbance sequence is not known a-priori, or if the uncertainty distribution changes with time. Note that the mixed worst-case disturbance sequence computed via scenarios of uncertainty in [21, 35] may in itself be over-conservative [67].*

4.3 Case study

4.3.1 Overview

In this section, we implement our proposed method (OA-SMPC) for simulating the optimal BESS dispatch strategy for a practical MG with PV, load and connection to the main grid in an EMPC framework. The MG setup is from the real-life MG at

Algorithm 1. Online Adaptive SMPC (OA-SMPC)

Initialization

1. Choose $x(0)$.
2. Choose $h(0)$ from domain knowledge.

Online solution

1. Solve (4.11) to get $u^*(t|t)$.

2a. If post-processing of nominal OA-SMPC computed optimal control inputs are not allowed: Set $u(t) \leftarrow u^*(t|t)$ and account for the uncertainties in $x(t+1)$ by (4.1). Calculate $V(t+1)$ from (4.12a).

2b. If post-processing of nominal OA-SMPC computed optimal control inputs are allowed: Post-process by (4.24) and (4.3) to account for the uncertainties to calculate $x(t+1)$ and $u(t)$. Calculate $V(t+1)$ similar to (4.25).

3. Calculate $Y(t+1)$ from (4.12b).
4. Calculate $h(t+1)$ from (4.18).
5. Set $t \leftarrow t+1$ and repeat from Step 1 of Online solution.

the Port of San Diego, described in [65]. The MG model incorporates electricity prices with demand and energy charges, realistic load and PV forecast, and a post-processing step for incorporating the forecast uncertainties in BESS dispatch. The yearly (2019) electricity costs were compared for the MG, for the traditional MPC, with hard constraints on the state (BESS SOC), and our OA-SMPC method with chance constraints on the state. The motivation for using chance constraints on BESS SOC in the OA-SMPC is to leverage some extra BESS capacity to reduce demand peaks and thus, demand charges, leading to significant electricity cost savings, while staying within a maximum violation probability bound to avoid adverse effects on BESS life. Additionally, we also compare our proposed OA-SMPC to the traditional EMPC method without chance constraints, and a state-of-the-art approach [21] from the literature with chance constraints and similar computational cost.

4.3.2 PV and load forecast

The MG model uses day-ahead PV and gross load forecasts with 15 minute time resolution as inputs. The k-Nearest Neighbor (kNN) algorithm is used for the gross load forecast. The training data comprises of 15-min resolution historical load observations from November 1, 2018 to November 20, 2019. For every MPC horizon, gross load observations for the previous 24 h (feature vector) are compared with the training sample and $k = 29$ nearest neighbors are identified by the kNN algorithm. Finally, the gross load forecast is calculated by averaging the gross load of the selected neighbors at every time-step of the forecast horizon [68]. The root mean square error (RMSE), mean absolute error (MAE), and mean bias error (MBE) for the gross load forecast for the entire year are 22.4 kW, 17.3 kW, and -1.2 kW respectively.

The PV generation forecast for the upcoming 24 h utilizes the kNN (with $k = 30$) algorithm as well. The feature vector is formed by three data sets: numerical weather prediction (NWP) model forecasts for the upcoming 24 h, the average of the preceding 1, 2, 3, and 4 h PV power generation, and the current time of the day. The NWP forecast utilized was the High-Resolution Rapid Refresh (HRRR) model developed by NOAA [69]. The PV power generation dataset was obtained by running simulations for the PV plant in the Solar Advisor Model (SAM) using the irradiance observation data obtained from the NSRDB database as an input. The training sample for PV power generation forecast includes NWP forecast and irradiance observations between January 1, 2019 to December 31, 2019. The RMSE, MAE and MBE for the PV forecast for the entire year are 20.3 kW, 9.1 kW, and -0.8 kW respectively.

4.3.3 MG model

The system state $x(t) = [x_1(t)]$ is the BESS state of charge (SOC). The control input is $u(t) = \begin{bmatrix} u_1(t) & u_2(t) \end{bmatrix}^\top$ where $u_1(t)$ is the BESS dispatch power (primary control source for handling uncertainty), and $u_2(t)$ is the grid import power (secondary control source for handling uncertainty). $u_1(t) > 0$ denotes charging, while $u_2(t) > 0$ denotes power import from the main grid to the MG. The PV generation and gross load is denoted by $\mathrm{PV}(t)$ and $L(t)$ respectively and are used as forecast inputs to the MPC. The uncertainty $w(t) = [w_1(t)]$ is the difference between the gross load and PV generation forecast uncertainties, i.e., $w_1(t) = \left(L^f(t) - L^r(t)\right) - \left(\mathrm{PV}^f(t) - \mathrm{PV}^r(t)\right)$ where the superscript f and r denote forecasted and real values. The MPC prediction horizon is one-day ahead, subdivided into $N = 96$ equal time-steps of $\Delta t = 0.25$ h (15 minutes) each.

The system matrices are $A = [1]$, $B = \begin{bmatrix} \frac{\Delta t}{\mathrm{BESS_{en}}} & 0 \end{bmatrix}$, and $E = [\frac{\Delta t}{\mathrm{BESS_{en}}}]$ where $\mathrm{BESS_{en}}$ is the energy capacity of the BESS. The system matrices handle the SOC update of the battery due to charging/discharging. For the hard control input constraints, $S = \begin{bmatrix} 1 & 0 \\ -1 & 0 \end{bmatrix}$ and $s = \begin{bmatrix} \mathrm{BESS_{max}} & \mathrm{BESS_{max}} \end{bmatrix}^\top$, which constrains the maximum charging/discharging power of the BESS. For the time varying equality constraints coupling the control inputs,

$M = \begin{bmatrix} 1 & -1 \end{bmatrix}$, $c(t) = [\mathrm{PV}^f(t) - L^f(t)]$, and $F = [1]$, which ensures power balance of the MG with the main grid. The MPC also has a terminal state constraint defined as $x_1(t+N|t) \geq \hat{x}_1$.

For this case study, we consider joint chance constraints (JCC) on the BESS SOC which considers a violation if the BESS SOC goes above or below predefined upper ($\mathrm{SOC_{max}}$) and lower bounds ($\mathrm{SOC_{min}}$) in closed-loop. The goal is to reduce electricity import costs from the grid by having controlled violations beyond the predefined upper and lower bounds by making a larger BESS capacity available for dispatch. Unrestricted violations are avoided as they can adversely affect the BESS lifetime. The chance constraints are defined by $G = \begin{bmatrix} 1 & -1 \end{bmatrix}^\top$, $g = \begin{bmatrix} \mathrm{SOC_{max}} & -\mathrm{SOC_{min}} \end{bmatrix}^\top$ and $h(t) = \begin{bmatrix} h_1(t) & h_2(t) \end{bmatrix}^\top$. We choose $h_1(t) = h_2(t)$ for adapting both the state constraints simultaneously by the same parameter as they are setup in JCC form. The maximum probability of the JCC violation is predefined by α. For the traditional EMPC (without chance constraints), violations are avoided and the state constraints are formulated as (4.26), while for the OA-SMPC the state constraints are formulated as (4.10).

$$Gx(t+k|t) \leq g \qquad \forall k \in \mathbb{N}_1^N, \forall t. \tag{4.26}$$

In the JCC formulation, when updating $h(t)$ by (4.18), it is ensured that $h_1(t) = \max\big(\mathrm{SOC_{max}} - 1, h_1(t)\big)$, and $h_2(t) = \max\big(-\mathrm{SOC_{min}}, h_2(t)\big)$ to ensure the state constraints do not violate physical limits of SOC above 1 or below 0. However, in our case study, $h_i(t)$ given by (4.18) never violate physical limits, obviating the above correction. We have practically ensured this by setting a high value of γ_i in (4.18), which is a design choice, at the cost of slower system adaptation (i.e., rate of change of $h_i(t)$), and setting the initial constraint relaxation parameter $h_i(0)$ such that $g_i - h_i(0)$ is sufficiently far away from physical limits for $i \in \{1,2\}$.

The objective function is formulated as in [65, 70], and is given by,

$$
\begin{aligned}
J(t) = & R_{\mathrm{NC}} \max\{u_2(t+k|t)\}_{k=0}^{N-1} + R_{\mathrm{OP}} \max\{u_2(t+l|t)\}_{l\in\mathbb{I}(t)} \\
& + R_{\mathrm{EC}} \Delta t \left[\sum_{k=0}^{N-1} u_2(t+k|t) + \frac{1-\eta}{2} \sum_{k=0}^{N-1} |u_1(t+k|t)| \right],
\end{aligned}
\tag{4.27}
$$

where R_{NC} is the non-coincident demand charge (NCDC) rate charged on the maximum grid import during the prediction horizon. Similarly, R_{OP} is the on-peak demand charge (OPDC) rate, charged on the maximum grid import between 16:00 and 21:00 h, called on-peak (OP) hours of the prediction horizon, and $\mathbb{I}(t)$ represents indices of prediction horizon time-steps coinciding with the OP hours. Naturally, the indices of OP hours in the prediction horizon are a function of the starting time-step t of the MPC prediction horizon. R_{EC} is the energy charge rate and η is the round-trip efficiency of the BESS accounting for BESS losses. After the net load for the entire month is realized, the monthly NCDC is computed based on maximum load demand from the grid during the month, while the monthly OPDC is computed based on maximum load demand between 16:00 and 21:00 h of all days of the month. The predefined parameters of the MG for the OA-SMPC operation are shown in Table 4.1 and a block diagram of the MG operational framework is shown in Fig. 4.1. Note that the one step controllability in Assumption 4.4(b), and ideal control policy in Assumption 4.8 is relaxed for the case study for realistic simulations. The satisfaction of Assumption 4.4(a) is ensured by choosing a sufficiently large γ_i which constrains the rate of $h_i(t)$ increase depending on the available control input power to satisfy (7.5). Note that due to Assumption 4.17(a), in our case study, the risk of violation of Assumption 4.4(a) can only arise when $h_i(t)$ increases.[6]

[6]The maximum absolute forecast uncertainty throughout the year for the case study is 261 kW, which still is lesser than half of the BESS power capacity of 700 kW. Thus, even in the case where Assumption 4.17(a) is relaxed, and the BESS is set up to handle all the uncertainty until reaching the physical limits, the practical viability of Assumption 4.4(a) is reinforced.

Table 4.1. Design Parameters of the OA-SMPC for the MG.

Parameter	Symbol	Value
NCDC rate	R_{NC}	\$24.48/kW
OPDC rate	R_{OP}	\$19.19/kW
Energy rate	R_{EC}	\$0.1/kWh
BESS round-trip efficiency	η	0.8
BESS energy capacity	BESS_{en}	2,500 kWh
BESS power capacity	BESS_{max}	700 kW
Upper bound of SOC for traditional EMPC 1	SOC_{max}	0.8
Lower bound of SOC for traditional EMPC 1	SOC_{min}	0.2
Maximum violation probability	α	0.1
Terminal state constraint	$\hat{x}_1$	0.5
Initial state	$x_1(0)$	0.5
Initial constraint relaxing parameter	$h(0)$	$\begin{bmatrix}-0.1 & -0.1\end{bmatrix}^\top$
Proportionality constant	γ_1 and γ_2	15

4.3.4 Operation strategy

This section presents the real-time operation strategy of the OA-SMPC for the economic MG dispatch probem under consideration. Although (4.18) updates h_i at every time-step, given the emphasis on additional OPDC penalties in our cost function, whenever the starting time-step of the MPC coincides with daily OP hours, we restrict the h_i increase between two time steps, overriding (4.18) when required. Decreasing h_i during the daily OP hours is still allowed, and if h_i increases it is reset manually to the previous value. The reasoning behind restricting the increase of h_i during OP times is to avoid the additional OPDC costs (on top of NCDC) by incurring preferential violations during OP hours (by deeper BESS discharge due to relaxed state constraints). The preferential OP hour violations may lead to state violations beyond the maximum allowable limit temporarily, but the adaptive rule (by virtue of $Y > \alpha$) pushes the BESS to compensate by lowering violations due to rapid increase of h_i during other times (when risk of penalty on peaks is lower). The simulations are carried out in CVX, a package for solving convex programs in the MATLAB environment [59, 60].

4.4 Results and discussions

We compare results of yearly simulations from 4 test cases: (i) Traditional EMPC 1 described in Section 4.3.3 to demonstrate the case without chance constraints; (ii) OA-SMPC which is our proposed method described in Section 4.3.3 to demonstrate the case with chance constraints on state; (iii) SMPC Lit from [21] which is similar in computational cost to our proposed method, with the chance constraints being represented by (4.9b), a corresponding adaptive constraint tightening rule given by $\tilde{h}_i(t) = \tilde{h}_i(t-1)\left[1 - \frac{\alpha_i - Y_i(t) + \frac{2\alpha_i - 1}{2t}}{\gamma_i}\right]$, with $\tilde{h}_i(t) > 0$, $\forall t,\ i \in \{1,2\}$, and $\tilde{h}_1(t) = \tilde{h}_2(t)$. As [21] only tightens the state constraints, violation is allowed in closed-loop by changing the feasible state set in the post-processing step in Assumption 4.17(a) to the physical limits of the system (i.e., SOC limits of 0 and 1). Similar to the OA-SMPC, $\tilde{h}_i$ increase during OP hours is avoided by resetting it manually to its previous value. The design parameters for SMPC Lit are the same as that of OA-SMPC (see Table 4.1), with $\tilde{h}(0) = -h(0)$; (iv) Traditional EMPC 2 which modifies Case (i) with $g = \begin{bmatrix} \mathrm{SOC}_{\max} - h_1(0) & -\mathrm{SOC}_{\min} - h_2(0) \end{bmatrix}^\top$ to demonstrate the MG performance with the state constraints always relaxed by the same initial relaxing parameter in Case (ii) to violate $\mathrm{SOC}_{\max}/\mathrm{SOC}_{\min}$ in closed-loop but without adaptation.

From the PV and gross load forecasting errors, we find that the mean and standard deviation (SD) of the uncertainty is -0.5 kW and 30.3 kW, respectively for the entire year of 2019. A greater (lesser) value of mean uncertainty would push the states higher (lower) in general causing more constraint violations due to the BESS exceeding (falling below) the $\mathrm{SOC}_{\max}$ ($\mathrm{SOC}_{\min}$). A higher SD of the uncertainty would cause the closed-loop behavior of the system to differ significantly from the open-loop solutions given by (4.11) which in addition to increasing the likelihood of violations may also compel expensive BESS dispatch to handle the uncertainty and satisfy Assumption 4.4(a).

Table 4.2. Results for the 4 test cases for the year 2019. Monthly costs are added to compute the yearly cost.

Costs	Traditional 1	OA-SMPC	SMPC Lit [21]	Traditional 2
NCDC	\$66,586	\$64,579	\$66,960	\$57,690
OPDC	\$1,959	\$1,274	\$2,087	\$1,148
Energy Cost	\$14,382	\$14,385	\$14,382	\$14,399
BESS loss	\$8,290	\$9,071	\$8,309	\$10,447
Total Cost	\$91,217	\$89,309	\$91,738	\$83,683
Total BESS cycles	165.8	181.4	166.2	208.9
Y at year end	0%	10.1%	2.2%	20.4%

Figure 4.2 and Table 4.2 summarize the simulation results of the 4 test cases for the year 2019. Note that the energy costs are similar across all cases as there is no arbitrage in the MG model. The minute differences in energy costs are due to the different ending BESS SOC at the end of the year for the different test cases.

The comparison between the Traditional EMPC 1 and OA-SMPC demonstrates the superior economic performance of our proposed algorithm while still staying within the maximum allowable violation probability bound. NCDC and OPDC decrease by 3% and 35% between Traditional EMPC 1 and OA-SMPC. The OPDC savings (as a %) are significantly more than NCDC because of the operation strategy (see Section 4.3.4) allowing preferential violations during OP hours. As extra BESS capacity is available for the OA-SMPC as compared to the Traditional EMPC 1 due to the adaptive relaxation of BESS SOC constraints beyond the $0.2-0.8$ SOC range, the BESS is used more aggressively in OA-SMPC resulting in 9.4% more BESS losses amounting to 15.6 extra BESS yearly cycles. Overall, OA-SMPC leads to 2.1% total yearly cost savings as compared to the Traditional EMPC 1. SMPC Lit performs the worst as it tightens the feasible SOC range and leads to highest yearly cost. Some violations are caused due to the effect of uncertainty in the closed-loop but it is unable to reduce costs as the timing of the uncertainty is critical in reducing demand charges. The NCDC and OPDC are greater in SMPC Lit as compared to both the Traditional EMPC 1 and OA-SMPC. SMPC Lit has similar BESS

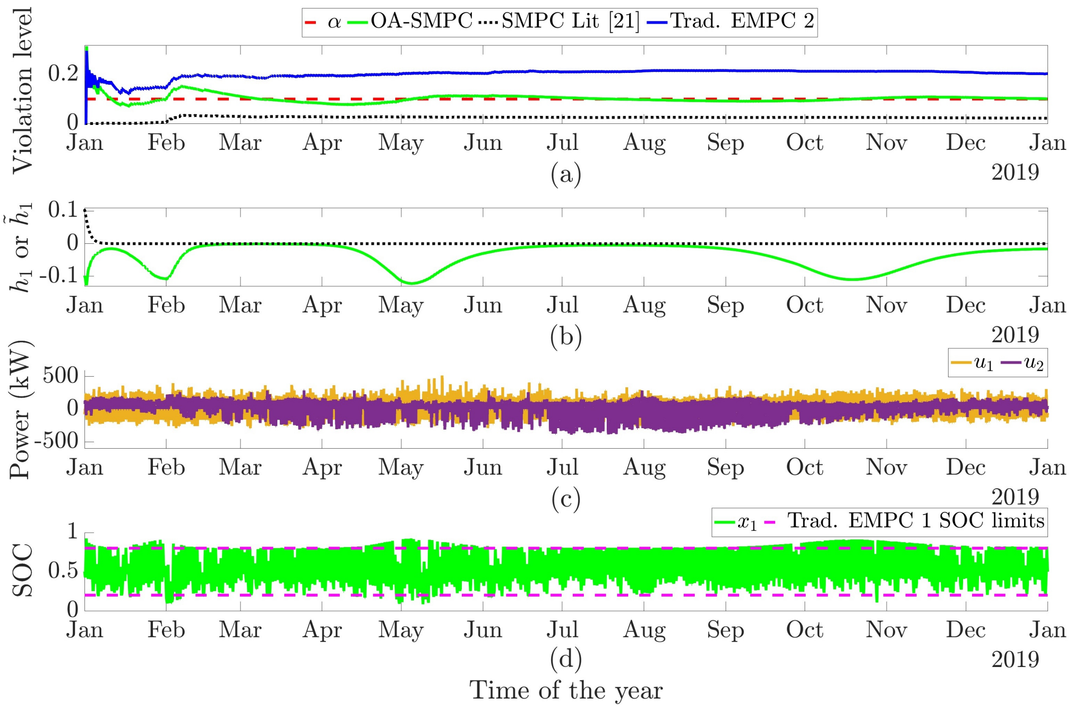

Figure 4.2. Yearly time-series for the: (a) time-average of state constraint violations (Y) for the OA-SMPC, SMPC Lit [21], and Traditional EMPC 2 case studies, and the maximum allowable state constraint violation probability ($\alpha = 0.1$), (b) adaptive state constraint relaxing/tightening parameters (h_1 and $\tilde{h}_1$, with $h_1 = h_2$, and $\tilde{h}_1 = \tilde{h}_2$ in these case studies) for the OA-SMPC and SMPC Lit, (c) closed-loop behavior of the control inputs for the OA-SMPC, (d) closed-loop behavior of the state for the OA-SMPC.

cycles as the Traditional EMPC 1 with 0.6% extra yearly costs. This serves as a proof of the concept alluded to in Remark 4.3 that adaptive constraint tightening methods (like SMPC Lit) can be over-conservative being unable to exploit the allowable violation limit which can be particularly disadvantageous in EMPC frameworks.

Figure 4.2(a) shows the variation of Y for the OA-SMPC (green line), and SMPC Lit (black dotted line) for the entire year. For the OA-SMPC, initially, Y is 0 until the first constraint violation occurs, after which it overshoots α, oscillating with a high frequency and magnitude until the first week of January. Then, consistent with the goal of Y converging to a value less than or equal to α, Y decreases and oscillates about α with lower frequency and magnitude, as the system evolves, and finally reaching a value of 10.1% at the end of the year (which is within a small margin of α). It is expected for Y to decrease below α if the OA-SMPC is run over a longer time period, resulting in satisfying the chance constraints, albeit nonconservatively, in closed-loop. Figure 4.2(b) shows that for the OA-SMPC, h_1 and h_2 increase and decrease depending on the overshoot and undershoot of Y with respect to α respectively, being able to expand and contract the feasible state set accordingly to keep Y near α. Figures 4.2(c) and 4.2(d) demonstrate the yearly closed-loop behavior of the BESS dispatch and grid import, and SOC respectively for the OA-SMPC. For a significant portion of the year, the grid import is negative because the PV system at the location is oversized generating excess power which is fed back to the grid. Significant violation of constraints can be seen in Figure 4.2(d) in the months of May and October, which are the two months that aid most is cost savings.

Figure 4.2(b) also shows that for the SMPC Lit, the $\tilde{h}_1$ and $\tilde{h}_2$ quickly drop down to 0 in the first week of January trying to encourage violations initially as the initial constraint tightening was too conservative. However, the system's Y still stays far below α, with the result that $\tilde{h}_1$ and $\tilde{h}_2$ stay close to 0^+ throughout the year behaving essentially like the Traditional EMPC 1 in the nominal MPC with allowance for SOC limits to range from 0 to 1 in closed-loop. In the months of February and March (not shown in Figures), SMPC Lit creates more NCDC than Traditional EMPC 1, because just before the NCDP time, a high uncertainty forces the SOC to go below the lower limit of 0.2, which causes a large BESS charging action at the next time-step to climb back to the feasible SOC range of above 0.2 causing demand peaks, a problem alluded to in Remark 4.19.

Traditional EMPC 2 demonstrates that relaxing the state (BESS SOC) constraints by the same initial relaxation parameter as in OA-SMPC without any adaptation causes the violations to exceed the maximum allowable violation probability bound in closed-loop (blue line in Fig. 4.2(a)). The Traditional EMPC 2 has lower total yearly electricity costs (due to lower NCDC and OPDC), than the OA-SMPC because the objective function in (4.27) penalizes peaks in grid import power (u_2) more than BESS dispatch power (u_1), resulting in prolonged aggressive dispatch of the BESS to serve the net load ($L-\mathrm{PV}$).

The aggressive BESS dispatch is more prolonged in Traditional EMPC 2 than OA-SMPC because the feasible BESS SOC range in Traditional EMPC 2 is not adapted due to past violations, and the feasible state set continues being larger than OA-SMPC throughout. The Traditional EMPC 2 shows higher frequency of oscillation and magnitude of overshoot of Y above α as compared to OA-SMPC, and additionally shows that Y consistently remains above 2α for the majority of the year. Thus, the Traditional EMPC 2 is unable to fulfill the chance constraints and may significantly harm BESS life, resulting in 27.5 more yearly BESS cycles as compared to OA-SMPC. The analysis serves as a proof of concept that it is the adaptive relaxation rule in OA-SMPC rather than the nature of uncertainties which ensure nonconservative chance constraint satisfaction in closed-loop in OA-SMPC.

Figure 4.3 and Table 4.3 present the results of the OA-SMPC analysis when it is repeated with different values of $\alpha \in \{0.05, 0.15, 0.2\}$, with the same other design parameters as in Table 4.1. Figure 4.3 shows that in all the cases, similar behavior is observed as in Fig. 4.2(a) with Y oscillating about α with lower frequency and magnitude as the system evolves with time along the year while ultimately settling at a value below α at year-end, thereby tightly satisfying the chance constraints. Table 4.3 demonstrates that superior cost savings are attained when α increases at the cost of more BESS cycles. Comparing the case with $\alpha = 0.2$ in Table 4.3 with Traditional EMPC 2 in Table 4.2 shows that the OA-SMPC is more effective at reducing costs with less violations and BESS cycles than the Traditional EMPC 2 due to the OA-SMPC's online adaptivity.

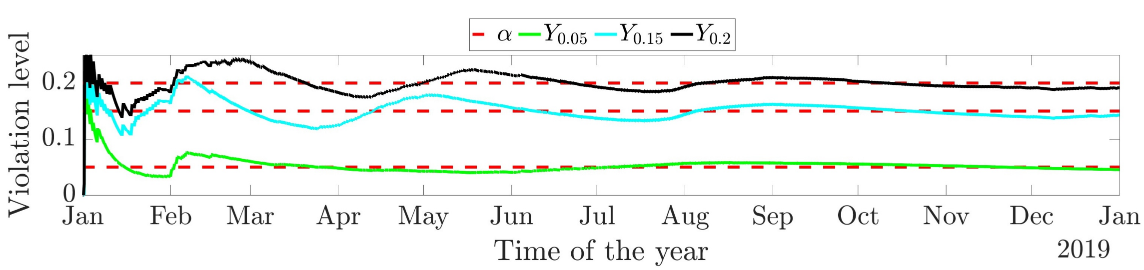

Figure 4.3. Yearly time-series for the time-average of state constraint violations (Y_α) for the OA-SMPC for the maximum allowable state constraint violation probability $\alpha \in \{0.05, 0.15, 0.2\}$.

Table 4.3. Results for the OA-SMPC with different values of maximum probability of violation of state constraints (α) for the year 2019.

Costs	$\alpha = 0.05$	$\alpha = 0.15$	$\alpha = 0.2$
NCDC	\$66,294	\$59,564	\$57,323
OPDC	\$1,865	\$1,036	\$540
Energy Cost	\$14,383	\$14,395	\$14,395
BESS loss	\$8,473	\$9,747	\$10,336
Total Cost	\$91,014	\$84,742	\$82,593
Total BESS cycles	169.5	194.9	206.7
Y at year end	4.5%	14.3%	19.1%

Acknowledgements

This chapter, in full, is a reprint of the material as it appears in 'Adaptive Relaxation-Based Nonconservative Chance Constrained Stochastic MPC' authored by Avik Ghosh, Cristian Cortes-Aguirre, Yi-An Chen, Adil Khurram, and Jan Kleissl, in the IEEE Transactions on Control Systems Technology, 2025. The dissertation author was the primary investigator and author of this paper.

Chapter 5

Deterministic EMPC with an online reference trajectory

5.1 Problem statement

EMPC instead of stabilizing a reference trajectory/state in the objective function like a Tracking MPC, optimizes the economic performance over the prediction horizon, making it particularly attractive for economical MG dispatch. However, the demand charge component in the monthly electricity cost, which is based on the maximum monthly grid import power of the MG from the main grid, make it difficult to be encapsulated in additive stage costs, and can make solutions violate the principle of optimality if naively introduced in the objective function. Moreover, previous EMPC based works mostly rely on a-priori knowledge of an optimal economic steady state or optimal periodic trajectory for performance guarantees, which are not useful or possibly don't exist respectively, for real-time economical MG dispatch where load/generation forecasts are known only $24-48$ h in advance.

In this chapter, we propose an EMPC formulation for a generic deterministic discrete non-linear time varying system with hard state and input constraints, without any a-priori requirements of an optimal economic steady state or optimal periodic trajectory. It is proved that under mild assumptions on terminal cost and region, the asymptotic average economic cost of the proposed method is no worse than the asymptotic average economic cost of any other non-fixed arbitrary reference trajectory which is known only until the current time-step.

5.2 Problem formulation

5.2.1 System description

The dynamics of the deterministic (i.e., uncertainty-free) discrete non-linear time-varying system is governed by,

$$x(t+1) = f(x(t), u(t), t), \qquad \forall t, \tag{5.1}$$

where the state x at time $t \in \mathbb{T}$, belongs to a set defined as $\mathbb{X}(t)$, implying $x(t) \in \mathbb{X}(t)$. Similarly, the control input $u(t) \in \mathbb{U}(t)$. The composite sets $\mathbb{X}$ and $\mathbb{U}$ are defined by $\mathbb{X} := \bigcup_{t\in\mathbb{T}} \mathbb{X}(t)$ and $\mathbb{U} := \bigcup_{t\in\mathbb{T}} \mathbb{U}(t)$, which overall implies $f : \mathbb{X}(t) \times \mathbb{U}(t) \times \mathbb{T} \to \mathbb{X}(t+1)$.

We denote the solution to (5.1) over a horizon N starting from an initial state x_0 and time t_0 (i.e., $x(t_0) = x_0 \in \mathbb{X}(t_0)$), under the control sequence parameterized by x_0 and t_0, i.e., $\mathbf{u}(x_0,t_0) = \big(u(t_0;(x_0,t_0)), u(t_0+1;(x_0,t_0)), \ldots, u(t_0+N-1;(x_0,t_0))\big)^\top$, as the state sequence $\mathbf{x}^{\mathbf{u}}(x_0,t_0) = \big(x_0, x(t_0+1;(x_0,t_0)), \ldots, x(t_0+N;(x_0,t_0))\big)^\top$.[1] From hereon, for ease of notation we will denote $u(t_0+k;(x_0,t_0))$ as $u(t_0+k)$, $\forall k \in \mathbb{N}_0^{N-1}$. Similarly $x(t_0+k;(x_0,t_0))$ is denoted by $x(t_0+k)$, $\forall k \in \mathbb{N}_0^{N}$.

We consider an arbitrary solution for the system (5.1), denoted by the sequence of states and control inputs that satisfy (5.2), as the reference trajectory. The dynamics of the reference trajectory are thus,

$$x^r(t+1) = f(x^r(t), u^r(t), t), \qquad \forall t, \tag{5.2}$$

[1]Note that to avoid confusion, a state and control input sequence are denoted by boldface $\mathbf{x}$ and $\mathbf{u}$, respectively. The state and control input sequences are composed of a collection of individual state and control inputs varying over time. The individual state and control inputs at time t are denoted by non-boldface $x(t)$ and $u(t)$ respectively.

where $x^r(t) \in \mathbb{X}(t)$ and $u^r(t) \in \mathbb{U}(t)$. Unlike [45], in this work, the reference trajectory is not assumed to be fixed (and known) a-priori for all times under consideration, but is only known until the current time t. This means that at time t, $\{\big(x^r(t'), u^r(t'), x^r(t'+1)\big), \forall t' \leq t\}$ is known. At time t, $x^r(t+1)$ is known because of the substitution of $\{x^r(t), u^r(t)\}$ in the uncertainty-free dynamics (5.2).[2] The reference trajectory can be generated online from a separate optimization or rules-based method and its knowledge only until the current time is more realistic than [45], especially for applications such as BESS control for VRE integrated MGs involving a variety of forecasts. For example, for optimal BESS dispatch in VRE intensive MGs, forecasts for VRE generation and load are required. These forecasts are typically known only hours or a few days in advance [44], unlike [45] where forecasts have to be assumed months or weeks in advance to fix the reference trajectory a-priori which is unrealistic.

5.2.2 Receding horizon EMPC

The economic MPC problem to be solved over a receding prediction horizon of length N, initialized from state $x(t)$ and time t, is given by

$$\begin{aligned} V_N^0(x(t),t) &= \underset{\mathbf{u}(x(t),t)\in\mathbb{U}^N}{\text{minimize}} \; V_N(x(t),\mathbf{u}(x(t),t),t) \\ &= \underset{\mathbf{u}(x(t),t)\in\mathbb{U}^N}{\text{minimize}} \sum_{k=0}^{N-1} l(x(t+k|t),u(t+k|t),t+k) + V_f(x(t+N|t),t+N), \end{aligned} \tag{5.3a}$$

subject to

$$x(t+k+1|t) = f(x(t+k|t),u(t+k|t),t+k), \qquad \forall k \in \mathbb{N}_0^{N-1}, \forall t \in \mathbb{T}, \tag{5.3b}$$

$$x(t+k|t) \in \mathbb{X}(t+k), \qquad \forall k \in \mathbb{N}_0^{N-1},\ \forall t \in \mathbb{T}, \tag{5.3c}$$

[2]Note that at time t, although $x^r(t+1)$ is known, $u^r(t+1)$ is unknown.

$$u(t+k|t) \in \mathbb{U}(t+k), \qquad \forall k \in \mathbb{N}_0^{N-1}, \forall t \in \mathbb{T}, \tag{5.3d}$$

$$x(t+N|t) \in \mathbb{X}_f(t+N) \subseteq \mathbb{X}(t+N), \qquad \forall t \in \mathbb{T}, \tag{5.3e}$$

where V_N in the objective function defined as $V_N : \mathbb{X}(t) \times \mathbb{U}^N \times \mathbb{T} \to \mathbb{R}$, which consists of the additive economic stage cost function $l : \mathbb{X}(t) \times \mathbb{U}(t) \times \mathbb{T} \to \mathbb{R}$, and the terminal cost function $V_f : \mathbb{X}_f(t) \times \{\mathbb{T} \cap \mathbb{N}_{\geq N}\} \to \mathbb{R}$. The composite terminal constraint set is defined by $\mathbb{X}_f := \bigcup_{t \in \mathbb{T} \cap \mathbb{N}_{\geq N}} \mathbb{X}_f(t)$.

The optimal control sequence on solving (5.3) is given by $\mathbf{u}^0(x(t),t) = \big(u^0(t|t), u^0(t+1|t), \ldots, u^0(t+N-1|t)\big)^\top$. Similarly, the optimal state sequence on applying the optimal control sequence is given by $\mathbf{x}^{\mathbf{u}^0}(x(t),t) = \big(x(t), x^0(t+1|t), \ldots, x^0(t+N-1|t), x^0(t+N|t)\big)^\top$. The closed-loop control law is given by the first element of $\mathbf{u}^0(x(t),t)$, represented as $\kappa_N(x(t),t) := u^0(t|t)$ which is applied to the system at time t. The closed-loop system is thus represented by,

$$x(t+1) = f(x(t), \kappa_N(x(t),t), t), \qquad \forall t \in \mathbb{T}, \tag{5.4}$$

where $\kappa_N : \mathbb{X}(t) \times \mathbb{T} \to \mathbb{U}(t)$, and after $x(t+1)$ is calculated from (5.4), the optimization in (5.3) is repeated from the updated state $x(t+1)$, and time $t+1$.

Assumption 5.1 (**Continuity of system and cost** [**45, 49**])**.** *The functions $f(\cdot)$, $l(\cdot)$ and $V_f(\cdot)$ are continuous.*

Assumption 5.2 (**Properties of constraint sets** [**45, 49**])**.** *For each $t \in \mathbb{T}$, $\mathbb{X}(t)$ is closed, and $\mathbb{U}(t)$ is compact. For each $t \in \mathbb{T} \cap \mathbb{N}_{\geq N}$, $\mathbb{X}_f(t)$ is closed. $x^r(t) \in \mathbb{X}(t)$ and $u^r(t) \in \mathbb{U}(t)$. The composite set $\mathbb{U}$ is bounded.*

Remark 5.3 (**Existence of a solution of the optimal control problem** (5.3) [**45, 49**])**.** *From Assumptions 5.1 and 5.2, a solution of* (5.3) *exists for $x(t) \in \mathbb{X}(t)$, $\forall t \in \mathbb{T}$*

if (5.3b)*,* (5.3c)*,* (5.3d) *and* (5.3e) *is satisfied over the prediction horizon* N *[49, Proposition 2.29].*

Assumption 5.4 (**Uniqueness of the solution to the optimal control problem** (5.3) [**45, Remark 1**]). *For* $x(t) \in \mathbb{X}(t)$, $\forall t \in \mathbb{T}$*, the control sequence associated with solving* (5.3) *is unique.*

Assumption 5.5 (**Properties of terminal cost, region and control law**). *For each* $t \in \mathbb{T} \cap \mathbb{N}_{\geq N}$*, if* $x(t) \in \mathbb{X}_f(t)$*, there exists a terminal control law* $\kappa_f : \mathbb{X}_f(t) \times \{\mathbb{T} \cap \mathbb{N}_{\geq N}\} \rightarrow \mathbb{U}(t)$*, such that,*

$$
\begin{aligned}
V_f\big(f(x(t),\kappa_f(x(t),t),t),t+1\big) - V_f(x(t),t) \leq \\
- l\big(x(t),\kappa_f(x(t),t),t\big) + l\big(x^r(t-N),u^r(t-N),t-N\big).
\end{aligned}
$$

The reason for using $l\big(x^r(t-N),u^r(t-N),t-N\big)$ for the last term in the RHS of Assumption 5.5 instead of $l\big(x^r(t),u^r(t),t\big)$ as in [45, Assumption 3] is to widen the practical applicability of the present study as compared to [45], and is discussed later in Remark 5.8. Note that Assumption 5.5 implicitly implies that, applying the terminal control law κ_f to $x(t) \in \mathbb{X}_f(t)$, leads to $f\big(x(t),\kappa_f(x(t),t),t\big) \in \mathbb{X}_f(t+1), \forall t \in \mathbb{T} \cap \mathbb{N}_{\geq N}$. In other words, the sequence of sets $\mathbb{X}_f(t)$, $\forall t \in \mathbb{T} \cap \mathbb{N}_{\geq N}$ is sequentially control invariant for (5.1) [49, Definition 2.27].

Assumption 5.6 (**Lower boundedness of stage and terminal cost [45, 49]**). *The function* $l(\cdot)$ *is uniformly bounded below for* $\big\{x(t),u(t),t\big\} \in \mathbb{X}(t) \times \mathbb{U}(t) \times \mathbb{T}$*. Similarly, the function* $V_f(\cdot)$ *is uniformly bounded below for* $\{x(t),t\} \in \mathbb{X}_f(t) \times \{\mathbb{T} \cap \mathbb{N}_{\geq N}\}$*.*

Theorem 5.7 (**Asymptotic average cost guarantee of the receding horizon EMPC**). *Let Assumptions 5.1, 5.2, 5.4, 5.5, and 5.6 hold. The asymptotic average economic cost of the closed-loop system given by* (5.4) *is no worse than the asymptotic* *average economic cost of the reference trajectory given by* (5.2). *Specifically,*

$$\limsup_{T\to\infty} \sum_{t=t_0}^{t_0+T-1} \frac{1}{T}\Big(l\big(x(t),u(t),t\big) - l\big(x^r(t),u^r(t),t\big)\Big) \le 0,$$

where $u(t) = \kappa_N(x(t),t)$, $\forall t \in \mathbb{T}$.

Proof. The proof of Theorem 5.7 is similar to [45, Theorem 1], but extends the asymptotic average cost guarantee from [45] to the case when the reference trajectory is not fixed (and thus not completely known) a-priori for the entire time period under consideration, but is only known until the current time t.

From Remark 5.3 and Assumption 5.4, we know that at time t, a unique optimal solution to (5.3) exists and is given by $\mathbf{u}^0(x(t),t)$, with $V_N^0(x(t),t) = V_N(x(t),\mathbf{u}^0(x(t),t),t)$. A feasible control sequence at time $t+1$ is given by the final $N-1$ control inputs of $\mathbf{u}^0(x(t),t)$, and appending a terminal control input by following Assumption 5.5, as $x(t+N|t) \in \mathbb{X}_f(t+N)$. Specifically, after $\kappa_N(x(t),t)$ is applied to $x(t)$ which makes the system state evolve to $x(t+1)$, a feasible control sequence at $t+1$ for (5.3) is given by $\mathbf{u}(x(t+1),t+1) = \big(u^0(t+1|t),\ldots,u^0(t+N-1|t),\kappa_f(x^0(t+N|t),t+N)\big)^\top$. As the optimal cost is a lower bound of any feasible cost at any time, we conclude $V_N^0(x(t+1),t+1) \le V_N(x(t+1),\mathbf{u}(x(t+1),t+1),t+1)$. Thus, it follows that,

$$\begin{aligned}
V_N^0(x(t+1),t+1) - V_N^0(x(t),t) &\le V_N(x(t+1),\mathbf{u}(x(t+1),t+1),t+1) - V_N^0(x(t),t)\\
&= l(x^0(t+N|t),\kappa_f(x^0(t+N|t),t+N),t+N)\\
&+V_f\big(f(x^0(t+N|t),\kappa_f(x^0(t+N|t),t+N),t+N),t+N+1\big)\\
&-l(x(t),\kappa_N(x(t),t),t) - V_f(x^0(t+N|t),t+N)\\
&\le -l(x(t),\kappa_N(x(t),t),t) + l(x^r(t),u^r(t),t)
\end{aligned} \tag{5.5}$$

Summing the inequality in (5.5) from an initial time t_0 to t_0+T-1 and dividing by the number of time steps T gives,

$$\sum_{t=t_0}^{t_0+T-1} \frac{V_N^0(x(t+1),t+1) - V_N^0(x(t),t)}{T} \leq \sum_{t=t_0}^{t_0+T-1} \frac{-l(x(t),\kappa_N(x(t),t),t) + l(x^r(t),u^r(t),t)}{T} \tag{5.6}$$

Rearranging by interchanging the LHS and RHS of (5.6) and taking the limit superior of both sides (as the LHS limit may not exist after rearranging) at $T \to \infty$ gives us,

$$\begin{aligned}&\limsup_{T\to\infty} \sum_{t=t_0}^{t_0+T-1} \frac{1}{T}\Big(l\big(x(t),\kappa_N(x(t),t),t\big) - l\big(x^r(t),u^r(t),t\big)\Big)\\ &\leq \limsup_{T\to\infty} \frac{1}{T}\Big(V_N^0(x(t_0),t_0) - V_N^0(x(t_0+T),t_0+T)\Big)\end{aligned} \tag{5.7}$$

We know from Assumption 5.6 that $V_N^0(x(t),t)$ is lower bounded by some constant $C \in \mathbb{R}$, $\forall t \in \mathbb{T}$, and $V_N^0(x(t_0),t_0)$ is also a constant. Thus, the RHS of (5.7) can be written as

$$\limsup_{T\to\infty} \frac{1}{T}\Big(V_N^0(x(t_0),t_0) - V_N^0(x(t_0+T),t_0+T)\Big) \leq \limsup_{T\to\infty} \frac{1}{T}\Big(V_N^0(x(t_0),t_0) - C\Big) = 0 \tag{5.8}$$

Combining (5.7) and (5.8) completes the proof with $u(t) = \kappa_N(x(t),t)$, $\forall t$. □

Remark 5.8 (Wider practical applicability of Assumption 5.5 as compared to [45]). *Assumption 5.5 modifies [45, Assumption 3] to make analysis possible when the reference trajectory is not fixed (and thus not completely known) a-priori for the time period under consideration, and is known only until the current time-step, and is thus more realistic and has wider practical applicability than [45]. This is because if [45, Assumption 3] is used instead of Assumption 5.5, the last term in the RHS of* (5.5) *would be $l(x^r(t+N),u^r(t+N),t+N)$, which at time t is assumed to be known for [45], making it restrictive,*[3] *but can be unknown for our system.*

[3]This is because [45] assumes knowledge of the reference trajectory for all times under consideration from the start which is practically impossible for problems like economic MG dispatch involving a variety of forecasts (see Section 5.2.1 for a detailed discussion)

5.3 Extension of EMPC to optimal MG dispatch

In this section, we will apply the EMPC structure from Section 5.2.2 to the optimal MG dispatch problem. Here, we consider a MG with local gross load demand, PV generation, with an installed BESS and connection to the main grid. The goal of the receding horizon EMPC based optimal MG dispatch problem is: *At each time t, under a given perfect forecast of load and VRE (PV in this case) generation over a prediction horizon N, compute the optimal BESS dispatch profile to minimize electricity costs (defined later in Section 5.3.2) over the prediction horizon, with the goal of reducing monthly electricity costs as well.*

5.3.1 MG model

In this section, we first consider the original MG model which is a linear-time-invariant (LTI) system consisting of one constituent state $x_1(t)$, and two constituent control inputs represented by $u(t) = \begin{bmatrix} u_1(t) & u_2(t) \end{bmatrix}^\top$. Later, we will augment this original MG model to add other constituent states $x_2(t)$, $x_3(t)$ with the motivation and dynamics for $x_2(t)$ and $x_3(t)$ becoming clear in Section 5.3.2 and formulations presented in Sections 5.3.3 and 5.3.4 respectively. The original MG model is represented in the structure of the receding horizon EMPC as in Section 5.2.2 as follows

$$x_1(t+1) = Ax_1(t) + Bu(t), \qquad \forall t, \tag{5.9a}$$

$$Su(t) \leq s, \qquad \forall t, \tag{5.9b}$$

$$Mu(t) = c(t), \qquad \forall t, \tag{5.9c}$$

$$Gx_1(t) \leq g, \qquad \forall t, \tag{5.9d}$$

where $x_1(t) \in \mathbb{R}_{\geq 0}$ is the BESS state of charge (SOC). The control inputs are $u(t) = \begin{bmatrix} u_1(t) & u_2(t) \end{bmatrix}^\top$ where $u_1(t) \in \mathbb{R}$ is the BESS dispatch power, and $u_2(t) \in \mathbb{R}$ is the grid import power. $u_1(t) > 0$ denotes charging, while $u_2(t) > 0$ denotes power import from the main grid to the MG. The EMPC prediction horizon is subdivided into N equal time-steps of Δt duration each.

The system matrices are $A = [1]$, $B = \begin{bmatrix} \frac{\Delta t}{\text{BESS}_{\text{en}}} & 0 \end{bmatrix}$, where BESS_{en} is the energy capacity of the BESS. The system matrices handle the SOC update of the battery due to charging/discharging by (5.9a). For the hard control input constraints (5.9b),

$$S = \begin{bmatrix} 1 & 0 \\ -1 & 0 \\ 0 & 1 \\ 0 & -1 \end{bmatrix}, \text{ and, } s = \begin{bmatrix} \text{BESS}_{\text{max}} \\ \text{BESS}_{\text{max}} \\ \hat{b} \\ -\hat{a} \end{bmatrix},$$

which constrains the maximum charging/discharging power of the BESS and MG power exchange with the main grid. Practically, $|\hat{a}|$ and $|\hat{b}|$ is chosen to be very large so that the MG power exchange with the grid constraints are never active so as to negate the risk of violating (5.9c) as the main grid can be conceptualized as an infinite bus. The PV generation and gross load are denoted by $\text{PV}(t)$ and $L(t)$ respectively and are used as forecast inputs to the MPC which are assumed to be known perfectly for the prediction horizon. For the time varying equality constraints coupling the control inputs given by (5.9c), $M = \begin{bmatrix} 1 & -1 \end{bmatrix}$, $c(t) = [\text{PV}(t) - L(t)]$, which ensures power balance of the MG with the main grid. The hard state constraints represented by (5.9d) limits the SOC of the BESS between upper (SOC_{max}) and lower bounds (SOC_{min}) making $G = \begin{bmatrix} 1 & -1 \end{bmatrix}^\top$, and $g = \begin{bmatrix} \text{SOC}_{\text{max}} & -\text{SOC}_{\text{min}} \end{bmatrix}^\top$.

5.3.2 Electricity cost structure

In general, the monthly electricity costs for a MG involves volumetric energy charges (\$/kWh) and demand charges (\$/kW). Two distinct time-of-use demand charges are used: one based on maximum grid imports for the whole month called non-coincident demand peak (NCDP), added on top of maximum grid import between $16:00-21:00$ h of all days of the month, called on-peak demand peak (OPDP). The demand charges associated with NCDP and OPDP are called non-coincident demand charges (NCDC), and on-peak demand charges (OPDC) respectively. The pricing structure can be extended to other forms of demand charges or adjusted to account for NCDC only by setting the OPDC terms to 0.

As demand charges are calculated over a monthly window, consider a month being equally subdivided into T equal time-steps of Δt duration each. For each month, let $\mathscr{T}_w \subset \mathbb{T}$ be the set of all time-steps for the monthly window. Specifically, $\mathscr{T}_w = \{0, 1, 2, \ldots, T-1\}$. $\mathscr{T}'_w \subset \mathscr{T}_w$ denotes the set of time-steps of the month over which OPDC is calculated.

The monthly electricity costs are formulated as [65, 70]

$$\sum_{t=0}^{T-1} \Big[R_{\mathrm{EC}}(t) \Delta t \Big(u_2(t) + \frac{(1-\eta)}{2} |u_1(t)| \Big) \Big] + R_{\mathrm{NC}} \max_{k \in \mathscr{T}_w} u_2(k) + R_{\mathrm{OP}} \max_{k \in \mathscr{T}'_w} u_2(k), \tag{5.10}$$

where the first, second, third, and fourth terms cover the energy charges, BESS losses, NCDC, and OPDC. respectively. Note that demand charges can never be negative.[4] The time-of-use energy charge rate, NCDC rate, OPDC rate, and round-trip efficiency of the BESS are denoted by $R_{\mathrm{EC}}(t)$, R_{NC}, R_{OP} and η, respectively. The first two terms in (5.10), i.e., the terms inside the summation, can be encapsulated as an additive economic stage cost, being dependent only on the current input and time. However, because of the

[4] In (5.10), it is implicitly assumed that $\max_{k \in \mathscr{T}_w} u_2(k) \geq 0$, implying that at some time within the month the grid import is positive, which is a reasonable assumption for a MG with BESS installation. The third term in (5.10) can be generalized further to $R_{\mathrm{NC}} \max(0, \max_{k \in \mathscr{T}_w} u_2(k))$ to incorporate the non-negativity of demand charges explicitly but is avoided here for brevity. A similar implicit assumption entails for the OPDC term, where it is implicitly assumed that $\max_{k \in \mathscr{T}'_w} u_2(k) \geq 0$.

presence of demand charges which involve a maximization over multiple time-steps, it is challenging to encapsulate the demand charges, i.e., the third and fourth term in (5.10) as an additive economic stage cost being dependent only on the current state, input and time as in Section 5.2.2. Thus, to mitigate this issue, inspired by [45], we formulate the dynamics of the second and third constituent state, $x_2(t)$ and $x_3(t)$ respectively by augmenting the original MG model in Section 5.3.3 to represent the demand charge term as an additive economic stage cost as in Section 5.2.2.

5.3.3 Augmented system

For the augmented system, an additional constituent state $x_2(t) \in \mathbb{R}_{\geq 0}$, $\forall t$, is defined, which tracks the 'running' NCDP (i.e., the maximum grid import until the current time $t \in \mathscr{T}_w$) as

$$x_2(t+1) = \max\big(x_2(t), u_2(t)\big), \qquad \forall t. \tag{5.11}$$

To incorporate the OPDC, we define another state $x_3(t) \in \mathbb{R}_{\geq 0}$, $\forall t$, which tracks the 'running' OPDP (i.e., maximum grid import during OP hours until the current time $t \in \mathscr{T}_w$) as

$$x_3(t+1) = \max\big(x_3(t), \beta(t)u_2(t)\big), \qquad \forall t. \tag{5.12}$$

where

$$\beta(t) := \begin{cases} 1, & t \in \mathscr{T}'_w, \\ 0, & \text{otherwise.} \end{cases}$$

The augmented state is then denoted as $x(t) = \begin{bmatrix} x_1(t) & x_2(t) & x_3(t) \end{bmatrix}^\top$ with the augmented MG dynamics and additive economic stage cost being rewritten in (5.13a) and (5.13b) respectively.

$$x(t+1) = f(x(t),u(t),t) := \begin{pmatrix} Ax_1(t) + Bu(t) \\ \max\big(x_2(t),u_2(t)\big) \\ \max\big(x_3(t),\beta(t)u_2(t)\big) \end{pmatrix}, \qquad \forall t, \tag{5.13a}$$

$$\begin{aligned} l(x(t),u(t),t) :=\ & R_{\text{EC}}(t)\Delta t\Big(u_2(t) + \frac{(1-\eta)}{2}|u_1(t)|\Big) + R_{\text{NC}}\Big(a(t+1)x_2(t+1) - a(t)x_2(t)\Big) \\ & + R_{\text{OP}}\Big(b(t+1)x_3(t+1) - b(t)x_3(t)\Big), \qquad \forall t, \end{aligned} \tag{5.13b}$$

where, $a : \mathbb{T} \to \mathbb{R}$ is a function defining coefficients for $x_2(t)$, $\forall t \in \mathscr{T}_w$ with $a(T) = 1$, and $b : \mathbb{T} \to \mathbb{R}$ is a function defining coefficients for $x_3(t)$, $\forall t \in \mathscr{T}_w$ with $b(T) = 1$.[5]

Proposition 5.9 (**Encapsulating monthly electricity costs by the augmented additive economic stage cost [45, Remark 8]**). *The monthly electricity costs in* (5.10) *are exactly represented by the augmented additive stage cost in* (5.13b) *which is dependent only on the current augmented state, control input and time over the demand charge window, i.e., a month, represented by* $\mathscr{T}_w$.

Proof. Considering the demand charge window as $\mathscr{T}_w = \{0,1,2,\ldots,T-1\}$, $\mathscr{T}_w' \subset \mathscr{T}_w$, and summing (5.13b) over all the time-steps in $\mathscr{T}_w$ gives

$$\begin{aligned} \sum_{t=0}^{T-1} l(x(t),u(t),t) &= \sum_{t=0}^{T-1} \Big[R_{\text{EC}}(t)\Delta t\Big(u_2(t) + \frac{(1-\eta)}{2}|u_1(t)|\Big) \\ &\quad + R_{\text{NC}}\Big(a(t+1)x_2(t+1) - a(t)x_2(t)\Big) + R_{\text{OP}}\Big(b(t+1)x_3(t+1) - b(t)x_3(t)\Big)\Big] \\ &= \sum_{t=0}^{T-1} \Big[R_{\text{EC}}(t)\Delta t\Big(u_2(t) + \frac{(1-\eta)}{2}|u_1(t)|\Big)\Big] + R_{\text{NC}}\Big(a(T)x_2(T) - a(0)x_2(0)\Big) \\ &\quad + R_{\text{OP}}\Big(b(T)x_3(T) - b(0)x_3(0)\Big). \end{aligned} \tag{5.14}$$

[5] Note that $x(t+1)$ is a function of $\{x(t),u(t),t\}$ by (5.1). Thus, the terms multiplying R_{NC} and R_{OP} in the R.H.S. of (5.13b) is still implicitly dependent only on the current state, input and time.

Note, $x_2(0)=0$, $a(T)=1$, and $x_2(T)=\max_{k\in\mathscr{T}_w} u_2(k)$. Also, $x_3(0)=0$, $b(T)=1$, and $x_3(T)=\max_{k\in\mathscr{T}_w'} u_2(k)$. Substituting the above in (5.14), makes the last equality in (5.14) exactly equal to (5.10) which completes the proof. □

Remark 5.10 (**Implication of the augmented stage cost** (5.13b) **on Theorem 5.7 for optimal MG dispatch**). *For Theorem 5.7 to apply to the optimal dispatch problem where the demand charges are levied over a month, T in the upper limit of Theorem 5.7 has to correspond to the end of the month, i.e., the granularity of the control inputs should be infinitely large, i.e., $\Delta t \to 0$.*[6] *Theorem 5.7 applies on a monthwise basis for the optimal MG dispatch problem as the augmented stage cost* (5.13b) *encapsulates the complete demand charges only when added over the entire monthly window.*

5.3.4 Candidate terminal cost function, terminal region, and terminal control law for the augmented system: Choice 1

Having set up the the optimal MG dispatch problem in the standard EMPC form with additive stage costs in the objective function, in this section and Section 5.3.5, we will investigate terminal cost functions, regions and control laws which satisfy Assumptions 5.1, 5.2, 5.4, 5.5, and 5.6. Satisfaction of the above assumptions ensures that optimal MG dispatch problem has the same structure as the EMPC in Section 5.2.2, as a consequence of which the results of Theorem 5.7 hold. To determine a candidate terminal cost function, region, and control law, we first introduce Assumption 5.11 next.

Assumption 5.11 (**Length of the prediction horizon**). *For the optimal MG dispatch problem, the prediction horizon N is at least equal to the minimum required to traverse the entire admissible SOC set.*

Assumption 5.11, though theoretically limiting, is generally true for MG dispatch problems with prediction horizons generally being $24-48$ h, which is enough to traverse

[6] A more detailed discussion pertaining to a practical MG as in our case study can be found in Section 5.4.3.

the entire SOC set with the BESS dispatch power. From the MG model in Section 5.3.1 and 5.3.3, the admissible state set can thus be represented as $\mathbb{X}(t) \in [\mathrm{SOC}_{\min}, \mathrm{SOC}_{\max}] \times [0, \hat{b}] \times [0, \hat{b}]$, $\forall t \in \mathbb{T}$, where $\hat{b} < \infty$ for any practical scenario. The admissible control input set is given by $\mathbb{U}(t) \in [-\mathrm{BESS}_{\max}, \mathrm{BESS}_{\max}] \times [\hat{a}, \hat{b}]$, $\forall t \in \mathbb{T}$, where $-\infty < \hat{a} < \hat{b} < \infty$ for practical scenarios.

With Assumption 5.11 active, an obvious choice of the terminal cost and region is $V_f(t) := 0$ and $\mathbb{X}_f(t) := \{x_r(t-N)\}$ respectively, $\forall t \in \mathbb{T} \cap \mathbb{N}_{\geq N}$. However, such a choice would render a restrictive terminal control law requiring $l\big(x(t), \kappa_f(x(t),t), t\big) \leq l\big(x^r(t-N), u^r(t-N), t-N\big)$ with $x(t) = x^r(t-N)$, $\forall t \in \mathbb{T} \cap \mathbb{N}_{\geq N}$ to satisfy Assumption 5.5. Because of the structure of the iterated max operation in (5.13a), the above terminal region makes $x_2^r(t-N)$ and $x_3^r(t-N)$ a hard upper bound on $x_2(t-N+k|(t-N))$ and $x_3(t-N+k|(t-N))$ respectively, $\forall k \in \mathbb{N}_0^N, \forall t \in \mathbb{T} \cap \mathbb{N}_{\geq N}$ within the optimization in (5.3) which may lead to infeasibility. In addition, the above terminal region gives no incentive for the system within the optimization to choose $x_2(t-N+k|(t-N)) < x_2^r(t-N)$ or $x_3(t-N+k|(t-N)) < x_3^r(t-N)$, $\forall k \in \mathbb{N}_0^N, \forall t \in \mathbb{T} \cap \mathbb{N}_{\geq N}$ which could be advantageous if the reference trajectory is economically suboptimal.[7] An additional restriction arises for the optimal MG problem with the above terminal region. Note that according to (5.9a), and the structure of the control input matrix $\boldsymbol{B}$, the BESS SOC, $x_1(t)$, is only affected by the BESS dispatch, $u_1(t)$. As (5.9c) has to be satisfied for the optimal MG dispatch at all times to maintain power balance of the MG with the main grid, the above terminal region necessitates the following terminal control law

$$\kappa_f(x(t),t) := \left\{ \begin{pmatrix} u_1^r(t-N) \\ u_1^r(t-N) - c(t) \end{pmatrix} \right\}, \qquad \forall t \in \mathbb{T} \cap \mathbb{N}_{\geq N}, \tag{5.15}$$

where, $\max\big(x_2(t), u_1^r(t-N) - c(t)\big) = x_2^r(t-N+1)$, and $\max(x_3(t), \beta(t)\big(u_1^r(t-N) - c(t)\big) =$

[7]These findings are similar to [45, Sec. III-C].

$x_3^r(t-N+1)$ to ensure sequential control invariance of $\mathbb{X}_f(t)$, $\forall t \in \mathbb{T} \cap \mathbb{N}_{\geq N}$. The above equalities are highly restrictive and may not be satisfied for practical applications.

To mitigate the above restrictiveness, we design the following terminal cost function, region and control law, which allows the reference bound to be exceeded or not realized depending on the economic objective. The terminal region is defined as

$$\mathbb{X}_f(t) := \left\{ \begin{pmatrix} x_1^r(t-N) \\ x_2(t) \\ x_3(t) \end{pmatrix} \right\}, \qquad \forall t \in \mathbb{T} \cap \mathbb{N}_{\geq N}, \tag{5.16}$$

which implies that the BESS SOC in the optimization (5.3) must terminate (at the end of the prediction horizon) exactly at the current reference SOC, while the running NCDP $x_2(t)$, and running OPDP $x_3(t)$ can terminate at any value depending on the economic objective. The terminal control law is still represented by (5.15), however without the restrictive requirement of the reference and actual demand peaks to be the same. The terminal cost function is defined by (5.17) where the operational Assumption 5.12 has to be enforced by design to satisfy Assumption 5.5.

$$\begin{aligned} V_f(x(t),t) := {} & R_{\mathrm{NC}}\Big[\max\Big(a(t)x_2(t), a(t-N+1)x_2^r(t-N+1)\Big) - a(t-N+1)x_2^r(t-N+1)\Big] \\ & + R_{\mathrm{OP}}\Big[\max\Big(b(t)x_3(t), b(t-N+1)x_3^r(t-N+1)\Big) - b(t-N+1)x_3^r(t-N+1)\Big] \\ & - h(t), \qquad \forall t \in \mathbb{T} \cap \mathbb{N}_{\geq N}, \end{aligned} \tag{5.17}$$

where $h : \mathbb{T} \to \mathbb{R}$ is a bounded strictly increasing function, and Assumption 5.12 holds. $h(\cdot)$ is chosen as bounded in (5.17) to satisfy Assumption 5.6. The strictly increasing property of $h(\cdot)$ helps satisfy Assumption 5.5 as described next.

Assumption 5.12 (**Operational assumption for the optimal MG dispatch problem with terminal cost** (5.17) **to satisfy Assumption 5.5**). *Let* $A_1(t) = a(t)x_2(t)$, $B_1(t) =$

$b(t)x_3(t)$, $A_2(t) = a(t)x_2^r(t)$, and $B_2(t) = b(t)x_3^r(t)$. Then, the following holds $\forall t \in \mathbb{T} \cap \mathbb{N}_{\geq N}$:

$$\begin{aligned} h(t+1) - h(t) \geq & R_{\text{EC}}(t)\Delta t\Big(u_1^r(t-N) - c(t) + \frac{(1-\eta)}{2}|u_1^r(t-N)|\Big) \\ & - R_{\text{EC}}(t-N)\Delta t\Big(u_1^r(t-N) - c(t-N) + \frac{(1-\eta)}{2}|u_1^r(t-N)|\Big) \\ & + R_{\text{NC}}\Big[A_1(t+1) - A_1(t) + \max\Big(A_1(t+1), A_2(t-N+2)\Big) \\ & - \max\Big(A_1(t), A_2(t-N+1)\Big) + A_2(t-N) - A_2(t-N+2)\Big] \\ & + R_{\text{OP}}\Big[B_1(t+1) - B_1(t) + \max\Big(B_1(t+1), B_2(t-N+2)\Big) \\ & - \max\Big(B_1(t), B_2(t-N+1)\Big) + B_2(t-N) - B_2(t-N+2)\Big]. \end{aligned} \tag{5.18}$$

Note that although Assumption 5.12 might be theoretically limiting as $t \to \infty$ because $\lim_{t\to\infty}\big(h(t+1) - h(t)\big)$ is 0, but under practical scenarios under finite-time it is always possible to satisfy by choosing an appropriate $h(\cdot)$. However, for the rest of work we will ignore this possible theoretical limitation and let Assumption 5.12 hold $\forall t \in \mathbb{T} \cap \mathbb{N}_{\geq N}$.

Remark 5.13 (**Implication of the possible failure of Assumption 5.12 on Theorem 5.7 as $t \to \infty$ for practical scenarios**). *For practical MG operation scenarios, while Assumption 5.12 may fail to hold as $t \to \infty$, given a sufficiently large control input granularity, i.e., T is sufficiently (even though not infinitely) large, Theorem 5.7 would be modified to,*

$$\sum_{t=t_0}^{t_0+T-1} \frac{1}{T}\Big(l\big(x(t), u(t), t\big) - l\big(x^r(t), u^r(t), t\big)\Big) \leq \varepsilon,$$

where $\varepsilon > 0$ is small. The implication is that the average economic cost difference between the proposed system given by (5.4) *and reference trajectory given by* (5.2) *is upper bounded by a small positive constant, $\varepsilon \propto \frac{1}{T}$.*

Proposition 5.14 (**Satisfaction of Assumption 5.5 for the optimal MG dispatch problem with terminal cost** (5.17)). *The candidate terminal region, control law and* *terminal cost for the optimal MG dispatch problem as defined in* (5.16)*,* (5.15)*, and* (5.17) *respectively, for the system dynamics and additive stage cost as defined in* (5.13a) *and* (5.13b) *respectively, satisfies Assumption 5.5, if Assumption 5.12 holds.*

Proof. The result follows straightforwardly by substituting $x(t) \in \mathbb{X}_f(t)$ defined in (5.16), $\kappa_f(x(t),t)$ defined in (5.15), $V_f(x(t),t)$ defined in (5.17), $f\big(x(t),\kappa_f(x(t),t),t\big)$ from (5.13a) and $l\big(x(t),\kappa_f(x(t),t),t\big)$ and $l\big(x^r(t-N),u^r(t-N),t-N\big)$ from (5.13b) in the inequality of Assumption 5.5. The above terminal region, control law and dynamics also ensure the sequential control invariance of $\mathbb{X}_f(t)$. $\square$

Substituting (5.13b) and (5.17) in the objective function of the EMPC (5.3a) and simplifying yields,

$$\begin{aligned}
V_N(x(t),\mathbf{u}(x(t),t),t) = \sum_{k=0}^{N-1} &\Big[R_{\text{EC}}(t+k)\Delta t\Big(u_2(t+k|t)+\frac{(1-\eta)}{2}|u_1(t+k|t)|\Big)\Big] \\
&+\Bigg[R_{\text{NC}}\Bigg(a(t+N)x_2(t+N|t)-a(t)x_2(t) \\
&+\max\Big(a(t+N)x_2(t+N|t),a(t+1)x_2^r(t+1)\Big)-a(t+1)x_2^r(t+1)\Bigg)\Bigg] \\
&+\Bigg[R_{\text{OP}}\Bigg(b(t+N)x_3(t+N|t)-b(t)x_3(t) \\
&+\max\Big(b(t+N)x_3(t+N|t),b(t+1)x_3^r(t+1)\Big)-b(t+1)x_3^r(t+1)\Bigg)\Bigg] \\
&-h(t+N).
\end{aligned} \tag{5.19}$$

Remark 5.15 (Behavior of the terminal cost (5.17) **in the objective function** (5.19)**).** *The behavior of the chosen terminal cost* (5.17) *in the objective function can be seen in the third and fourth term in the second and third square bracket of* (5.19)*. Note that at time* t*,* $x^r(t+1)$ *is already known through a separate online optimization or rules-based method (see Section 5.2.1). The terminal cost term penalizes any increase of* *the scaled terminal running NCDP,* $a(t+N)x_2(t+N|t)$*, in the optimization (performed at* t*) from the scaled (already) realized reference running NCDP,* $a(t+1)x_2^r(t+1)$*. However, when* $a(t+N)x_2(t+N|t) < a(t+1)x_2^r(t+1)$*, the terminal cost term is conservative and does not reward the optimizer, as any reward might be premature which can lead to a later increase of running NCDP over the reference trajectory which is undesirable (negating predicted savings), as the complete reference trajectory has not been realized yet unlike [45]. Also note that the first term in the second square bracket of* (5.19) *coming from additive stage cost already penalizes an increase of* $a(t+N)x_2(t+N|t)$ *beyond necessary. A similar structure is followed for penalization of scaled running OPDP,* $b(t+N)x_3(t+N|t)$*, in the optimization (performed at* t*) from the scaled (already) realized reference running OPDP,* $b(t+1)x_3^r(t+1)$*, along with a secondary penalty on* $b(t+N)x_3(t+N|t)$ *from the additive stage cost.*[8]

The objective function and constraints of the optimal MG dispatch problem are now set up in the EMPC structure of Section 5.2.2. Next, we present the receding horizon EMPC formulation, akin to (5.3) using (5.19) as the objective function for the optimal MG dispatch problem. The EMPC formulation with (5.16) and (5.17) as terminal region and cost function, respectively, is refereed to as Choice 1 and is presented in Appendix 7.2.1 (excluded here for brevity). Appendix 7.2.1 also shows that the value of $h(\cdot)$ does not affect the optimal control sequence (i.e., the solution $\mathbf{u}^0$) on solving the EMPC. Thus, while $h(\cdot)$ theoretically has to exist to satisfy Assumption 5.12,[9] it is discussed in Appendix 7.2.1, that in practical scenarios $h(\cdot)$ need not be designed at all and the $h(t+N)$ term can be dropped from the optimization. The result, while counterintuitive, facilitates practical application while still preserving the guarantee of Theorem 5.7 and avoiding design complexity.

[8]Remark 5.15 can be understood in a more intuitive way by substituting $a(t) = b(t) = 1, \forall t \in \mathbb{T}$, but the original formulation is retained here for generality.

[9]For the optimal MG dispatch problem, by inspection we can additionally conclude that in practical scenarios Assumptions 5.1, 5.2, 5.4, and 5.6 are also satisfied.

5.3.5 Candidate terminal cost function, terminal region, and terminal control law for the augmented system: Choices 2 and 3

Although the terminal cost function, region, and control law in Section 5.3.4 ensure the asymptotic average cost guarantee of Theorem 5.7, the terminal region (specifically the requirement of BESS SOC at the end of the optimization ending at the current reference SOC as formulated in (7.10) due to terminal constraint (5.16)) may lead to suboptimal finite-time economic performance. We now seek to take advantage of Assumption 5.11 in further relaxing the conditions for constructing a terminal region, control law, and cost function.

Choice 2

As Assumption (5.11) holds, we can define $\mathbb{X}_f(t) := \mathbb{X}(t)$, $\forall t \in \mathbb{T} \cap \mathbb{N}_{\geq N}$, i.e., each of the terminal SOC and running NCDP and OPDP are free variables. In this case, any control input, $u(t) = \begin{bmatrix} u_1(t) & u_1(t) - c(t) \end{bmatrix}^\top$ and successor state $x(t+1)$, satisfying (5.9b), and (5.13a), (5.9d) respectively, can be a terminal control law (an obvious example is $u(t) = \begin{bmatrix} 0 & -c(t) \end{bmatrix}^\top$). Specifically, it means,

$$\mathbb{X}_f(t) := \left\{ \begin{pmatrix} x_1(t) \\ x_2(t) \\ x_3(t) \end{pmatrix} \right\}, \qquad \forall t \in \mathbb{T} \cap \mathbb{N}_{\geq N}, \tag{5.20}$$

$$\kappa_f(x(t),t) := \left\{ \begin{pmatrix} u_1(t) \\ u_1(t) - c(t) \end{pmatrix} \right\}, \qquad \forall t \in \mathbb{T} \cap \mathbb{N}_{\geq N}. \tag{5.21}$$

At this stage, (5.17) can be used as a terminal cost function with the requisite changes in the energy cost and battery loss terms in Assumption 5.12, due to (5.21), i.e., replacing $u_1^r(t-N)$ in the first and third term in the RHS of (5.18) by $u_1(t)$. The EMPC formulation with (5.20) as the terminal region and (5.17) as the terminal cost function is referred to as Choice 2 and is presented in Appendix 7.2.2. The EMPC formulation for Choice 2 is the same as that of Choice 1, but with a relaxed terminal constraint as the terminal BESS SOC is free. Note that the terminal region and control law for Choice 2 subsume the ones defined for Choice 1.

Choice 3

The candidate terminal region and control law is same as Choice 3 as for Choice 2 with the difference being in the terminal cost function. As discussed in Remark 5.15, the objective function in (5.19), which is borne out of the terminal cost function (5.17), penalizes the terminal running NCDP $x_2(t+N|t)$, and terminal running OPDP $x_3(t+N|t)$ twice, once from the additive stage cost and another time from the terminal cost. This makes the second penalization of $x_2(t+N|t)$ and $x_3(t+N|t)$ from the terminal cost redundant to the optimizer when peak demand charges dominate the objective function as compared to BESS losses and energy cost within a prediction horizon (i.e., when peak demand penalty is orders of magnitude higher than penalty on grid import or BESS losses). Thus, in certain cases, it might be helpful to remove this redundancy of double penalizing $x_2(t+N|t)$ and $x_3(t+N|t)$ by formulating the terminal cost to penalize the increase of $x_2(t+1|t)$ rather than $x_2(t+N|t)$ from $x_2^r(t+1|t)$. Similarly, penalizing an increase of $x_3(t+1|t)$ rather than $x_3(t+N|t)$ from $x_3^r(t+1|t)$ might be helpful. A motivation for such a penalty is given in Section 5.4.2. Thus, assuming for now, that such a penalization of $x_2(t+1|t)$ and $x_3(t+1|t)$ holds value in addition to penalizing $x_2(t+N|t)$ and $x_3(t+N|t)$, we can formulate another terminal cost function as defined by (5.22) where the operational Assumption 7.1 has to be enforced by design to satisfy Assumption 5.5.

$$\begin{aligned} V_f(x(t),t) := R_{\mathrm{NC}}\Big[&\max\Big(a(t-N+1)x_2(t-N+1), a(t-N+1)x_2^r(t-N+1)\Big) \\ &- a(t-N+1)x_2^r(t-N+1)\Big] \\ &+ R_{\mathrm{OP}}\Big[\max\Big(b(t-N+1)x_3(t-N+1), b(t-N+1)x_3^r(t-N+1)\Big) \\ &- b(t-N+1)x_3^r(t-N+1)\Big] - h(t), \qquad \forall t \in \mathbb{T} \cap \mathbb{N}_{\geq N}, \end{aligned} \tag{5.22}$$

where $h : \mathbb{T} \to \mathbb{R}$ is a bounded strictly increasing function as in (5.17), and Assumption 7.1 (see Appendix 7.2.2) holds. Assumption 7.1 is similar to Assumption 5.12 with the first elements of the max terms replaced and the energy cost and BESS loss terms modified due to the change of BESS dispatch and grid import, and is given in Appendix 7.2.2 for brevity.[10]

Proposition 5.16 (**Satisfaction of Assumption 5.5 for the optimal MG dispatch problem with terminal cost** (5.22))**.** *The candidate terminal region, control law, and terminal cost for the optimal MG dispatch problem as defined in* (5.20), (5.21), *and* (5.22), *respectively, for the system dynamics and additive stage cost as defined in* (5.13a) *and* (5.13b) *respectively, satisfy Assumption 5.5, if Assumption 7.1 (see Appendix 7.2.2) holds.*

Proof. Similar to the proof of Proposition 5.14. □

The receding horizon EMPC formulation of the optimal MG dispatch problem with (5.20) and (5.22) as the terminal region and cost respectively is referred to as Choice 3 and is presented in Appendix 7.2.2 for brevity. Note that dropping the terminal constraint in Choices 2 and 3 is supposed to improve the finite-time electricity costs, with the formulation still ensuring that the guarantees of Theorem 5.7 hold.

[10] Note that $V_f(\cdot)$ in (5.22) is implicitly a function of only t as $x(t)$ does not appear in the RHS.

5.4 Case study

5.4.1 Overview

In this section, we implement our proposed method given in Appendices 7.2.1 (Choice 1) and 7.2.2 (Choices 2 and 3), for simulating the optimal BESS dispatch strategy for a grid-connected MG with PV and load. The MG setup is from the real-life MG at the Port of San Diego, described in [44, 65, 71]. The MG model incorporates electricity prices with non-coincident (NC) and on-peak (OP) demand and energy charges. We assume a perfect day-ahead load and PV forecast for the analyses consistent with our dynamics.

It is by definition that the (best case) optimal electricity cost for the month can only be achieved if (5.10) is used as the objective in an optimization spanning the entire month necessitating availability of perfect forecast for the entire month a-priori, which is unrealistic. Thus, generally the standard method in the literature [44, 45] is to carry out a receding horizon optimization using the economic objective function similar to (5.10). However, such an optimization is carried out over a day-ahead prediction horizon with memory of previous running NCDP and OPDP (see (7.14)), rather than a monthly horizon, which is more realistic. The trajectory generated by this standard method generally followed in the literature is called henceforth as the standard reference method. The use of other methods to generate a reference trajectory is discussed in Section 5.4.2.

In addition to the asymptotic average economic guarantees (see Theorem 5.7), we show in this case study that, in practice, our method has the potential to produce better finite-time (i.e., non-asymptotic) economic performance, even when compared to the reference method which directly optimizes the economic cost function, as in (7.14). While our method cannot theoretically guarantee better finite-time economic performance in general, this case study is a proof of concept of our method having good finite-time performance while having robust asymptotic theoretical guarantees, which might be of importance to MG operators.

5.4.2 Motivation for using Choice 3 for certain reference trajectories

The standard reference method referred to in Section 5.4.1 optimizes the actual economic cost over a prediction horizon subject to input and state constraints. However, as we perform a finite horizon optimization over a much smaller duration than a month, and additionally the standard reference method might have terminal constraints according to the MG operator's choice (which although unknown to the MG operator at the time of operation – might not have to be satisfied in real-time to get economical performance once more information gets available as the EMPC moves forward in time and has access to more forecast data), the standard reference method might perform poorly in closed-loop despite high quality open-loop solutions. That is because, once the standard reference method optimizer concludes a predicted peak will be reached within the prediction horizon (howsoever far from the present it might be), the optimizer does not have an incentive to aggressively discharge the BESS at the first time-step to beyond what is necessary to equalize the grid import with the future predicted peak. However, the future predicted peak might never be realized as more forecast data becomes available as the standard reference method moves ahead in time. However, once a poor decision has been made in the present time-step as MPC applies only the first time-step computed control in closed-loop, it cannot be corrected later and overall higher NCDP and OPDP may be realized.

It is discussed in [70] that if $\frac{R_{\text{NC}}}{R_{\text{OP}}} < \frac{\delta_{\text{off}}}{\delta_{\text{on}}}$, where δ_{off} and δ_{on} are the off-peak[11] and on-peak hours of the day, it is economical to spread the grid import over the off-peak hours and keep the on-peak load 0. The intuition behind the condition lies in the analysis of an increase of NCDP, δ_{NCDP}, and an increase of OPDP, δ_{OPDP} from importing δ_{GI} from the grid in either off-peak or on-peak times. If $R_{\text{NC}}\delta_{\text{NCDP}} < R_{\text{OP}}\delta_{\text{OPDP}}$, then adding the grid import over the off-peak period is more economical. Substituting $\delta_{\text{NCDP}} = \frac{\delta_{\text{GI}}}{\delta_{\text{off}}}$ and

[11] Off-peak hours are all hours of the day except the on-peak hours, i.e., all hours except 16:00 – 21:00 h.

$\delta_{\text{OPDP}} = \frac{\delta_{\text{GI}}}{\delta_{\text{on}}}$ in the above equality proves the result.

Thus, taking inspiration from the above discussion, we formulate another reference trajectory with the objective function minimizing deviation of grid import from an ideal trajectory formed by spreading the entire forecasted net load over only the off-peak period. The objective function for such a reference trajectory is given in (7.15) in Appendix 7.2.3 with a detailed explanation of the procedure and logic behind the ideal trajectory. The reference trajectory created from the method in this section is referred to as the tracking reference method, as opposed to the standard reference method.

As the tracking reference method tries to minimize deviation from an ideal grid import trajectory, it typically dispatches the BESS more aggressively than the standard reference method. Therefore, in open-loop, the tracking reference method might be worse (or at best no better) than the standard reference method, but in closed-loop the tracking reference method might be superior. However, the technique used in the tracking reference does not have any theoretical guarantees and is based only on empirical findings. Thus, Choice 3 incorporates the best aspects of the reference tracking method while having the economic cost explicitly in the objective function (Appendix 7.2.2). The objective function for Choice 3 in (7.13) – instead of redundantly double penalizing the predicted terminal peaks as in Choices 1 and 2 (see (7.11)) – penalizes both the predicted terminal peaks and the increase of the predicted peaks up to the next time-step (i.e., $x_2(t+1|t)$ and $x_3(t+1|t)$, which will be realized in closed-loop because of perfect forecasts) from the (already realized) reference peaks $x_2^r(t+1)$ and $x_3^r(t+1)$. This gives the proposed method in Choice 3 the ability to relatively weigh the penalty on the predicted peaks in the prediction horizon temporally, as a peak predicted later has lesser significance than a peak predicted closer to the current time in closed-loop.

5.4.3 EMPC framework

The EMPC based optimization framework for our proposed method for Choices 1, 2, and 3 are given in Appendices 7.2.1, 7.2.2 and 7.2.2 respectively. The standard reference method has (7.14) as the objective function, with (7.6), (7.7), (7.8), (7.9) as constraints with superscript 'r' in the state and control input variables signifying the reference trajectory. Similarly, the tracking reference method has (7.15) as the objective function with (7.6), (7.7), (7.8), (7.9) as constraints. Terminal constraints are sometimes added to both the reference methods based on varied scenarios of MG operator's operational choices and are described in Section 5.5. Note that while Prop C1 has terminal constraints, Prop C2 and Prop C3 do not, with all the proposed methods still preserving the guarantee of Theorem 5.7.

Note that the knowledge of $x^r(t+1)$ at time t before the implementation of our proposed method is not unrealistic under a perfect forecast assumption. The scenario just implies that at time t, the reference optimization is first carried out to compute $u^r(t)$, which is then plugged into (5.2) to get $x^r(t+1)$. Note that the closed-loop control input $u^r(t)$ for the reference method would not change from the MPC computed one, as perfect forecasts are assumed.

The MPC prediction horizon for both our and the reference method is one-day ahead, subdivided into N equal time-steps of $\Delta t = 0.25$ h (15 minutes) each, implying $N = \frac{24\text{ h}}{\Delta t} = 96$. The predefined design parameters of the MG are shown in Table 5.1. The time-steps within the month are represented by $\mathscr{T}_w = \{0, 1, 2, \ldots, T-1\}$, where $T = NM_{\text{day}}$, with M_{day} being the number of days in the month over which the demand charge window extends for. Note that the above relationship shows that $T \propto \frac{1}{\Delta t}$, which implies that the asymptotic average cost guarantee in Theorem 5.7 can be interpreted as applying when $\Delta t \to 0$, as $T \to \infty$ and $\Delta t \to 0$ are mathematically equivalent.

Table 5.1. Design Parameters of the MG at the Port of San Diego [71].

Parameter	Symbol	Value
NCDC rate	R_{NC}	\$24.48/kW
OPDC rate	R_{OP}	\$19.19/kW
Energy rate	$R_{\mathrm{EC}}(t), \forall t$	\$0.1/kWh
BESS round-trip efficiency	η	0.8
BESS energy capacity	$\mathrm{BESS}_{\mathrm{en}}$	2,500 kWh
BESS power capacity	$\mathrm{BESS}_{\mathrm{max}}$	700 kW
Upper bound of SOC	$\mathrm{SOC}_{\mathrm{max}}$	0.8
Lower bound of SOC	$\mathrm{SOC}_{\mathrm{min}}$	0.2
Initial SOC	$x_1(0)$ and $x_1^r(0)$	0.5

5.5 Results and discussion

5.5.1 Reference method terminal constraints and case study settings

We analyze the results from January 2019 by comparing our proposed method to 3 reference method test cases: (i) The reference method with the terminal constraint set being the entire state space; (ii) the reference method with the terminal SOC ending at the starting SOC for the MPC given by

$$x^r(t+N|t) = \begin{pmatrix} x_1^r(t) \\ x_2^r(t+N|t) \\ x_3^r(t+N|t) \end{pmatrix}, \qquad \forall t \in \mathbb{T},$$

symbolizing a case where the MG operator wants to ensure that the BESS does not have any net energy export or import from the grid over the prediction horizon; (iii) the reference method with the terminal SOC ending above the 50% SOC for the MPC given by

$$x^r(t+N|t) \geq \begin{pmatrix} 0.5 \\ x_2^r(t+N|t) \\ x_3^r(t+N|t) \end{pmatrix}, \qquad \forall t \in \mathbb{T},$$

symbolizing a case where the MG operator is anxious about future demand peaks and wants to have enough storage in the BESS at the terminal time-step of each MPC run. The results for the case study when considering NCDC only is presented in Section 5.5.2 where the third constituent state above is dropped as there is no OPDC with $R_{\mathrm{OP}} = 0$. The results when considering both NCDC and OPDC are presented in Section 5.5.3. All our simulations are run with $a(t) = b(t) = 1, \forall t \in \mathbb{T}$. Note that as arbitrage is not considered for energy charges, the energy cost differences between the different cases is minor and is only a result of different ending SOC of the BESS at the end of the month, and is not important for this analysis. When considering NCDC only (Section 5.5.2), the standard reference method is compared against Choice 1 and Choice 2 of the proposed method. Use of Choice 3 of the proposed method is only carried out when considering both NCDC and OPDC (Section 5.5.3), as comparison of Choice 3 makes sense only with the tracking reference trajectory where spreading of grid import power over the off/on peak period has a significant impact on total electricity costs. In Sections 5.5.2 and 5.5.3, we abbreviate the standard and tracking reference methods by 'Std Ref' and 'Track Ref' respectively, with 'Prop C1', 'Prop C2', and 'Prop C3' as abbreviations for the Proposed method Choice 1, 2, and 3, respectively.

5.5.2 NCDC only

Table 5.2 shows that for Case (i), where the Std Ref is free to choose the most suitable BESS SOC at the terminal time-step, performs better than Prop. C1 with respect to NCDC. However, Prop C1 (almost totally) compensates for its excess NCDP, which happened because of its terminal constraints, by lower BESS usage loss. Prop C1 has lower BESS usage loss as once a higher demand peak has been reached, the BESS has no incentive to discharge aggressively as reducing the grid import below the already realized peak incurs no benefit. Overall, the total costs for Std Ref are (almost) equal to Prop C1 when the energy costs are ignored as they are irrelevant for comparative analysis in the long run. The results for Prop C2 are equivalent to the Std Ref as expected, as the only difference between them is the double penalization of the terminal running NCDP in Prop C2 due to the terminal cost, where the demand charge terms already dominate the costs inside the prediction horizon and are already considered in the additive stage cost, making the terminal cost penalty redundant (see Section 5.3.5).

For Case (ii), the Std Ref has almost equivalent performance to Prop C1 as expected, as the formulations are equivalent but for the double penalization of terminal running NCDP in Prop C2 (as the initial state is the same for both) which has negligible effects. Prop C2 outperforms both the Std Ref and Prop C1 because of the relaxation in the terminal region in Prop C2 as compared to both Std Ref and Prop C2. Overall, Prop C2 has an ≈13.3% NCDC reduction, and ≈3.3% total cost reduction as compared to Std Ref and Prop C1.

The biggest performance improvement comes in Case (iii) with a 4.1% reduction of NCDC in Prop C1 as compared to Std Ref with a total cost reduction of 0.8%. As Prop C2 does not have terminal constraints, it leads to the best cost reduction with an additional 4.7% and 1.3% reduction in NCDC and total cost respectively over Prop C1.

Note that, Prop C2 performs similar to or better than Prop C1 and Std Ref for all cases. Additionally, note that the performance of Prop C2 in all cases is almost same, which is further equivalent to Std Ref Case (i), further illustrating that while the terminal cost in (5.17) (or a slight variation of it for Prop C2 as discussed in Section 5.3.5) is important for ensuring the long-term guarantee of Theorem 5.7, it has little significance in improving performance in finite-time for redundancy in double-penalization of terminal running NCDP and OPDP (see above and Section 5.3.5 for an explanation).

Table 5.2. Result comparison for the Std Ref, Prop C1, and Prop C2 methods for the 3 test cases considering only NCDC for January 2019.

Costs	**Case (i)**			**Case (ii)**			**Case (iii)**		
	Std Ref	Prop C1	Prop C2	Std Ref	Prop C1	Prop C2	Std Ref	Prop C1	Prop C2
NCDC	\$3,450	\$3,569	\$3,459	\$3,983	\$3,970	\$3,453	\$3,782	\$3,627	\$3,455
Energy Cost	\$5,676	\$5683	\$5,675	\$5,716	\$5,715	\$5,676	\$5,718	\$5,719	\$5,676
BESS loss	\$385	\$268	\$385	\$137	\$139	\$385	\$220	\$298	\$385
Total Cost	\$9,511	\$9,519	\$9,519	\$9,837	\$9,823	\$9,514	\$9,721	\$9,644	\$9,516

5.5.3 Both NCDC and OPDC

When both the NCDC and OPDC are considered in the MG, the results in Table 5.3 follow almost the same trends as in the NCDC only case (see Table 5.2), and a detailed discussion is avoided here for brevity. The key takeaways are: (i) Prop C2 performs similarly in all cases as in Section 5.5.2 and is either better or at least as good as Prop C1 and Std Ref for all cases; (ii) Case (iii) has the largest performance improvement with Prop C1 outperforming Std. Ref, which is further outperformed by Prop C2.

However, an interesting performance improvement is observed by using the Track Ref method over the Std Ref method for Cases (ii) and (iii), as can be observed by comparing Tables 5.3 and 5.4. Note that Track Ref has the same terminal constraints as in Std Ref for all cases. The Track Ref method – despite having different terminal constraints in all cases – performs similarly, which is a coincidence owing to the large prediction horizon, where the predicted control inputs at the start of the prediction horizon is minimally affected by the terminal constraints. However, the performance improvement in Track Ref as compared to Std Ref in Cases (ii) and (iii) as elucidated in Section 5.4.2 is empirical, without theoretical guarantees, with the objective function (7.15) not having economics at all. Prop C3 can however, combine the economics explicitly in the cost function while also considering the trajectory (i.e., demand peaks) of Track Ref to achieve a tradeoff. The tradeoff is important so that even when the Track Ref fails to give good economic performance, Prop C3 will still not perform 'pathologically' in closed-loop because of the explicit consideration of economics.

The advantage of explicit consideration of economics can be seen in Table 5.4 where Prop C3 outperforms the Track Ref in all the cases, which makes Prop C3 outperform Std Ref in all cases except Case (i) where Prop C3 has 1.1% more total costs than Std Ref.

While one might argue that the finite-time performance improvement of the proposed methods (either Prop C1/C2/C3) over the Std Ref in the concerned cases is a result of the change (as in Prop C1) or removal of terminal constraints (as in Prop C2 and C3) in the optimization, it is important to note that addition of terminal constraints in Std Ref is a MG operator design condition keeping in mind different level of conservativeness and experience. The MG operator would not know in real-time if the decision to keep terminal constraints is good from a closed-loop monthly cost perspective until the end of the month has been reached (which is too late to make changes). As forecasts only for the prediction horizon (i.e., 24 h in advance) is known, it is possible to have a situation where addition of terminal constraints as in Cases (ii) and (iii) can outperform Case (i) with Std Ref technique in closed-loop monthly electricity cost.[12] There, our proposed methods hold value in the long term because of application of Theorem 5.7, and especially if reference trajectories like Track Ref is used by the MG operator (where the terminal cost in Prop C3 plays a critical role) which has been empirically shown to have better performance than Std Ref in some cases.

[12]We have not demonstrated this for our case study but it is possible for such a situation to arise with different prediction horizons and/or forecast data.

Table 5.3. Result comparison for the Std Ref, Prop C1, and Prop C2 methods for the 3 test cases considering both NCDC and OPDC for January 2019.

Costs	**Case (i)**			**Case (ii)**			**Case (iii)**		
	Std Ref	Prop C1	Prop C2	Std Ref	Prop C1	Prop C2	Std Ref	Prop C1	Prop C2
NCDC	\$4,358	\$3,438	\$4,357	\$3,988	\$3,978	\$4,357	\$5,000	\$4,760	\$4,357
OPDC	\$0	\$2,217	\$0	\$3,081	\$3,079	\$0	\$972	\$0	\$0
Energy Cost	\$5,652	\$5,697	\$5,652	\$5717	\$5,714	\$5,652	\$5,691	\$5,685	\$5,652
BESS loss	\$584	\$380	\$584	\$136	\$138	\$584	\$431	\$518	\$584
Total Cost	\$10,595	\$11,733	\$10,594	\$12,924	\$12,910	\$10,594	\$12,093	\$10,964	\$10,595

Table 5.4. Result comparison for the Track Ref, and Prop C3 methods for the 3 test cases considering both NCDC and OPDC for January 2019.

Costs	**Case (i)**		**Case (ii)**		**Case (iii)**	
	Track Ref	Prop C3	Track Ref	Prop C3	Track Ref	Prop C3
NCDC	\$4,803	\$4,511	\$4,803	\$4,511	\$4,803	\$4,511
OPDC	\$162	\$0	\$162	\$0	\$162	\$0
Energy Cost	\$5,689	\$5,648	\$5,689	\$5,648	\$5,689	\$5,648
BESS loss	\$847	\$560	\$843	\$560	\$847	\$560
Total Cost	\$11,502	\$10,719	\$11,498	\$10,719	\$11,502	\$10,719

Acknowledgements

This chapter, in full, is currently being prepared for submission for publication of the material as ‘Economic Model Predictive Control with a Non-Fixed Reference Trajectory for Optimal Microgrid Dispatch’ authored by Avik Ghosh, Adil Khurram, Jan Kleissl, and Sonia Martínez, in Automatica. The dissertation author was the primary investigator and author of this paper.

Chapter 6

Conclusions and future work

In this dissertation, we first analyzed the economically optimal EV charging effects on building electricity costs, and developed analytical expressions to quantify the optimal EV charging benefits. Other than highlighting the most important factors that affected the total electricity cost deviation from building to building and between different charging strategies (V0G/V1G/V2B), the work is intended to aid in appropriately sizing EV charging infrastructure and quickly quantifying the optimal EV charging benefits worldwide, even without performing economic optimization.

Second, we developed application-agnostic, computationally inexpensive, real-time MPC algorithms with provable guarantees. Specifically, we focused on developing nonconservative chance constrained stochastic MPC (SMPC) and economic MPC (EMPC) based algorithms. Then, we applied the developed algorithms for economically optimal BESS dispatch in VRE integrated MGs (on realistic MG load and generation data and tariff profiles), and demonstrated the superior performance of our developed algorithms with respect to the traditional and state-of-the-art approaches in the field for both electricity cost savings and other relevant metrics. In the following, we summarize the key findings of the dissertation and point towards future research directions.

6.1 Conclusions and extensions

6.1.1 Effects of number of EV charging/discharging on total electricity costs in commercial buildings with time-of-use energy and demand charges

In Chapter 3, we carry out a techno-economic analysis of three different types of workplace EV charging strategies (V0G, V1G and V2B) in 14 commercial buildings with real load profiles. We primarily base our analysis on an idealized uniform EV commuter fleet case study with a layover period of 06:30 – 19:30 h for the year 2019.

V0G incurs the highest year-around electricity costs followed by V1G and V2B. For V0G, the building-to-building difference in EV charging costs depends on the intersection of the original NC demand peak time with the EV charging time, and the difference between the original NC demand peak and the maximum original load during the EV charging time. For V2B, the building-to-building difference in EV charging costs depends on the intersection of the original NC and OP demand peak times with the EV layover time. For V1G and V2B, the building-to-building difference depends on the difference between the original demand peaks and the mean original load during the on and off-peak layover periods.

The V1G and V2B total electricity costs initially diverge with increasing daily charging demand (or number of EV charging stations) and then become parallel to each other. As the daily charging demand increases, the cost savings of V2B charging over V1G reduce and the V2B charging costs exceed the original (pre-EV) costs. A longer layover period generally leads to more cost savings over a shorter layover period for V1G and V2B, as the charging is spread out over a longer duration for V1G, while for V2G there is an additional flexibility of shifting on-peak loads to off-peak periods. Correspondingly, a longer layover period also leads to a higher number of optimal V2B charging stations (the number of V2B charging stations to be installed at a building such that its operating electricity costs do not exceed the pre-EV original electricity costs), as compared to a shorter layover period. Generally, with increasing difference between the original NCDP and mean off-peak period load and the original OPDP and mean on-peak period load, weighed over the off-peak and on-peak layover times respectively, the optimal number of V2B charging stations increases.

Sensitivity analyses based on changing both initial and final SOC of EVs while keeping the energy demand constant for all the buildings for both layover periods show that, as the final SOC decreases from 90 to 80% (with the initial SOC decreasing from 50 to 40%), the total electricity costs remain the same for V0G and V1G, while for V2B the total electricity costs decrease because of the additional flexibility of discharging during the on-peak period. A realistic case study based on historical data for 5 high charging demand weekdays in February 2020 for 14 EV charging stations shows that the V2G and V1G charging strategy results in 54.4% and 40.3% total electricity cost savings respectively over the original V0G charging schedule.

While the results discussed so far were all based on convex optimization, we also provided general analytical expressions that allow estimating V1G and V2B benefits based on a pre-EV building load profile and EV and tariff data. Although the number of V2B charging stations such that the original (pre-EV) operating electricity bill is not exceeded cannot be predicted exactly without carrying out the convex optimization, we provided a framework (using (3.17), in conjunction with Tables 3.1 and 3.5) to approximate the optimal number of V2B charging stations without carrying out the convex optimization, which may be of interest to building owners.

One of the limitations of this study is the assumption of 100% charging/discharging efficiency for the EVs. In reality, each time an EV charges/discharges there are costs due to energy losses and battery degradation. Therefore, if the losses were considered, the V2G/V2B charging economic benefits, which depend on more charging/discharging cycles, would reduce. Another limitation of the study is that uncertainties in layover periods and battery capacity (which may occur due to ageing) are not considered. Future work will focus on tackling these limitations to make the study more robust and accurate and increase its applicability to more realistic scenarios.

6.1.2 Adaptive relaxation-based nonconservative chance constrained SMPC

In Chapter 4, we present a novel online adaptive state constraint relaxation-based SMPC (OA-SMPC) framework for nonconservative chance constraint satisfaction in closed-loop. An adaptive state constraint relaxation rule is developed for a generic discrete LTI system based on the time-average of past constraint violations without any a-priori assumptions about the probability distribution of the uncertainty set or its statistics, or sample uncertainties from historical data. The time-average of the state constraint violations, under the assumption of ideal control inputs which can cause/prevent constraint violations almost surely, is proven to asymptotically converge to the maximum allowable violation probability. The time-average of the state constraint violations is also proven to exhibit martingale-like behavior asymptotically, even without the ideal control input assumption.

The proposed method (OA-SMPC) is applied for minimizing monthly electricity costs by optimal BESS dispatch for a grid connected MG in an economic MPC (EMPC) framework. We perform simulations for the Port of San Diego MG using realistic PV and load forecast data for the year 2019. Chance constraints are applied on the BESS SOC to make use of excess BESS capacity in our proposed OA-SMPC as compared to the traditional EMPC without chance constraints (which uses hard constraints on BESS SOC). The OA-SMPC outperforms the traditional EMPC and a state-of-the-art chance constrained approach from the literature, striking an effective trade off between high BESS utilization (i.e., higher cost savings) and full SOC constraint satisfaction (i.e., longer BESS lifetime). The OA-SMPC lowers MG electricity costs by nonconservative chance constraint satisfaction in closed-loop, thereby having minimal adverse effect on BESS lifetime.

Future work will incorporate the BESS degradation cost and a life-cycle analysis of the MG to aid in a more realistic analysis. While we have demonstrated the practical efficacy of the method for the case study presented, the formal guarantees of nonconservative chance constraint satisfaction is presented under the strong ideal control policy in Assumption 4.8, which needs to be relaxed in future work to better approximate real-life controllers. A way to avoid the strong requirements of Assumption 4.8 can be to learn the distribution of the uncertainty from historical data while using the present algorithm, and once learned — leveraging the information about the distribution to solve the problem, relaxing Assumption 4.8.

6.1.3 Deterministic EMPC with an online reference trajectory

In Chapter 5, we present an EMPC formulation for a generic deterministic (i.e., uncertainty free) discrete non-linear time-varying system. We first prove that under some mild assumptions, the asymptotic average closed-loop cost of the proposed EMPC is no worse than the asymptotic average closed-loop cost of an arbitrary non-fixed reference trajectory for the same system (see Theorem 5.7). The reference trajectory is not known a-priori for all time-steps like [45] but is only known until the current time-step and thereafter recomputed at every time-step through an online optimization/rules-based method to better reflect realistic conditions. We then show that the optimal MG dispatch problem can be reformulated such that it meets the conditions for our proposed EMPC formulation. A realistic case study using PV and load forecast data from the MG at the Port of San Diego shows that the method is also capable of reducing monthly (i.e., finite-time) electricity costs as compared to reference trajectories generated by directly optimizing the electricity cost function over the prediction horizon or by tracking an ideal grid import curve.

The methodologies as described in Sections 5.3.4 and 5.3.5 can give rise to many other possibilities of constructing terminal cost functions, control laws and regions, and the Proposed method Choices 1, 2 and 3 are by no means exhaustive but only a proof of existence. Further study is required to investigate different terminal cost functions, regions, and controls laws to give better finite-time closed-loop guarantees without sacrificing on the asymptotic guarantees in Theorem 5.7. There is also a need for further research in developing reference trajectories and their pairing with different EMPC formulations for achieving better finite-time closed-loop performance, ideally with finite-time guarantees. Here, different choices of coefficients, $a(t)$ and $b(t)$ which would lead to different control laws depending on the weighing of running NCDP and OPDP respectively in the objective function, can be investigated. Moreover, investigation into techniques which can relax Assumption 5.11, and extension of similar guarantees in this work for stochastic systems (see [51] for related work) are needed. Lastly, analyses need to be carried out for different MGs and sites, and for longer periods of time (seasonally/yearly) to exhaustively investigate the performance of the proposed controller under varied exogenous input conditions.

6.2 Future research directions

The contributions in this dissertation are based on the assumption that the model of the system to be controlled is known. However in real-life complex systems, it may not be possible to always know the model a-priori. Thus, it becomes essential in these cases to implement the controllers in a model-free, learning based setting for future works. As model-free controllers have the ability to adapt to changing input-output data, it can be naturally leveraged to consider complicated operating-regime-dependent, non-linear dynamics (such as BESS/EV degradation), or when the uncertainty distribution is time varying, which is oftentimes the case in practice.

The controller setup investigated in this dissertation is based on a centralized structure. However, for networked systems (such as a combination of several individual

MGs, where each MG controller is local but the overall network needs to achieve some common goal with minimal/no communication between the individual MGs) there is a need for development of algorithms which leverages distributed control for reasons such as privacy, cybersecurity, reliability, scalability, etc. A direction for future work will be to extend similar guarantees as investigated in this dissertation for distributed control systems.

The methodologies developed and suggested as extensions of this dissertation — beyond their application to control of VRE integrated MGs — naturally extend to related domains such as HVAC control in commercial buildings and traffic management systems. At a broader level, a promising future research direction lies in addressing challenges within the water-energy nexus, particularly in developing regions of the world where economically efficient real-time plant operation is of paramount importance.

Acknowledgements

This chapter, in part, is a reprint of the material as it appears in 'Effects of number of electric vehicles charging/discharging on total electricity costs in commercial buildings with time-of-use energy and demand charges' authored by Avik Ghosh, Monica Zamora Zapata, Sushil Silwal, Adil Khurram, and Jan Kleissl, in the Journal of Renewable and Sustainable Energy, 2022; and 'Adaptive Relaxation-Based Nonconservative Chance Constrained Stochastic MPC' authored by Avik Ghosh, Cristian Cortes-Aguirre, Yi-An Chen, Adil Khurram, and Jan Kleissl, in the IEEE Transactions on Control Systems Technology, 2025; as well as 'Economic Model Predictive Control with a Non-Fixed Reference Trajectory for Optimal Microgrid Dispatch' authored by Avik Ghosh, Adil Khurram, Jan Kleissl, and Sonia Martínez, which is currently being prepared for submission for publication in Automatica. The dissertation author was the primary investigator and author of these papers.

Chapter 7

Appendix

7.1 Adaptive relaxation-based nonconservative chance constrained SMPC

7.1.1 Conditions for testing Assumption 4.4(a)

A test for Assumption 4.4(a) entails solving the following optimization problem [72, Section 5.8.1] at each time t, given $x(t)$, $c(t|t)$ and $h(t)$.

$$f^* = \min\ 0, \tag{7.1}$$

subject to

$$x(t+1|t) = Ax(t) + Bu(t|t), \tag{7.2}$$

$$Su(t|t) \leq s, \tag{7.3}$$

$$Mu(t|t) = c(t|t), \tag{7.4}$$

$$G(x(t+1|t)) \leq g - h(t). \tag{7.5}$$

If $f^* = 0$, then the optimization problem defined above is feasible and we can guarantee Assumption 4.4(a) holds. If $f^* = \infty$, then the optimization problem above is infeasible and Assumption 4.4(a) fails to hold. Note that if (4.3) and (4.11d) are not considered in the problem formulation, we can drop (7.4).

7.2 Deterministic EMPC with an online reference trajectory

7.2.1 Optimal MG dispatch problem formulation for the proposed method Choice 1

$$\underset{\mathbf{u}(x(t),t)\in\mathbb{R}^{2N}}{\text{minimize}}\,(5.19)$$

subject to

$$x(t+k+1|t) = \begin{pmatrix} Ax_1(t+k|t)+Bu(t+k|t) \\ \max\big(x_2(t+k|t),u_2(t+k|t)\big) \\ \max\big(x_3(t+k|t),\beta(t+k)u_2(t+k|t)\big) \end{pmatrix}, \qquad \forall k\in\mathbb{N}_0^{N-1},\ \forall t\in\mathbb{T}, \tag{7.6}$$

$$Su(t+k|t)\leq s, \qquad \forall k\in\mathbb{N}_0^{N-1},\ \forall t\in\mathbb{T}, \tag{7.7}$$

$$Mu(t+k|t)=c(t+k|t), \qquad \forall k\in\mathbb{N}_0^{N-1},\ \forall t\in\mathbb{T}, \tag{7.8}$$

$$G'x(t+k|t)\leq g', \qquad \forall k\in\mathbb{N}_0^{N},\ \forall t\in\mathbb{T}, \tag{7.9}$$

$$x(t+N|t) = \begin{pmatrix} x_1^r(t) \\ x_2(t+N|t) \\ x_3(t+N|t) \end{pmatrix}, \qquad \forall t\in\mathbb{T}, \tag{7.10}$$

where

$$G' = \begin{bmatrix} G & \mathbb{0}^2 & \mathbb{0}^2 \\ 0 & 1 & 0 \\ 0 & -1 & 0 \\ 0 & 0 & 1 \\ 0 & 0 & -1 \end{bmatrix}, \; g' = \begin{bmatrix} g \\ \hat{b} \\ 0 \\ \hat{b} \\ 0 \end{bmatrix},$$

and Assumption 5.12 is enforced.

Note that some terms, namely, $a(t)x_2(t)$, $a(t+1)x_2^r(t+1)$, $b(t)x_3(t)$, $b(t+1)x_3^r(t+1)$ and $h(t+N)$ of (5.19) are independent of $\mathbf{u}(x(t),t)$ for a given initial state $x(t)$, reference states $x^r(t)$, $x^r(t+1)$ and time t, as they are just additive constants. Thus, the optimization with the objective function (5.19) has the same optimal control input sequence $\mathbf{u}^0(x(t),t)$ (i.e., solution) when using the objective function in (7.11) provided we use the same constraints (7.6), (7.7), (7.8), (7.9), (7.10), as (5.19) and (7.11) differ by additive constants.

$$\begin{aligned} V_N(x(t),\mathbf{u}(x(t),t),t) = \sum_{k=0}^{N-1} \Big[R_{\mathrm{EC}}(t+k)\Delta t \Big(u_2(t+k|t) + \frac{(1-\eta)}{2} |u_1(t+k|t)| \Big) \Big] \\ + \left[R_{\mathrm{NC}} \left(a(t+N)x_2(t+N|t) + \max\Big(a(t+N)x_2(t+N|t), a(t+1)x_2^r(t+1) \Big) \right) \right] \\ + \left[R_{\mathrm{OP}} \left(b(t+N)x_3(t+N|t) + \max\Big(b(t+N)x_3(t+N|t), b(t+1)x_3^r(t+1) \Big) \right) \right]. \end{aligned} \tag{7.11}$$

Note that use of (7.11) relaxes the design requirement of choosing $h(\cdot)$ in practical scenarios to satisfy Assumption 5.12.

7.2.2 Optimal MG dispatch problem formulation for the proposed method Choices 2 and 3

Receding horizon EMPC formulation for Choice 2

The receding horizon EMPC formulation of the optimal MG dispatch problem for Choice 2 is presented as follows.

$$\underset{\mathbf{u}(x(t),t)\in\mathbb{R}^{2N}}{\text{minimize}}\ (7.11)$$

subject to (7.6), (7.7), (7.8) and (7.9). Note that there is no additional terminal constraint like (7.10) in this case on account of (5.20).

Statement of Assumption 7.1 for Choice 3

Assumption 7.1 (**Operational assumption for the optimal MG dispatch problem with terminal cost** (5.22) **to satisfy Assumption 5.5**)**.** *Let* $A_1(t) = a(t)x_2(t)$*,* $B_1(t) = b(t)x_3(t)$*,* $A_2(t) = a(t)x_2^r(t)$*, and* $B_2(t) = b(t)x_3^r(t)$*. Then, the following holds* $\forall t \in \mathbb{T}\cap\mathbb{N}_{\geq N}$*.*

$$\begin{aligned}
h(t+1)-h(t) \geq\, & R_{\mathrm{EC}}(t)\Delta t\Big(u_1(t)-c(t)+\frac{(1-\eta)}{2}|u_1(t)|\Big)\\
& - R_{\mathrm{EC}}(t-N)\Delta t\Big(u_1^r(t-N)-c(t-N)+\frac{(1-\eta)}{2}|u_1^r(t-N)|\Big)\\
& + R_{\mathrm{NC}}\Big[A_1(t+1)-A_1(t)+\max\Big(A_1(t-N+2),A_2(t-N+2)\Big)\\
& - \max\Big(A_1(t-N+1),A_2(t-N+1)\Big)+A_2(t-N)-A_2(t-N+2)\Big]\\
& + R_{\mathrm{OP}}\Big[B_1(t+1)-B_1(t)+\max\Big(B_1(t-N+2),B_2(t-N+2)\Big)\\
& - \max\Big(B_1(t-N+1),B_2(t-N+1)\Big)+B_2(t-N)-B_2(t-N+2)\Big].
\end{aligned} \tag{7.12}$$

Receding horizon EMPC formulation for Choice 3

The receding horizon EMPC formulation of the optimal MG dispatch problem for Choice 3 is presented after removing the additive constants similar to (7.11) as follows.

$$
\begin{aligned}
\underset{\mathbf{u}(x(t),t)\in\mathbb{R}^{2N}}{\text{minimize}} \sum_{k=0}^{N-1} & \Big[R_{\text{EC}}(t+k)\Delta t\Big(u_2(t+k|t)+\frac{(1-\eta)}{2}|u_1(t+k|t)|\Big)\Big] \\
&+\Bigg[R_{\text{NC}}\Bigg(a(t+N)x_2(t+N|t)+\max\Big(a(t+1)x_2(t+1|t),a(t+1)x_2^r(t+1)\Big)\Bigg)\Bigg] \\
&+\Bigg[R_{\text{OP}}\Bigg(b(t+N)x_3(t+N|t)+\max\Big(b(t+1)x_3(t+1|t),b(t+1)x_3^r(t+1)\Big)\Bigg)\Bigg],
\end{aligned}
\tag{7.13}
$$

subject to (7.6), (7.7), (7.8) and (7.9). Similar to Choice 2, there is no additional terminal constraint like (7.10) in this case too, on account of (5.20).

7.2.3 Objective function for the optimal MG dispatch problem for the reference methods

The objective function for the standard reference method is presented as follows

$$
\begin{aligned}
\tilde{V}_N(x^r(t),\mathbf{u}^r(x^r(t),t),t)=\sum_{k=0}^{N-1}&\Big[R_{\text{EC}}(t+k)\Delta t\Big(u_2^r(t+k|t)+\frac{(1-\eta)}{2}|u_1^r(t+k|t)|\Big)\Big] \\
&+R_{\text{NC}}\Big(a(t+N)x_2^r(t+N|t)\Big)+R_{\text{OP}}\Big(b(t+N)x_3^r(t+N|t)\Big).
\end{aligned}
\tag{7.14}
$$

The objective function for the tracking reference method is given as follows

$$
\tilde{V}_N(x^r(t),\mathbf{u}_r(x^r(t),t),t)=P(t)\,\|\mathbf{u}_2^r(x_r(t),t)-\bar{\mathbf{u}}_2^r(t)\| \tag{7.15}
$$

where $\bar{\mathbf{u}}_2^r(t)$ is the ideal grid import trajectory over the prediction horizon and $P(t)$ is the penalty matrix. $\bar{\mathbf{u}}_2^r(t)$ is composed of 0 for the on-peak period time-steps of the prediction horizon, with the off-peak period elements being $\max\Big(x_2^r(t),-\frac{\sum_{k=0}^{N-1}c(t+k|t)}{N_{\text{off}}}\Big)$, where N_{off} is the length of the prediction horizon coinciding with the off-peak period. $\boldsymbol{P}(t)$ is a diagonal matrix that penalizes the deviation of the predicted grid import from the ideal, with more weighing for on-peak periods, as OPDC are charged on top of NCDC. $\boldsymbol{P}(t)$ is composed of 1 for off-peak period time-steps of the prediction horizon, and $\frac{R_{\text{NC}}+R_{\text{OP}}}{R_{\text{NC}}}$ for the OP period time-steps of the prediction horizon, symbolizing that increasing demand during OP periods can increase both NCDC and OPDC.

We do not use the running OPDP $x_3^r(t)$, in $\bar{\mathbf{u}}_2^r(t)$ as increasing the ideal grid import trajectory in the OP period time-steps could further aggravate it rather than forcing it to stay close to 0 even when a prior non-zero value of grid import has been reached in the OP period. However, in some situations, not increasing the ideal grid import trajectory over the OP period time-steps when a prior OPDP has been reached could increase the NCDP beyond necessary, especially if the NCDP happens after the OPDP. If the running OPDP is included in the ideal grid import trajectory, the time-steps of $\bar{\mathbf{u}}_2^r(t)$ corresponding to the OP period would be modified as $\max\left(0, x_3^r(t)\right)$.

Bibliography

[1] Peng Kou, Feng Gao, and Xiaohong Guan. Stochastic predictive control of battery energy storage for wind farm dispatching: Using probabilistic wind power forecasts. *Renewable Energy*, 80:286–300, aug 2015.

[2] K Mongird, V Fotedar, V Viswanathan, V Koritarov, P Balducci, B Hadjerioua, and J Alam. Energy Storage Technology and Cost Characterization Report. Technical report, 2019.

[3] Margaret Smith and Jonathan Castellano. Costs associated with non-residential electric vehicle supply equipment. *U.S. Department of Energy Vehicle Technologies Office*, 2015.

[4] Zeyu Wang, Ahlmahz Negash, and Daniel S Kirschen. Optimal scheduling of energy storage under forecast uncertainties. *IET Generation, Transmission & Distribution*, 11(17):4220–4226, 2017.

[5] Abby Brown, Stephen Lommele, Alexis Schayowitz, and Emily Klotz. Electric vehicle charging infrastructure trends from the alternative fueling station locator: First quarter 2020. Technical Report NREL/TP-5400-77508, National Renewable Energy Laboratory, Golden, CO, 2020.

[6] B Aluisio, A Conserva, M Dicorato, G Forte, and M Trovato. Optimal operation planning of v2g-equipped microgrid in the presence of ev aggregator. *Electric Power Systems Research*, 152:295–305, 2017.

[7] M Huda, T Koji, and M Aziz. Techno economic analysis of vehicle to grid (v2g) integration as distributed energy resources in indonesia power system. *Energies*, 13, 2020.

[8] Ruifeng Shi, Shaopeng Li, Penghui Zhang, and Kwang Y Lee. Integration of renewable energy sources and electric vehicles in v2g network with adjustable robust optimization. *Renewable Energy*, 153:1067–1080, 2020.

[9] Mahdi Kiaee, Andrew Cruden, and Suleiman Sharkh. Estimation of cost savings from participation of electric vehicles in vehicle to grid (v2g) schemes. *Journal of Modern Power Systems and Clean Energy*, 3(2):249–258, 2015.

[10] Zhile Yang, Kang Li, and Aoife Foley. Computational scheduling methods for integrating plug-in electric vehicles with power systems: A review. *Renewable and Sustainable Energy Reviews*, 51:396–416, 2015.

[11] Alexander Schuller, Benjamin Dietz, Christoph M Flath, and Christof Weinhardt. Charging strategies for battery electric vehicles: Economic benchmark and v2g potential. *IEEE Transactions on Power Systems*, 29(5), 2014.

[12] Ujjwal Datta, Nithya Saiprasad, Akhtar Kalam, Juan Shi, and Aladin Zayegh. A price-regulated electric vehicle charge-discharge strategy for g2v, v2h, and v2g. *International Journal of Energy Research*, 43(2):1032–1042, 2019.

[13] C Zhou, Y Xiang, Y Huang, X Wei, Y Liu, and J Liu. Economic analysis of auxiliary service by v2g: city comparison cases. *Energy Reports*, 6:509–514, 2020.

[14] Viviani Caroline Onishi, Carlos Henggeler Antunes, and João Pedro Fernandes Trovão. Optimal energy and reserve market management in renewable microgrid-pevs parking lot systems: V2g, demand response and sustainability costs. *Energies*, 13(8):1884, 2020.

[15] Xinzhou Li, Yitong Tan, Xinxin Liu, Qiangqiang Liao, Bo Sun, Guangyu Cao, Cheng Li, Xiu Yang, and Zhiqin Wang. A cost-benefit analysis of v2g electric vehicles supporting peak shaving in shanghai. *Electric Power Systems Research*, 179:106058, 2020.

[16] Seth Mullendore. An introduction to demand charges. *Clean Energy Group, National Renewable Energy Laboratory (NREL)*, 2017.

[17] Guanchen Zhang, Shaoqing Tim Tan, and G Gary Wang. Real-time smart charging of electric vehicles for demand charge reduction at non-residential sites. *IEEE Transactions on Smart Grid*, 9(5):4027–4037, 2017.

[18] Yi He, Ziqi Song, and Zhaocai Liu. Fast-charging station deployment for battery electric bus systems considering electricity demand charges. *Sustainable Cities and Society*, 48:101530, 2019.

[19] Nan Qin, Azwirman Gusrialdi, R Paul Brooker, and Ali T-Raissi. Numerical analysis of electric bus fast charging strategies for demand charge reduction. *Transportation Research Part A: Policy and Practice*, 94:386–396, 2016.

[20] Sumeet Singh, Marco Pavone, and Jean-Jacques E. Slotine. Tube-based mpc : a contraction theory approach. 2016.

[21] Frauke Oldewurtel, David Sturzenegger, Peyman Mohajerin Esfahani, Göran Andersson, Manfred Morari, and John Lygeros. Adaptively constrained stochastic model predictive control for closed-loop constraint satisfaction. In *American Control Conference*, pages 4674–4681, 2013.

[22] Diego Muñoz-Carpintero, Guoqiang Hu, and Costas J Spanos. Stochastic model predictive control with adaptive constraint tightening for non-conservative chance constraints satisfaction. *Automatica*, 96:32–39, 2018.

[23] Yushen Long and Lihua Xie. Iterative learning stochastic mpc with adaptive constraint tightening for building hvac systems. *IFAC-PapersOnLine*, 53(2):11577–11582, 2020.

[24] Milan Korda, Ravi Gondhalekar, Frauke Oldewurtel, and Colin N Jones. Stochastic mpc framework for controlling the average constraint violation. *IEEE Transactions on Automatic Control*, 59(7):1706–1721, 2014.

[25] Frauke Oldewurtel, Line Roald, Göran Andersson, and Claire Tomlin. Adaptively constrained stochastic model predictive control applied to security constrained optimal power flow. In *American Control Conference*, pages 931–936, 2015.

[26] Xiaogang Guo, Zhejing Bao, Hongji Lai, and Wenjun Yan. Model predictive control considering scenario optimisation for microgrid dispatching with wind power and electric vehicle. *The Journal of Engineering*, 2017(13):2539–2543, 2017.

[27] G. Liu, M. Starke, B. Xiao, X. Zhang, and K. Tomsovic. Microgrid optimal scheduling with chance-constrained islanding capability. *Electric Power Systems Research*, 145:197–206, Apr 2017.

[28] Zhi Peng Yuan, Jing Xia, and Peng Li. Two-Time-Scale Energy Management for Microgrids with Data-Based Day-Ahead Distributionally Robust Chance-Constrained Scheduling. *IEEE Transactions on Smart Grid*, 12(6):4778–4787, Nov 2021.

[29] Kaitlyn Garifi, Kyri Baker, Behrouz Touri, and Dane Christensen. *Stochastic Model Predictive Control for Demand Response in a Home Energy Management System; Stochastic Model Predictive Control for Demand Response in a Home Energy Management System*. 2018.

[30] Marko Gulin, Jadranko Matusko, and Mario Vasak. Stochastic model predictive control for optimal economic operation of a residential dc microgrid. volume 2015-June, pages 505–510. Institute of Electrical and Electronics Engineers Inc., 6 2015.

[31] Yifu Ding, Thomas Morstyn, and Malcolm D McCulloch. Distributionally robust joint chance-constrained optimization for networked microgrids considering contingencies and renewable uncertainty. *IEEE Transactions on Smart Grid*, 13(3):2467–2478, 2022.

[32] Farid Hamzeh Aghdam, Navid Taghizadegan Kalantari, and Behnam Mohammadi-Ivatloo. A stochastic optimal scheduling of multi-microgrid systems considering emissions: A chance constrained model. *Journal of Cleaner Production*, 275:122965, 2020.

[33] Hang Wang, Haijun Xing, Yangfan Luo, and Wenbo Zhang. Optimal scheduling of micro-energy grid with integrated demand response based on chance-constrained

programming. *International Journal of Electrical Power & Energy Systems*, 144:108602, 2023.

[34] Okan Ciftci, Mahdi Mehrtash, and Amin Kargarian. Data-driven nonparametric chance-constrained optimization for microgrid energy management. *IEEE Transactions on Industrial Informatics*, 16(4):2447–2457, 2019.

[35] Xiaogang Guo, Zhejing Bao, Zhijie Li, and Wenjun Yan. Adaptively Constrained Stochastic Model Predictive Control for the Optimal Dispatch of Microgrid. *Energies 2018, Vol. 11, Page 243*, 11(1):243, Jan 2018.

[36] Basil Kouvaritakis, Mark Cannon, and Diego Muñoz-Carpintero. Efficient prediction strategies for disturbance compensation in stochastic mpc. *International Journal of Systems Science*, 44(7):1344–1353, 2013.

[37] Basil Kouvaritakis, Mark Cannon, Saša V Raković, and Qifeng Cheng. Explicit use of probabilistic distributions in linear predictive control. *Automatica*, 46(10):1719–1724, 2010.

[38] Marcello Farina, Luca Giulioni, Lalo Magni, and Riccardo Scattolini. An approach to output-feedback mpc of stochastic linear discrete-time systems. *Automatica*, 55:140–149, 2015.

[39] Giuseppe C Calafiore and Lorenzo Fagiano. Stochastic model predictive control of lpv systems via scenario optimization. *Automatica*, 49(6):1861–1866, 2013.

[40] Daniele Bernardini and Alberto Bemporad. Scenario-based model predictive control of stochastic constrained linear systems. In *Proceedings of the 48h IEEE Conference on Decision and Control (CDC) held jointly with 2009 28th Chinese Control Conference*, pages 6333–6338. IEEE, 2009.

[41] James Fleming and Mark Cannon. Time-average constraints in stochastic model predictive control. In *2017 American Control Conference (ACC)*, pages 5648–5653. IEEE, 2017.

[42] Alexandre Capone, Tim Brdigam, and Sandra Hirche. Online constraint tightening in stochastic model predictive control: A regression approach. *IEEE Transactions on Automatic Control*, 2024.

[43] James B Rawlings, David Angeli, and Cuyler N Bates. Fundamentals of economic model predictive control. In *2012 IEEE 51st IEEE conference on decision and control (CDC)*, pages 3851–3861. IEEE, 2012.

[44] Cristian Cortes-Aguirre, Yi-An Chen, Avik Ghosh, Jan Kleissl, and Adil Khurram. Economic mpc with an online reference trajectory for battery scheduling considering demand charge management. *IEEE Transactions on Smart Grids (Under review); arXiv:2412.10851*, 2024.

[45] Michael J Risbeck and James B Rawlings. Economic model predictive control for time-varying cost and peak demand charge optimization. *IEEE Transactions on Automatic Control*, 65(7):2957–2968, 2019.

[46] Morgan Jones and Matthew M Peet. Solving dynamic programming with supremum terms in the objective and application to optimal battery scheduling for electricity consumers subject to demand charges. In *2017 IEEE 56th Annual Conference on Decision and Control (CDC)*, pages 1323–1329. IEEE, 2017.

[47] David Angeli, Rishi Amrit, and James B Rawlings. On average performance and stability analysis of economic model predictive control. *IEEE Transactions on Automatic Control, DOI*, 10, 2012.

[48] Rishi Amrit, James B Rawlings, and David Angeli. Economic optimization using model predictive control with a terminal cost. *Annual Reviews in Control*, 35(2):178–186, 2011.

[49] James Blake Rawlings, David Q Mayne, Moritz Diehl, et al. *Model predictive control: theory, computation, and design*, volume 2. Nob Hill Publishing Madison, WI, 2017.

[50] Lars Grüne. Economic receding horizon control without terminal constraints. *Automatica*, 49(3):725–734, 2013.

[51] Robert D McAllister and James B Rawlings. A suboptimal economic model predictive control algorithm for large and infrequent disturbances. *IEEE Transactions on Automatic Control*, 69(2):1242–1248, 2023.

[52] David Angeli, Alessandro Casavola, and Francesco Tedesco. On average performance of economic model predictive control with time-varying cost and terminal constraints. In *2015 American Control Conference (ACC)*, pages 2974–2979. IEEE, 2015.

[53] David Angeli, Alessandro Casavola, and Francesco Tedesco. Theoretical advances on economic model predictive control with time-varying costs. *Annual Reviews in Control*, 41:218–224, 2016.

[54] Stefan Ambec and Claude Crampes. Real-time electricity pricing to balance green energy intermittency. *Energy economics*, 94:105074, 2021.

[55] Lars Grüne and Simon Pirkelmann. Closed-loop performance analysis for economic model predictive control of time-varying systems. In *2017 IEEE 56th Annual Conference on Decision and Control (CDC)*, pages 5563–5569. IEEE, 2017.

[56] David Williams. *Probability with martingales*. Cambridge university press, 1991.

[57] Robert Gardner Bartle and Robert G Bartle. *The elements of real analysis*, volume 2. Wiley New York, 1964.

[58] Sushil Silwal, Colton Mullican, Yi-An Chen, Avik Ghosh, John Dilliott, and Jan Kleissl. Open-source multi-year power generation, consumption, and storage data in a microgrid. *Journal of Renewable and Sustainable Energy*, 13(2), 2021.

[59] Michael Grant and Stephen Boyd. CVX: Matlab software for disciplined convex programming, version 2.1. http://cvxr.com/cvx, March 2014.

[60] Michael Grant and Stephen Boyd. Graph implementations for nonsmooth convex programs. In V. Blondel, S. Boyd, and H. Kimura, editors, *Recent Advances in Learning and Control*, Lecture Notes in Control and Information Sciences, pages 95–110. Springer-Verlag Limited, 2008. http://stanford.edu/~boyd/graph_dcp.html.

[61] How long does it take to charge an electric car? https://pod-point.com/guides/driver/how-long-to-charge-an-electric-car?srsltid=AfmBOoqYSgI9TvyXnXUzFKpLFEAv7AeDIAiuChFAkSNgicn1uT4kx_70. Accessed: 2025-05-12.

[62] Levels of ev charging. https://www.power-sonic.com/blog/levels-of-ev-charging/. Accessed: 2025-05-12.

[63] Evs explained: Battery capacity, gross versus net. https://www.caranddriver.com/features/a36051980/evs-explained-battery-capacity-gross-versus-net/. Accessed: 2025-05-12.

[64] Electric vehicle charging station locations. https://afdc.energy.gov/fuels/electricity-locations#/find/nearest?fuel=ELEC. Accessed: 2025-05-12.

[65] Avik Ghosh, Cristian Cortes-Aguirre, Yi-An Chen, Adil Khurram, and Jan Kleissl. Adaptive chance constrained mpc under load and pv forecast uncertainties. In *IEEE PES Grid Edge Technologies Conference & Exposition (Grid Edge)*, pages 1–5, 2023.

[66] Georg Schildbach, Giuseppe C Calafiore, Lorenzo Fagiano, and Manfred Morari. Randomized model predictive control for stochastic linear systems. In *2012 American Control Conference (ACC)*, pages 417–422. IEEE, 2012.

[67] Matthias Lorenzen, Fabrizio Dabbene, Roberto Tempo, and Frank Allgöwer. Constraint-tightening and stability in stochastic model predictive control. *IEEE Transactions on Automatic Control*, 62(7):3165–3177, 2016.

[68] Rui Zhang, Yan Xu, Zhao Yang Dong, Weicong Kong, and Kit Po Wong. A composite k-nearest neighbor model for day-ahead load forecasting with limited temperature forecasts. volume 2016-November. IEEE Computer Society, 11 2016.

[69] Stanley G. Benjamin, Stephen S. Weygandt, John M. Brown, Ming Hu, Curtis R. Alexander, Tatiana G. Smirnova, Joseph B. Olson, Eric P. James, David C. Dowell, Georg A. Grell, Haidao Lin, Steven E. Peckham, Tracy Lorraine Smith, William R. Moninger, Jaymes S. Kenyon, and Geoffrey S. Manikin. A north american hourly

assimilation and model forecast cycle: The rapid refresh. *Monthly Weather Review*, 144(4):1669 – 1694, 2016.

[70] Avik Ghosh, Mónica Zamora Zapata, Sushil Silwal, Adil Khurram, and Jan Kleissl. Effects of number of electric vehicles charging/discharging on total electricity costs in commercial buildings with time-of-use energy and demand charges. *Journal of Renewable and Sustainable Energy*, 14(3), 2022.

[71] Avik Ghosh, Cristian Cortes-Aguirre, Yi-An Chen, Adil Khurram, and Jan Kleissl. Adaptive relaxation-based nonconservative chance constrained stochastic mpc. *IEEE Transactions on Control Systems Technology*, 2025.

[72] Stephen Boyd and Lieven Vandenberghe. *Convex optimization*. Cambridge university press, 2004.